

Functional reconstitution
of the human lysosomal peptide transporter TAPL
reveals the substrate specificity

Dissertation
zur Erlangung des Doktorgrades
der Naturwissenschaften

vorgelegt beim Fachbereich
Biochemie, Chemie und Pharmazie
der Johann Wolfgang Goethe-Universität
in Frankfurt am Main

von Chenguang Zhao
aus Huhehaote/China

Frankfurt am Main, 2009
(D30)

Vom Fachbereich Biochemie, Chemie und Pharmazie der
Johann Wolfgang Goethe-Universität als Dissertation angenommen.

Dekan: Prof. Dr. Dieter Steinhilber

1. Gutacher: PD. Dr. Rupert Abele

2. Gutachter: Prof. Dr. Clemens Glaubitz

Datum der Disputation:

Teile der vorliegenden Arbeit wurden veröffentlicht in:

Zhao C, Haase W, Tampé R, Abele R.

Peptide Specificity and Lipid Activation of the Lysosomal Transport Complex ABCB9 (TAPL).

J Biol Chem (2008) 283: 17083-17091

Zhao C, Tampé R, Abele R.

TAP and TAP-like — brothers in arms?

Naunyn-Schmiedeberg's Arch Pharmacol (2006) 372: 444–450

Table of Contents

Deutsche Zusammenfassung	4
Abstract	8
1 Introduction	10
1.1 ABC Transporters	10
1.1.1 Structural organization	10
1.1.2 Transport mechanism	17
1.2 Transporter associated with antigen processing-like (TAP-like or TAPL)	18
1.2.1 Phylogenetic relationship and gene organization	18
1.2.2 Topology model and homodimerization	20
1.2.3 TAPL functions as a peptide transporter	22
1.2.4 Nucleotide-dependent peptide transport	23
1.2.5 Tissue distribution and cellular localization	24
1.2.6 Physiological function	25
1.3 Objective	27
2 Materials	28
2.1 Chemicals	28
2.2 Primers	31
2.3 Peptides	33
3 Methods	34
3.1 Molecular cloning	34
3.1.1 Plasmid DNA preparation	34
3.1.2 Ligase chain reaction for site-directed <i>in vitro</i> mutagenesis	34
3.1.3 Plasmid DNA restriction analysis	35
3.1.4 Subcloning the gene of interest by restriction digestion and ligation	36
3.1.5 Subcloning the cDNAs of Haf-4 and Haf-9 by PCR	36
3.1.6 Isolation of the recombinant Bacmid DNA	37
3.2 Microbiological techniques	37
3.2.1 Bacterial culture	37
3.2.2 Preparation of competent cells	38
3.2.3 Transformation of plasmid DNA into chemical competent bacterial cells	38
3.3 Cell biology techniques	39
3.3.1 Thawing and freezing of <i>Sf9</i> insect cells	39
3.3.2 <i>Sf9</i> insect cells culture	40
3.3.3 Transfecting <i>Sf9</i> cells with recombinant Bacmid DNA	40
3.3.4 Amplification of the recombinant baculovirus	40
3.3.5 Virus titer determination	41
3.3.6 Recombinant membrane protein expression	41
3.4 General biochemical methods	42

3.4.1 Protein concentration determination	42
3.4.2 SDS-PAGE	43
3.4.3 Immunoblotting	43
3.5 Biochemical assays for TAPL	45
3.5.1 Peptide labeling with 5-iodoacetamidofluorescein	45
3.5.2 Peptide labeling with Na ¹²⁵ I	45
3.5.3 Membrane preparation	46
3.5.4 Membrane solubilization	46
3.5.5 Determination of critical micelle concentration	47
3.5.6 Purification	47
3.5.7 Gel filtration	48
3.5.8 Blue native PAGE	48
3.5.9 Reconstitution	50
3.5.10 Freeze fracture electron microscopy	51
3.5.11 ATPase activity assay	51
3.5.12 Peptide transport assay	52
3.5.13 Peptide transport assay (glycosylation assay)	52
3.5.14 Co-immunoprecipitation	53
4 Results	54
4.1 Functional expression of TAPL	54
4.2 Solubilization of TAPL	55
4.3 Purification of TAPL	57
4.4 Oligomeric status	59
4.5 Functional reconstitution of TAPL	61
4.6 Lipid activation of TAPL	64
4.7 Key positions for substrate recognition	66
4.8 Sequence specificity of TAPL	67
4.9 ATPase activity	70
4.10 Functional solubilization and purification of TAPL by dodecylmaltoside	72
4.11 Functional expression of TAPL cysteine-less mutant and single cysteine mutants	77
4.12 Characterization of TAPL orthologs from <i>Caenorhabditis elegans</i>	81
4.12.1 Expression of Haf-4 and Haf-9 in <i>Sf9</i> insect cells	81
4.12.2 Haf-4 and Haf-9 are ATP-dependent peptide transporters	82
4.12.3 Interaction between Haf-4 and Haf-9	86
5 Discussions	87
5.1 Solubilization, purification and reconstitution	87
5.1.1 Solubilization	87
5.1.2 Purification	88
5.1.3 Reconstitution	89
5.2 Oligomeric status	93
5.3 Substrate specificity	95

5.4 ATP hydrolysis	97
5.5 TAPL cys-less and single cysteine mutants	99
5.6 Haf-4 and Haf-9	99
6 Abbreviations	102
7 References	105
Acknowledgments	122
Curriculum Vitae	123

Deutsche Zusammenfassung

ABC-Transporter kommen in allen Organismen von Archaeen, Bakterien bis hin zu Eukaryoten vor. Sie sind an zahlreichen zellulären Prozessen beteiligt, z.B. an der Nährstoffaufnahme, am Lipidtransport und der Antigenprozessierung. ABC-Transporter können eine Vielzahl chemisch diverser Substrate, unter anderem Kohlenhydrate, Antibiotika, Lipide sowie Polypeptide und Proteine mit mehr als 100 kDa Molekulargewicht durch zelluläre Membranen transportieren. Die humanen ABC-Transporter werden nach Sequenzhomologie innerhalb der ATP-Bindungskassette (ATP-binding cassette, ABC) in sieben Unterfamilien eingeteilt, die mit ABCA bis ABCG bezeichnet werden. Grundsätzlich haben ABC-Transporter eine Minimalzusammensetzung aus zwei Nukleotidbindedomänen (NBD), welche die Energie für die Translokation zur Verfügung stellen und zwei wenig konservierten Transmembrandomänen (TMD), die die Transporter in der Plasmamembran oder in intrazellulären Membranen verankern und den Translokationspfad ausbilden.

Der humane ABC Transportkomplex ABCB9 wurde als lysosomaler Polypeptidtransporter identifiziert. ABCB9 hat eine hohe Sequenzidentität zu TAP1 („*transporter associated with antigen processing 1*“) und TAP2 und wird deshalb „*TAP-Like*“ (TAPL) genannt. In lysosomalen Membranen organisiert sich TAPL als Homodimer, wobei sich das Monomer aus der N-terminalen TMD mit 10 putativen Transmembranhelices fusioniert mit der C-terminalen NBD zusammensetzt.

Von humanem TAPL wurden Orthologe in Invertebraten, wie *Caenorhaditis elegans* und Pflanzen, nachgewiesen, was auf ein hohes evolutionäres Alter von TAPL hindeutet. Humanes TAPL wird in verschiedenen Geweben exprimiert, u.a. im zentralen Nervensystem und im Herz. Auffallenderweise wird die Expression von TAPL während der Differenzierung von Monozyten zu dendritischen Zellen und Makrophagen stark induziert, somit wird eine Funktion von TAPL in der Antigenprozessierung vermutet. Allerdings ist dieser Peptidtransporter nicht an den klassischen MHC Klasse I und II-Prozessierungswegen beteiligt. Im Gegensatz zu TAP besitzt TAPL eine niedrige Affinität verbunden mit einer breiten Längenspezifität (6mer bis zu 59mer) für die Substratpeptide. Grundsätzlich besitzen TAPL und TAP ein ähnliches Substraterkennungsprinzip, da beide Transporter Peptide mittels Peptidrückgrat, den freien N- und C-Termini und Seitenketteninteraktionen, binden.

Die zentrale Frage auf dem TAPL-Forschungsgebiet beschäftigt sich momentan damit, die physiologische Bedeutung dieses Transporters aufzuklären. Um diese Fragestellung beantworten zu können ist die Kenntnis der Substratspezifität von essentieller Bedeutung.

Die Ziele meiner Doktorarbeit waren (i) die funktionale Solubilisierung, Reinigung und Rekonstitution von humanem TAPL in Liposomen. (ii) Des weiteren sollte die Substratspezifität detailliert entschlüsselt werden. (iii) Die Generierung und Charakterisierung einer Cystein-freien TAPL Variante sollte den Grundstein legen um den Translokationsmechanismus und die Struktur aufzuklären. (iv) Weiterhin sollten Orthologe von TAPL, Haf-4 und Haf-9 aus *Caenorhabditis elegans*, biochemisch charakterisiert werden, um weitere Kenntnisse über die physiologische Funktion von humanem TAPL zu erhalten.

Da es nicht möglich war, an isolierten TAPL-haltigen Membranen die Substratspezifität von TAPL zu entschlüsseln, wurde eine Prozedur bestehend aus Expression in Sf9 Insektzellen, unter Verwendung des Baculovirus Expressionssystems, Solubilisierung, Reinigung und funktionaler Rekonstitution in Liposomen etabliert. Durch intensives „*Screening*“ von Detergenzien zur Solubilisierung von TAPL kristallisierten sich die nicht-ionischen Detergenzien Digitonin und *n*-Dodecyl- β -D-maltosid (DDM) bezüglich Langzeitstabilität und Funktionalität von TAPL heraus. Für Digitonin konnte eine Solubilisierungseffizienz von 56% und für DDM von 52% nachgewiesen werden, wohingegen *n*-Octyl- β -D-glucopyranosid TAPL nur schwach solubiliziert (13%). Das Detergenz 3-[(3-Cholamidopropyl)dimethylammonio]-1-propansulfonat (CHAPS) solubilizierte TAPL (40% Solubilisierungseffizienz), jedoch war TAPL in diesem Detergenz nicht stabil. Das Detergenz Foscholin 14 zerstörte sogar den Homodimer. Nach Solubilisierung wurde TAPL in einem zwei Stufen Prozess, bestehend aus Kationenaustauscher und Metall-Affinitätschromatographie, mit einer maximalen Ausbeute von 500 μ g TAPL/Liter Insektzellkultur gereinigt. Im Vergleich zu DDM konnte mit Digitonin eine höhere Reinheit während der Reinigung erzielt werden. Der Oligomerisierungszustand von TAPL in der Digitonin- bzw. DDM-Mizelle wurde durch Größenausschlußchromatographie und „*blue native*“ PAGE untersucht. TAPL bildete einen Komplex mit einem apparenten Molekulargewicht von 200 kDa aus, was auf einen Homodimer mit einem theoretischen Molekulargewicht von 172 kDa hinweist.

Zur Charakterisierung des Peptidtransports wurde eine Rekonstitution von TAPL in Liposomen etabliert. Dabei wurden die Liposomen mit Triton X-100 destabilisiert und die Detergenzien mit „*Bio-Beads*“ entfernt. Nach der funktionalen Rekonstitution wies TAPL

die gleichen kinetischen Parameter wie TAPL in Membranen von Insektenzellen auf. Der K_M -Wert für das Modellopeptid RRYC^fKSTEL (f steht für Acetamidfluorescein gekoppelt an eine Cysteinseitenkette) konnte auf $10,5 \pm 2,3 \mu\text{M}$ und für ATP auf $97,6 \pm 2,7 \mu\text{M}$ bestimmt werden. Somit ist die Funktionalität von rekonstituierten TAPL nicht beeinträchtigt.

Für den Peptidtransport konnte eine starke Abhängigkeit für die Lipidzusammensetzung detektiert werden. Interessanterweise stellten sich Lipide von *E. coli* im Vergleich zu Lipidextrakten aus Säugerzellen als bevorzugt heraus. Des Weiteren zeigte sich, dass Phosphatidylcholin, das meist verbreitete Lipid in eukaryontischen Zellen, einen Dosis-abhängigen Effekt auf die Transportaktivität von TAPL hat. Die höchste Peptidtransporteffizienz wurde in Liposomen bestehend aus 70% *E. coli* Lipidextrakt und 30% (w/w) 1,2-dioleoyl-*sn*-glycero-3-phosphocholin (DOPC) nachgewiesen, höhere Konzentrationen von DOPC reduzierten die Peptidtransporteffizienz. Des Weiteren wurde TAPL in Liposomen rekonstituiert bestehend aus rein synthetisch hergestellten Phospholipiden. Dabei stellte sich heraus, dass Proteoliposomen aus 100% DOPC inaktiv waren. Wurden allerdings DOPC mit negativ geladenen Phospholipiden 1,2-dioleoyl-*sn*-glycero-3-phosphat (DOPA) oder 1,2-dioleoyl-*sn*-glycero-3-phospho-L-serin (DOPS) gemischt, so konnte eine Dosis-abhängige Transportaktivität festgestellt werden. Für die ebenfalls negativ geladenen Lipide 1,2-dioleoyl-*sn*-glycero-3-phosphoethanolamin (DOPE) und L- α -phosphatidylglycerol (PG) trat dieser Effekt nicht auf. Somit beeinflusst nicht nur die Ladung der Lipide den Peptidtransport durch TAPL, sondern auch die spezifische Kopfgruppe der Lipide.

Rekonstituiertes TAPL zeigte eine spezifische ATP-Hydrolyseaktivität, welche durch ortho-Vanadat inhibiert werden konnte. Die ATP-Hydrolyseaktivität in Proteoliposomen war 6-fach höher als in gereinigtem TAPL. Dieser Effekt könnte durch die erniedrigte Proteinflexibilität auf Grund des lateralen Drucks und Krümmungsstress in den Liposomen erklärt werden. Des Weiteren konnte eine durch Peptid stimulierte ATP-Hydrolyseaktivität nicht nachgewiesen werden.

Nach funktionaler Rekonstitution und Charakterisierung von TAPL in Liposomen wurden mit Hilfe von kombinatorischen D-Amino Peptidbibliotheken die Schlüsselpositionen für die Substraterkennung identifiziert. Sowohl die N- als auch die C-terminale Position innerhalb des Substratpeptids haben einen wesentlichen Einfluß auf die Substraterkennung. Die C-terminale Position innerhalb des Peptids hat den stärksten Einfluss auf die Substraterkennung, da kovalente Modifikationen den Peptidtransport drastisch reduzieren. Zusätzlich wiesen die

N-terminalen Positionen 2 und 3 einen Einfluss auf die Peptidselektivität auf. Die weitere Charakterisierung der Schlüsselpositionen mittels detaillierten Peptidbibliotheken ergab, dass TAPL sowohl bei der N- als auch bei der C-terminalen Position positiv geladene, aromatische oder hydrophobe Aminosäuren bevorzugt. Negativ geladene Aminosäuren, Asparagin und Methionin sind nicht präferiert. Diese Selektivitätsregel für die Peptiderkennung durch TAPL konnte für Peptide mit verschiedener Länge verifiziert werden. Diese Regel kann in Bezug auf elektrostatische Interaktionen erweitert werden, da Substratpeptide mit einer positiven Nettoladung effektiver transportiert werden als welche mit einer negativen Nettoladung. Diese Ergebnisse deuten auf eine Interaktion von TAPL mit den Termini des Substratpeptids hin, wobei Länge als auch die Aminosäuresequenz zwischen diesen Ankerpositionen promiskuitiv sein können. Dadurch das die Peptide nur über zwei Seitenreste erkannt werden, wird sichergestellt, dass ein Transporter eine Vielzahl verschiedenster Peptide transportieren kann und somit nicht der limitierende Faktor in diesem Prozess darstellt.

Ein wichtiger Grundstein, um den Translokationsmechanismus und die Struktur von TAPL aufzuklären, ist die Generierung einer Cystein-freien TAPL Variante. Durch gezielte Mutagenese wurden acht Cysteine im TAPL Monomer durch Alanin bzw. Valin ersetzt. Die Cystein-freie TAPL Mutante zeigte eine gleiche Peptidtransportaktivität wie TAPL Wildtyp. Nach der Gewährleistung der Funktionalität von Cystein-freiem TAPL wurden einzelne Cysteine an strategischen Positionen wieder eingeführt. Die eingeführten Cysteine hatten keinen Einfluss auf die Faltung von TAPL, da alle TAPL-Varianten in vergleichbaren Mengen exprimiert wurden und der Peptidtransport durch diese Mutationen nicht beeinflusst wurde. Eine Ausnahme bildete die TAPL-Variante L701C, welche nahe der konservierten H-Schleife in der NBD lokalisiert ist und eine signifikant reduzierte Transportaktivität aufweist.

Die orthologen TAPL Varianten in *Caenorhabditis elegans*, Haf-4 und Haf-9, besitzen eine Sequenzidentität von 40% mit humanem TAPL und 50% untereinander. Insbesondere Haf-4 scheint ein funktionales Homolog von humanem TAPL zu sein, da TAPL in Haf-4 defizienten Tieren die Formierung von Darm-Granula wiederherstellt und die Lebenszeit von Nematoden unter Hungerbedingungen auf Wildtyp Niveau erhöht. Für eine detaillierte Charakterisierung der physiologischen Funktion und deren Substrate wurden Haf-4 und Haf-9 mit Hilfe des Baculovirussystems in Sf9-Insektzellen exprimiert. Beide Proteine transportieren in Abhängigkeit von ATP das Modellpeptid. Allerdings ist der Transport 10–20 mal geringer als von TAPL. Interessanterweise scheinen diese Halbtransporter sowohl als Homodimere wie auch als Heterodimere die Funktion als Peptidtransporter erfüllen zu können.

Abstract

The transporter associated with antigen processing-like (TAPL) acts as a lysosomal ATP-dependent polypeptide transporter with broad length selectivity. To characterize in detail its substrate specificity, a procedure for solubilization, purification and functional reconstitution of human TAPL was developed. TAPL was expressed in *Sf9* insect cells with the baculovirus expression system and solubilized from crude membranes. By intensive screening of detergents, the mild non-ionic detergents digitonin and dodecylmaltoside were found to be ideal for solubilization with respect to efficiency, long term stability, and functionality of TAPL. TAPL was isolated in a two-step procedure with a yield of 500 $\mu\text{g/L}$ cell culture and, subsequently, reconstituted into proteoliposomes. The $K_{M(\text{pep})}$ for the peptide RRYC^fKSTEL (f refers to fluorescence label) and $K_{M(\text{ATP})}$ were determined to be $10.5 \pm 2.3 \mu\text{M}$ and $97.6 \pm 27.5 \mu\text{M}$, respectively, which are in the same range as the Michaelis-Menten constants determined in the membranes. The peptide transport activity of the reconstituted TAPL strongly depends on the lipid composition. Interestingly, the *E. coli* lipids are preferred over other tested natural lipids extracts. Moreover, phosphatidylcholine, the most abundant phospholipid in eukaryotic cells influenced TAPL activity in a dose dependent manner. In addition, some negatively charged lipids like DOPA and DOPS increased peptide transport activity with preference for DOPS. However, DOPE or egg PG which are also negatively charged had no effect. It seems not only the charge but also the specific head group of phospholipids that has impact on the function of TAPL.

With the help of combinatorial peptide libraries containing D-amino acid residues at defined positions as well as bulky fluorescein labeled peptides, the key positions of the peptides were localized to the N- and C-terminal residues with respect to peptide transport. The C-terminal position has the strongest selectivity since modification at this position shows strongest impact on peptide transport. Additionally, positions 2 and 3 of the peptide also have weak influence on peptide selectivity. Subsequently, the residue preferences at the key positions were systematically investigated by combinatorial peptide libraries with defined residues at certain positions. At both ends, TAPL favors positively charged, aromatic, or hydrophobic residues and disfavors negatively charged residues as well as asparagine and methionine. The residue preferences at the key positions are valid for peptide substrates with different length, indicating a general rule for TAPL selectivity. Besides specific interactions of both terminal residues, electrostatic interactions are important, since peptides with positive net charge are

more efficiently transported than negatively charged ones.

By size exclusion chromatography (SEC) and blue native PAGE, TAPL purified in the presence of digitonin or dodecylmaltoside had an apparent molecular weight of 200 kDa which is close to the theoretical molecular mass of the TAPL homodimer (172 kDa). The purified and reconstituted TAPL showed specific ATP hydrolysis activity which can be inhibited by orthovanadate. TAPL in proteoliposomes showed 6-fold higher ATP hydrolysis than digitonin solubilized protein, indicating the phospholipids impact on TAPL function. However, no peptide substrate stimulated ATPase activity was observed.

For site-specific labeling of TAPL, eight cysteines in each half transporter were replaced by alanine or valine. The TAPL cys-less mutant showed the same peptide transport activity as TAPL wt. Based on the functional TAPL cys-less mutant, seven single cysteine mutants were introduced into strategic positions. All single cysteine mutants in the TMD did not influence peptide transport, whereas the mutant L701C, which is close to the conserved H-loop motif, displayed impaired transport.

TAPL orthologs Haf-4 and Haf-9 from *Caenorhabditis elegans* possess around 40% sequence identities with TAPL and 50% with each other. Both proteins are putative half transporters and reported to be involved in the intestinal granule formation (Bauer, 2006; Kawai et al., 2009). To further understand the physiological functions of these two proteins, they were expressed in *Sf9* insect cells. Haf-4 and Haf-9 showed weak but specific ATP- and peptide-dependent peptide transport activity for the given peptide RRYC^fKSTEL. Therefore, it was proposed that the physiological roles for Haf-4 and Haf-9 might be related to their peptide transport activity. Besides forming functional homodimeric complex as estimated by the peptide transport activities, both half transporter could also form heteromers which was confirmed by co-immunoprecipitation. However, the heteromers showed decreased transport activity.

1 Introduction

1.1 ABC Transporters

The ATP-binding cassette (ABC) transporters form a family of membrane proteins, which couple the energy of ATP hydrolysis with solute translocation (Higgins, 1992). The ABC transporter superfamily represents the largest class of active transporters in prokaryotes, and the second largest class (after the major facilitator superfamily) in eukaryotes. They are involved in many cellular processes and transport a wide variety of substrates, ranging from sugars and amino acids, hydrophilic drugs and lipids to large proteins (Higgins, 1992; Schmitt and Tampé, 2002). ABC transporters can be found in the plasma membrane as well as in membranes of various organelles. In eukaryotes, ABC transporters exclusively function as exporters, whereas in archaea and eubacteria, they can mediate solute uptake by the help of high-affinity solute-binding proteins in the periplasm (Davidson and Chen, 2004). There are 48 ABC genes in the human genome, which are divided into seven subfamilies (A-G) based on homology of the nucleotide-binding domain (Dean et al., 2001). The function of only 16 human ABC transporters is deciphered (Borst and Elferink, 2002). Notably, 17 members of this family are associated with defined human diseases (Dean and Annilo, 2005). For example, dysfunctions in the cystic fibrosis transmembrane conductance regulator (CFTR or ABCC7) cause genetic lung disease cystic fibrosis (Sheppard and Welsh, 1999); mutations in ABCA1, which is a major regulator in cellular cholesterol and phospholipids homeostasis, lead to Tangier disease (Oram and Vaughan, 2000); deficiencies of the transporter associated with antigen processing (TAP) are related to certain autoimmune diseases and tumor developments (Lankat-Buttgereit and Tampé, 2002).

1.1.1 Structural organization

ABC transporters contain a conserved core structure of two transmembrane domains (TMDs) and two nucleotide-binding domains (NBDs) facing the cytosol (Schmitt and Tampé, 2002). The TMDs of ABC exporters normally comprise 2×6 membrane-spanning helices (Dean et al., 2001; Seeger and van Veen, 2009). However, for ABC importers, the number of transmembrane helices is variable (Biemans-Oldehinkel et al., 2006; Davidson et al., 2008). The TMDs form the translocation pathway and, in the case of exporters, the substrate-binding site. The NBDs contain the highly conserved Walker A and Walker B motifs, as well as the

C-loop (ABC signature motif), which is the hallmark of ABC transporters. The NBDs bind and hydrolyze ATP via the conserved motifs and energize the solute transport.

More than two dozens of crystal structures of the NBDs have been determined in the presence or absence of nucleotides after the HisP protein from *Salmonella typhimurium* (Hung et al., 1998). The overall structures and arrangements of the NBDs are highly conserved and can be divided to two subdomains: a catalytical core domain (RecA-like domain) and a helical domain (Figure 1-1A). The two subdomains of the NBD monomer form an ‘L’ shaped structure (Hung et al., 1998). Upon ATP binding the two NBDs can dimerize. There are several conserved sequence motifs within the NBD, all with specific functions (Jones and George, 2004). These motifs include the Walker A motif or the P-loop (GXXGXXGK(S/T)) that binds nucleotides; the Walker B motif ($\phi\phi\phi\phi$ D, ϕ stands for a hydrophobic residue) providing an aspartate coordinates Mg^{2+} (Yuan et al., 2001; Verdon et al., 2003), and having the glutamate following the Walker B to bind and probably polarize a water molecule attacking ATP (Geourjon et al., 2001; Moody et al., 2002b); the C-loop that contacts the α -phosphate of nucleotide; the Q-loop believed to sense the γ -phosphate moiety via the glutamine, and to serve as a hinge involved in the rigid-body movement between two subdomains as well as the contact interface with the coupling helix of the TMD (Jones and George, 2002; Locher et al., 2002; Zaitseva et al., 2006); the H-loop (also called His-loop or switch region) required for ATP binding and hydrolysis (Zaitseva, 2005; Zaitseva et al., 2006); the A-loop, which stacks against the adenine moiety of bound nucleotide with its aromatic residue (Ambudkar et al., 2006); and the D-loop (also SALD motif) involved in the contact interface between two NBDs (Locher et al., 2002; Smith et al., 2002; Chen et al., 2003a). Residues of the D-loop in the *cis*-NBD contact residues in the *trans*-NBD (the aspartate of the *cis*-D-loop forms a hydrogen bond with the *trans*-Walker A serine whereas the alanine upstream of the aspartate interacts with the histidine in the *trans*-H-loop), and *vice versa*. Therefore, the D-loop seems to play an important role in NBD-NBD communication (Zaitseva et al., 2005a).

Similar in the isolated NBDs and intact ABC transporters, the ATP hydrolysis cycle starts with the dimerization of the NBDs in a so called ‘head-to-tail’ fashion upon ATP binding. Two ATP molecules are sandwiched at the dimer interface (Loo et al., 2002; Moody et al., 2002a; Smith et al., 2002; Chen et al., 2003a; Janas et al., 2003b; Zaitseva et al., 2005b; Dawson and Locher, 2006; Oldham et al., 2007). ATP binding induces a rigid-body rotation of the helical domain towards the catalytical domain. The ATP-binding site is formed by the Walker A/B and the

H-loop from one NBD and the C-loop from the other (Figure 1-1B). ATP hydrolysis induces dissociation of the dimer and, subsequently, ADP and inorganic phosphate are released. These nucleotide-dependent conformational changes in the NBDs drive the conformational changes in the TMDs via the contact interface (Locher et al., 2002), resulting in substrate translocation. Unlike the NBDs, the TMDs vary considerably in primary sequence, length, architecture and the number of transmembrane (TM) helices (Hollenstein et al., 2007a). Based on the architectures of the TMDs from the available intact ABC transporter structures (Locher et al., 2002; Dawson and Locher, 2006; Dawson and Locher, 2007; Hollenstein et al., 2007b; Hvorup, 2007; Pinkett et al., 2007; Ward et al., 2007; Gerber et al., 2008; Kadaba et al., 2008; Aller et al., 2009), the structures of ABC transporters are categorized to exporters, type I importers and type II importers (Locher, 2009; Rees et al., 2009) (Table 1-1).

Table 1-1. Structurally characterized ABC transporter systems, as classified by the TMD fold*

Transporter	Organism	Nucleotide state	Orientation	PDB code	Resolution
Type I ABC importer					
ModABC	<i>Archaeoglobus fulgidus</i>	Apo	Inward	2ONK	3.1 Å
MalFGK ₂	<i>Escherichia coli</i>	ATP-bound	Outward	2R6G	2.8 Å
MaModBC	<i>Methanosarcina acetivorans</i>	Apo	Inward	3D31	3.0 Å
MetNI	<i>Escherichia coli</i>	Apo	Inward	3DHW	3.7 Å
Type II ABC importer					
BtuCD	<i>Escherichia coli</i>	Apo or (VO ₂) ₄	Outward	1L7V	3.2 Å
Hi1470/1	<i>Haemophilus influenzae</i>	Apo	Inward	2NQ2	2.4 Å
BtuCDF	<i>Escherichia coli</i>	Apo	Occluded	2QI9	2.6 Å
ABC exporter					
Sav1866	<i>Staphylococcus aureus</i>	ADP-bound	Outward	2HYD	3.0 Å
		AMPPNP-bound	Outward	2ONJ	3.4 Å
MsbA	<i>Salmonella typhimurium</i>	AMPPNP-bound	Outward	3B60	3.7 Å
		ADP-VO ₄ ³⁻ -bound	Outward	3B5Z	4.2 Å
		Apo	Inward	3B5W	5.3 Å
	<i>Escherichia coli</i>	Apo	Inward	3B5X	5.5 Å
	<i>Vibrio cholerae</i>	Apo	Inward	3B5X	5.5 Å
P-gp	<i>Mus musculus</i>	Apo	Inward	3G5U	3.8 Å

* Note that while the outward-facing conformation generally corresponds to the ATP (or suitable analogue)-bound state, exceptions are evident in the structures of ADP bound to Sav1866 and nucleotide-free BtuCD. Btu, vitamin B₁₂ importer; Mal, maltose transporter; Met, Met transporter; Mod, molybdate transporter; P-gp, P-glycoprotein; PDB, Protein Data Bank; (VO₂)₄, cyclotetranadate; VO₄³⁻, orthovanadate (Rees et al., 2009).

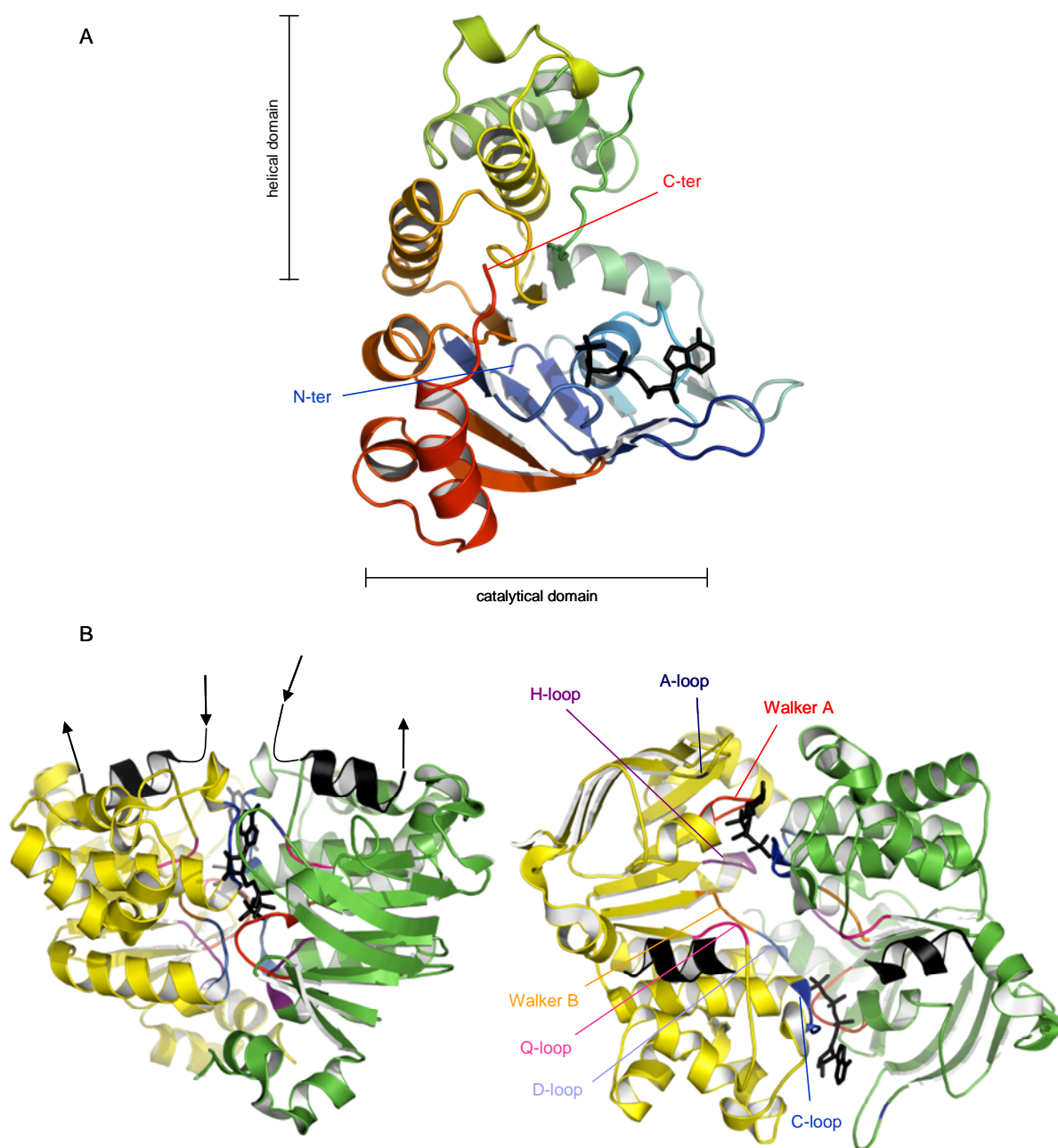


Figure 1-1 Structure and arrangement of the NBD. *A*, side view on the crystal structure of HisP monomer (PDB code: 1B0U). The structure is rainbow-colored starting with the N-terminus (N-ter) in blue and ending with the C-terminus (C-ter) in red. The catalytic core domain is composed of α -helices and β -sheets, whereas the helical domain is mostly made of α -helices. The bound ATP is demonstrated by *black sticks*. *B*, NBD arrangement in a functional ABC transporter. The NBDs of the multidrug ABC transporter Sav1866, crystallized with bound AMP-PNP (PDB code: 2ONJ), are shown in a view from the side (*left panel*) or from the membrane (showing the surface facing the TMDs, *right panel*). The two NBDs are in green and yellow, with mechanistically important sequence motifs colored and labeled with different colors. Bound AMP-PNP is shown as *black sticks*. Note that two AMP-PNP molecules are sandwiched between the P-loop of one NBD and the C-loop of the other, and *vice versa* ('head-to-tail' arrangement). The *short, black helices* are the coupling helices from the TMDs, with *arrows* indicating the direction of the polypeptide chain from the N-terminus to the C-terminus.

ABC exporters are found in the genomes of all sequenced organisms. The physiological functions of these transporters are diverse, but many of them are involved in multidrug resistance, which can lead to failure in cancer chemotherapy (Gottesman et al., 2002). Their TMDs share a core-complex of 12 TM helices (Figure 1-2) (Locher, 2009; Rees et al., 2009). The first high resolution crystal structure of the exporter Sav1866 from *Staphylococcus aureus* is an excellent model for the core architecture of ABC exporters (Stenham et al., 2003; Hollenstein et al., 2007a). In this structure, the TMDs for each subunit embrace each other and have a significant twist. The TMDs are organized into two ‘wings’ that are formed by helices TM1-2 from one subunit and TM3-6 for the other in the outward-facing conformation. Remarkably, no clear gating region was identified in Sav1866 (Dawson et al., 2007). The TMDs of exporters such as Sav1866 are fused to the NBDs, whereas the TMDs and the NBDs are often separate subunits in importers. Due to the long intracellular loops (ICLs), the NBDs are located approximately 25 Å away from the membrane surface (Dawson and Locher, 2006). In Sav1866, both intracellular loops, ICL1 (between TM2 and TM3) and ICL2 (connecting TM4 and TM5), have short ‘coupling helices’ oriented parallel to the membrane plane and are in contact with the NBDs. Coupling helix 1 contacts both NBDs, whereas coupling helix 2 interacts with the NBD of the opposite subunit. Such a swapping architecture forms another difference between exporters and importers. The latter, in contrast, have no swapping resulting in no direct contact between diagonally positioned TMD/NBD pairs and a large gap at the center of four subunits (Dawson and Locher, 2006). In the NBDs, residues around the Q-loop provide contacts with the TMDs in both exporters and importer. In addition to the Q-loop, the conserved glutamate of the X-loop motif found only in exporters forms contacts with both coupling helices of the opposite half transporter and is believed to play a prime role in the TMD-NBD interdomain communications (Dawson and Locher, 2006; Zolnerciks et al., 2007; Serohijos et al., 2008; Oancea et al., 2009; Seeger and van Veen, 2009). Conformational changes in the NBDs induced by ATP binding and hydrolysis are transmitted to the TMDs via the so called ‘transmission interface’ (NBD-TMD contact surface). Therefore, two distinct conformational changes (NBD dimerization and substrate translocation) are tightly coupled.

The type I importers including the molybdate/tungstate transporters *A. fulgidus* ModABC and the *M. acetivorans* MaModBC, as well as the *E. coli* maltose transporter MalFGK₂ and the methionine transporter MetNI, mediate the uptake of ions, sugars and other small substrates by utilizing a specific binding protein. The typical TMD of this type contains at least 5 TM helices (in the case of MetI) in each subunit (Kadaba et al., 2008; Rees et al., 2009).

Additional the N-terminal TM helices reach around and interact with the partner TMD, as in the case of ModABC, MalFGK₂ and MaModBC (Hollenstein et al., 2007b; Oldham et al., 2007; Gerber et al., 2008; Locher, 2009). This kind of intertwining organization of the TM helices is also present in MetI of which the N-terminal helix (TM1) wraps around and contacts with TM2-TM5 in the other TMD (Gerber et al., 2008; Rees et al., 2009). The numbers of TMDs among type I importers are different, thus the numbering of the following TMs is referred to that in the structure of ModB, which is the TMD of ModABC. The structures of ModABC and MalFGK₂ revealed an external gate beneath the interface with substrate binding protein. The gate is formed by the gating region 1 (located between TM3 and helix 3a) and the gating region 2 (located between TM5 and helix 5a) of each TMD (Hollenstein et al., 2007b; Oldham et al., 2007). The coupling helix in importers contains the consensus EAA motif (Saurin et al., 1994; Mourez et al., 1997), and in the case of ModB, it is helix 4a within the loop between TM4 and TM5. Similar to exporters, the coupling helix in type I importers also lies approximately parallel to the membrane bilayer and is embedded in a groove at the boundary between the catalytical core domain and the helical domain of the NBD. However, in contrast to exporters, the coupling helix forms contact mainly with the Q-loop of the NBD on the same side.

The type II importers represented by the *E. coli* vitamin B₁₂ transporter BtuC and *H. influenzae* Hi1471 have distinct TMD architecture from type I importers, with 10 TM helices from each subunit forming 20 transmembrane spans in total. Unlike the helix fold of exporters and type I importers, the 10 α -helices of each TMD form a single bundle and cross the membrane independently of the other TMD. Remarkably, helix TM2 is placed in the center of the subunit in proximate to most of the other helices. The N- and C-terminal halves of the BtuC subunit have similar helix packing, but opposite polarities through the membrane. The TMD-TMD interface is formed by helices TM5 and TM10. BtuCD revealed a closed internal gate formed by intracellular loops between TM4 and TM5 from each BtuC subunit. In contrast, Hi1470/1 revealed a closed external gating region formed by extracellular loops between TM5 and helix5a from each Hi1471 subunit. Moreover, the intracellular loops of BtuC and Hi1471 are shorter than in the Sav1866 structure, therefore, the NBDs are closer to the membrane region (Locher et al., 2002; Pinkett et al., 2007; Rees et al., 2009). The cytosolic loop between TM6 and TM7 in BtuC folds into two short helices. Because the shape of these two helices resembles a shape of an L, it is also called the L-loop. The L-loop is composed of helices L1 and L2, both extensively contact the NBD on the same side. The sequence of the L-loop is

similar to ICL4 of CFTR, ‘EAA loop’ of bacterial importers and ICL1 of exporters (Locher et al., 2002).

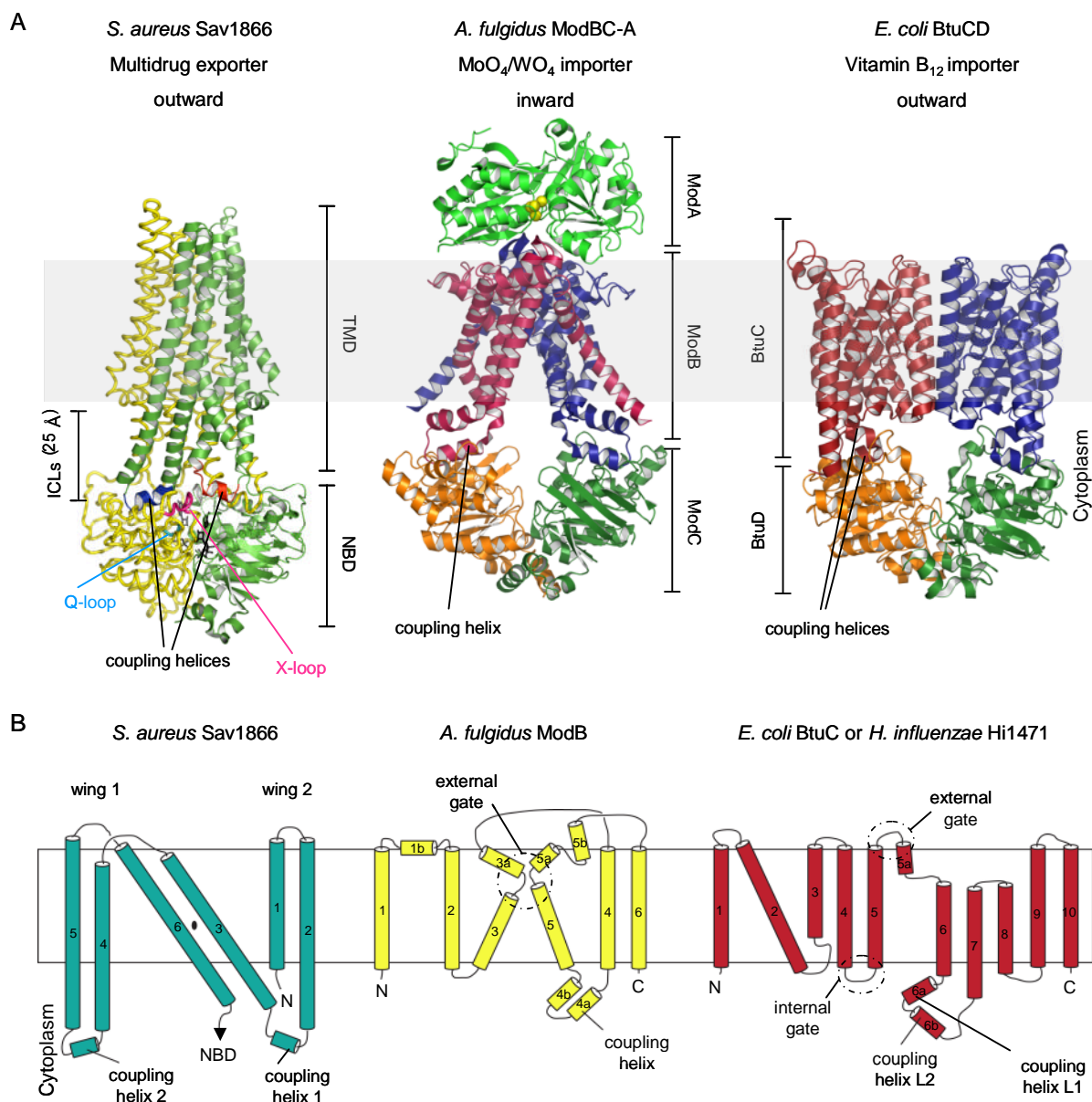


Figure 1-2. Crystal structures of ABC transporters and topology schemes of the TMDs. *A*, ribbon representation of three crystal structures of ABC transporters belong to three different families. The *gray box* depicts the position of the membrane. The TMDs of exporters such as Sav1866 are fused to the NBDs, whereas the TMDs and NBDs are separated subunits in importers. ModA is the substrate binding protein of ModBC. The stoichiometries of the assembled transporters are (Sav1866)₂, ModB₂C₂A and BtuC₂D₂. Note that one subunit of Sav1866 is in a *yellow coil* representation for clear demonstration of the transmission interface formed by coupling helix 1 (red), coupling helix 2 (blue), the X-loop (pink) and the Q-loop (cyan). *B*, topological schemes of the TMDs. The *open box* represents the membrane region. TM helices are numbered consecutively, and short helices following TM helices additionally carry letters. For Sav1866, the schematic emphasizes the long intracellular loops, the two ‘wings’ formed by TM1-2 and TM3-6, respectively, and the pseudo-twofold symmetry relating TM1-3 to TM4-6 (with the *black ellipse* depicting the approximate position of the rotation axis). For ModB, the schematic emphasizes the conserved gate formed by segments from TM3 and TM5. For BtuC (Hi1471), the schematic depicts the internal and external gates. The coupling helices in each TMD are the main site of contact with the NBD in the assembled transporter (Hollenstein et al., 2007a).

1.1.2 Transport mechanism

The similarities of ABC transporters suggest a common transport mechanism for both ABC importers and exporters. An ‘alternating access’ model (Jardetsky, 1966; Locher et al., 2002; Dawson et al., 2007) for transport has been accepted generally. In this model, the substrate-binding site can alternately access either the extracellular or intracellular side of the membrane, corresponding to the outward-facing and inward-facing conformations of the transporter. Binding and hydrolysis of ATP drive the switch between both conformations. In the case of ABC importers, the outward-facing conformation is expected to have a higher affinity for substrate than the inward-facing conformation, whereas the situation is the opposite in the ABC exporter (Rees et al., 2009). Comparing the crystal structures of ModABC (nucleotide-free state, ‘open’ conformation) and Sav1866 (ATP-bound state, ‘close’ conformation), the distance between the two coupling helices decreases drastically (10-15 Å) upon ATP binding (Dawson et al., 2007; Hollenstein et al., 2007a) (Figure 1-3). As the coupling helices approach, the TMDs flip from the inward-facing conformation to the outward-facing conformation. ABC importers can accept substrate from the cognate binding proteins. In contrast, ABC exporters might release substrates acquired previously. After ATP hydrolysis, the NBDs switch back to the ‘open’ conformation and then ADP as well as inorganic phosphate dissociates. Subsequently, the distance between coupling helices increase and the TMDs flip back to inward-facing conformation. As a consequence, importers might release the previously bound substrates, whereas exporters can recruit new substrates.

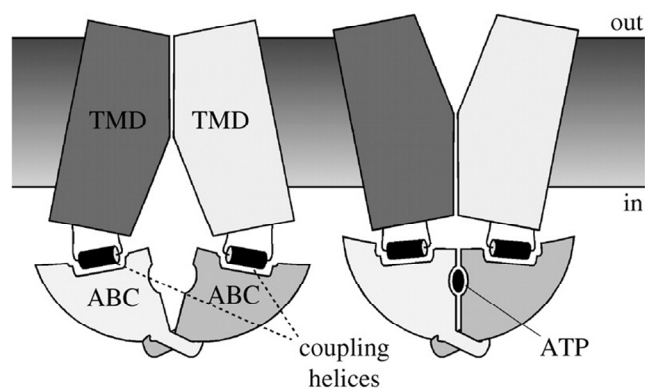


Figure 1-3. Conserved coupling mechanism of ABC transporters. The molecular motion induced by binding of ATP triggers the closing of a gap between the motor domains (NBDs). This moves the coupling helices, an architecturally conserved feature, closer together and flips the TMDs to an outward-facing conformation. Hydrolysis of ATP and NBD dissociation revert the TMDs to adopt an inward-facing conformation (Locher, 2009).

1.2 Transporter associated with antigen processing-like (TAP-like or TAPL)

The transporter associated with antigen processing like (TAPL, also called ABCB9) is a half transporter of the ABCB subfamily. Due to the significant homology with one of the best characterized ABC transporters, the transporter associated with antigen processing (TAP1 and TAP2 subunits), TAPL belongs to the TAP family together with TAP1 and TAP2. TAPL forms a homodimer which is localized in lysosomal compartment (Zhang et al., 2000; Demirel et al., 2007). It functions as an ATP-dependent peptide transporter with a broad peptide specificity (Wolters et al., 2005).

1.2.1 Phylogenetic relationship and gene organization

Phylogenetic analysis of TAPL with ABC transporters showed that it appeared to be closely related to TAP1 and TAP2, which shares 38% and 40% amino acid sequence identity with TAP1 and TAP2, respectively, while the identity between TAP1 and TAP2 is 39% (Zhang et al., 2000). Comparing the deduced primary structures of rat TAPL with the human and mouse counterparts, the mammalian TAPLs (rat, mouse, and human) are highly conserved, since about 99% of the amino acid residues are identical between rat and mouse, and 95% of the residues are identical between rodents and man in pairwise comparison. In contrast, only 75% of the residues from TAP1 or TAP2 are identical between rodents and human in spite of 90% identity between rat and mouse (Kobayashi et al., 2000). Therefore, the evolutionary rate of TAPL is much slower than those of TAP1 and TAP2 as deduced from sequence alignment analysis (Figure 1-4). Moreover, a sequence closely related to mammalian TAPL but not to TAP was found in the genome of the jawless vertebrate sea lamprey (*Petromyzon marinus*) (Uinuk-ool et al., 2003). TAPL seems to be the phylogenetic progenitor of TAP with a different physiological role, as lamprey does not possess an adaptive immune system. In addition, *Caenorhabditis elegans* has three TAPL orthologs with a sequence identity between 35-38%. They were identified as half ABC transporters (Sheps et al., 2004). *haf-2* is expressed in muscle cells, whereas the closest orthologs *haf-4* and *haf-9* are found in intestinal cells (Zhao et al., 2004). Haf-4 and Haf-9 were reported to be involved in intestinal granule formation (Bauer, 2006; Kawai et al., 2009).

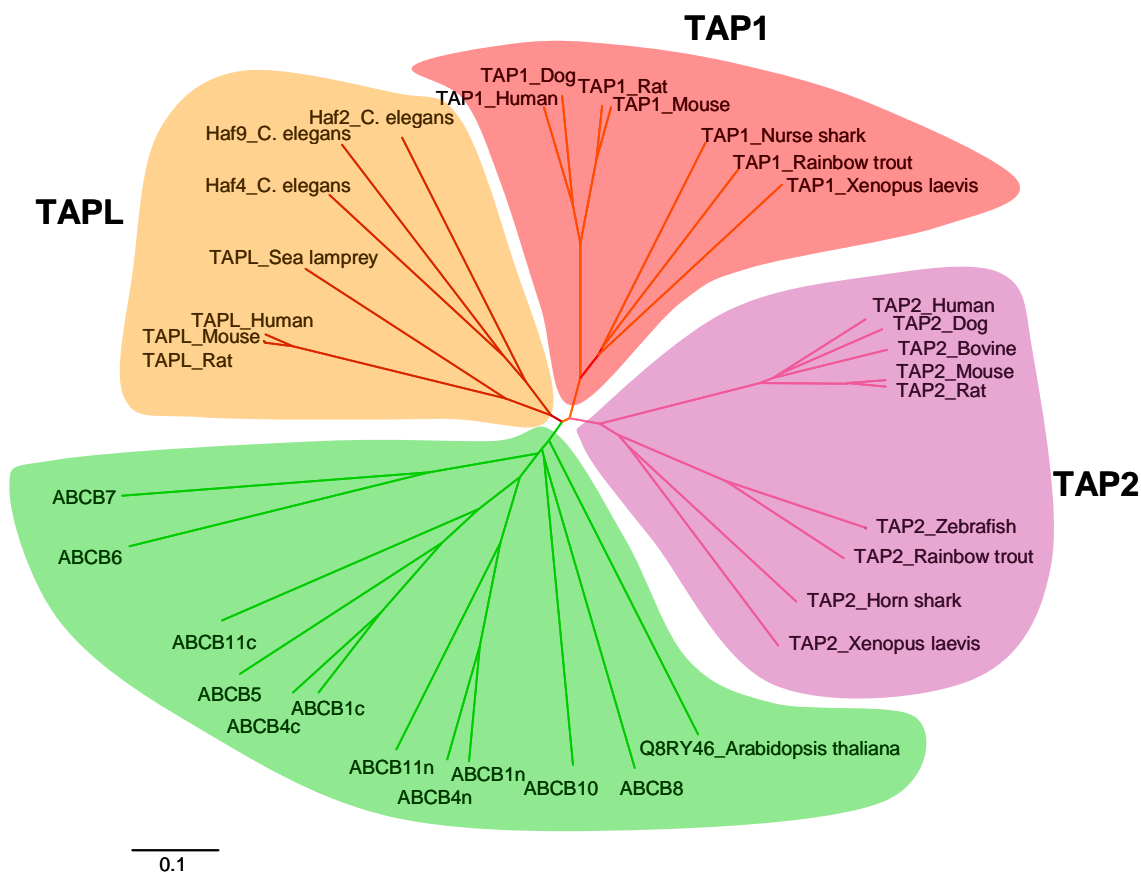


Figure 1-4. Phylogenetic relationship of TAPL to other ABC transporters. Predicted amino acid sequences from members of the human ABCB subfamily and its orthologs from other organisms were aligned using ClustalX. A neighbour-joining tree was generated with Phylo dendron (<http://www.iubio.bio.indiana.edu/treeapp/treeprint-form.html>). Full transporters were subdivided into an N- (*n*) and C-terminal (*c*) half for analysis. The horizontal bar indicates the genetic distance. Transporters without any given species name are human ABC transporters. The species of the ABC transporters used for generation of the phylogenetic tree are: human, *Homo sapiens*; dog, *Canis familiaris*; mouse, *Mus musculus*; rat, *Rattus norvegicus*; bovine, *Bos taurus*; rainbow trout, *Oncorhynchus mykiss*; zebrafish, *Brachydanio rerio*; nurse shark, *Ginglymostoma cirratum*; horn shark, *Heterodontus francisci*; sea lamprey, *Petromyzon marinus*; the nematode, *Caenorhabditis elegans*; *Xaenopus laevis*; and thale cress, *Arabidopsis thaliana*.

The TAPL gene is localized on chromosome 12 (12q24), which does not contain genes related to the adaptive immunity (Kobayashi et al., 2000). As shown in Figure 1-5, the TAPL gene consists of 12 exons, and translation starts at position 87 of exon 2 (Kobayashi et al., 2003; Uinuk-ool et al., 2003). The gene organization of TAPL is closely related to the TAP2 gene, since both genes have a first non-coding exon, and similar splicing pattern of exon 12 (Kobayashi et al., 2003; Penformis et al., 2003). In contrast, the TAP1 gene has only 11 exons and the translation starts at exon 1. Moreover, no other splicing isoform is reported for the TAP1 gene. Exon 1 in the TAP1 gene is corresponding to exon 2 in the TAPL and TAP2 genes, and is longer than the other exons. Exons 3 to 11 of the TAPL and TAP2 genes, exons 2 to 10

in the case for the TAP1 gene, have the same length. Nevertheless, the intron length in the TAPL gene is much longer than in the TAP1 and TAP2 genes. Four splicing isoforms of TAPL have been identified. Three of them named 12A, 12B and 12C, respectively, are generated by alternative splicing of exon 12 (Kobayashi et al., 2003). The full length TAPL cDNA (12A), containing an open reading frame of 2298 bp and coding for 766 amino acids, was cloned from human T-lymphoblast CEM cell line (Zhang et al., 2000). The splicing isoform 12B (683 amino acids) was cloned from HEK-293 cells, while isoform 12C (681 amino acids) was cloned from both HEK-293 and HeLa cells (Kobayashi et al., 2003; Uinuk-ool et al., 2003). Isoforms 12B and 12C lack 86 and 85 C-terminal amino acids, respectively, including the highly conserved H-loop. The fourth splicing isoform of TAPL has an internal deletion of 129 bp, which codes for 43 amino acids (residue 418 to 460), encompassing the last hydrophobic region (predicted TM9 and TM10) and contains exon 7 (Zhang et al., 2000). This splice variant of TAPL was speculated to have different substrate specificity than full length TAPL, since this region corresponds partially to the putative peptide-binding region. Interestingly, at least 4 different C-terminal splicing isoforms were found for rat TAPL, with a length of 693, 708, 762 and 766 amino acids, respectively (Yamaguchi et al., 2004).

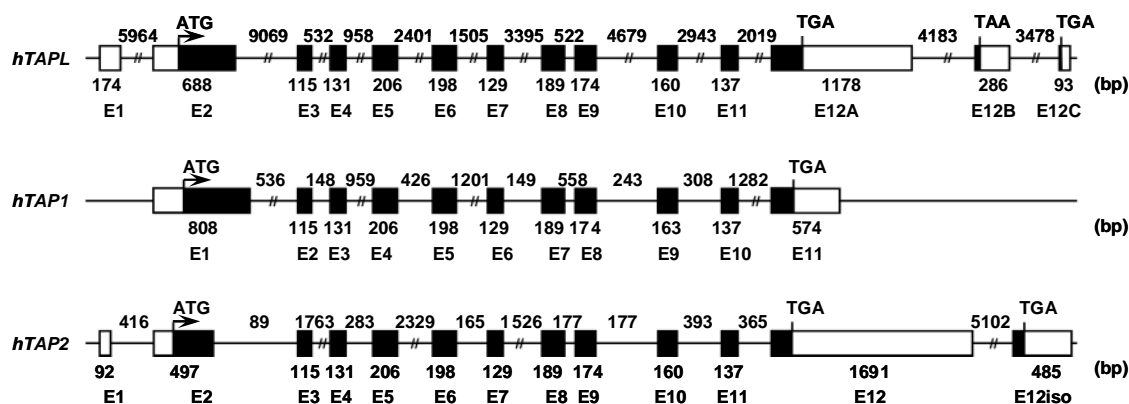


Figure 1-5. Comparison of the exon-intron organization of human TAPL, TAP1 and TAP2 genes. *Boxes* indicate exons, in which *filled boxes* represent coding sequences and *open boxes* untranslated sequences. Introns are shown by *horizontal lines*. Exons are drawn in proportion to real length. The exon and intron size (bp) is given by the *numbers* below and above the exons and introns, respectively. The position of the translation initiation codon is indicated with *ATG* and those of termination codons by *TGA* and *TAA*

1.2.2 Topology model and homodimerization

TAPL is a half transporter composed of the N-terminal hydrophobic domain and C-terminal hydrophilic NBD. On the basis of hydrophobicity analysis and sequence alignment with TAP subunits, we propose a topology model of TAPL with 10 transmembrane helices (Figure 1-6).

The sequence comparison with TAP subunits shows that the transmembrane domain can be subdivided into two regions. The core transmembrane domain comprising the six C-terminal transmembrane helices (TMD1) shows a high sequence identity to TAP1 as well as TAP2, and appears to form the binding pocket and pathway for the cargo, whereas the extra N-terminal domain composed of four putative transmembrane helices (TMD0) are distinct. In homology to TAP (Koch et al., 2004), the N-terminal domain could be involved in recruiting accessory factors, while the core unit of six helices may assemble a functional transport complex similar to TAP1 and TAP2. The N- and C-termini of TAPL as well as the putative peptide-binding site are located in the cytosol. Based on the sequence identities with the predicted peptide-binding region of TAP1 and TAP2 (Nijenhuis and Hammerling, 1996; Ritz et al., 2001), the putative peptide-binding region of TAPL is localized at the cytosolic loop between transmembrane helix 4 and 5 of the TMD1 (peptide-binding region 1 (PBR1)) and a stretch of 15 residues at the C-terminal of the last transmembrane helix connecting the TMD with the NBD (PBR2). The NBDs contain highly conserved sequences, which are involved in ATP binding (Walker A and B) and hydrolysis (C-loop, H-loop and D-loop), thus driving active transport across the membrane.

The eukaryotic ABC transporters are encoded either as full transporters consisting of a polypeptide with two TMDs and two NBDs, or as half transporters comprising only one TMD and one NBD. The latter must form either homo- or heterodimers to act as transporter (Jones and George, 2004). The members of the TAP family are half transporters. Therefore, the formation of dimers is essential for a functional transporter. TAP1, together with TAP2, forms an active transport complex (Powis et al., 1991; Spies and DeMars, 1991). TAP1 or TAP2 alone are not active in peptide binding and transport (Meyer et al., 1994). Since TAPL shows the same sequence identity to TAP as the TAP subunits do to one another, the dimerization of TAPL was studied. In dihydrofolate reductase protein-fragment complementation assays in SKOV3 cells (human ovarian carcinoma cell line) (Leveson-Gower et al., 2004), pull down assays with different tagged TAPL (Wolters et al., 2005), and cross-linking assays (Ohara et al., 2008), the homodimerization of TAPL was demonstrated. TAPL showed no functional interaction with TAP subunits and no ER localization (Zhang et al., 2000; Demirel et al., 2007). The information for the assembly of the transporter monomer was reported recently to reside in the core domain (Arg¹⁴¹-Ala⁷⁶⁶) (Kamakura et al., 2008). Similar to TAP, the core domain transporter (core-TAPL) is fully functional in respect of ATP-dependent peptide transport (Ö. Demirel, I. Bangert, R. Tampé and R. Abele, unpublished data).

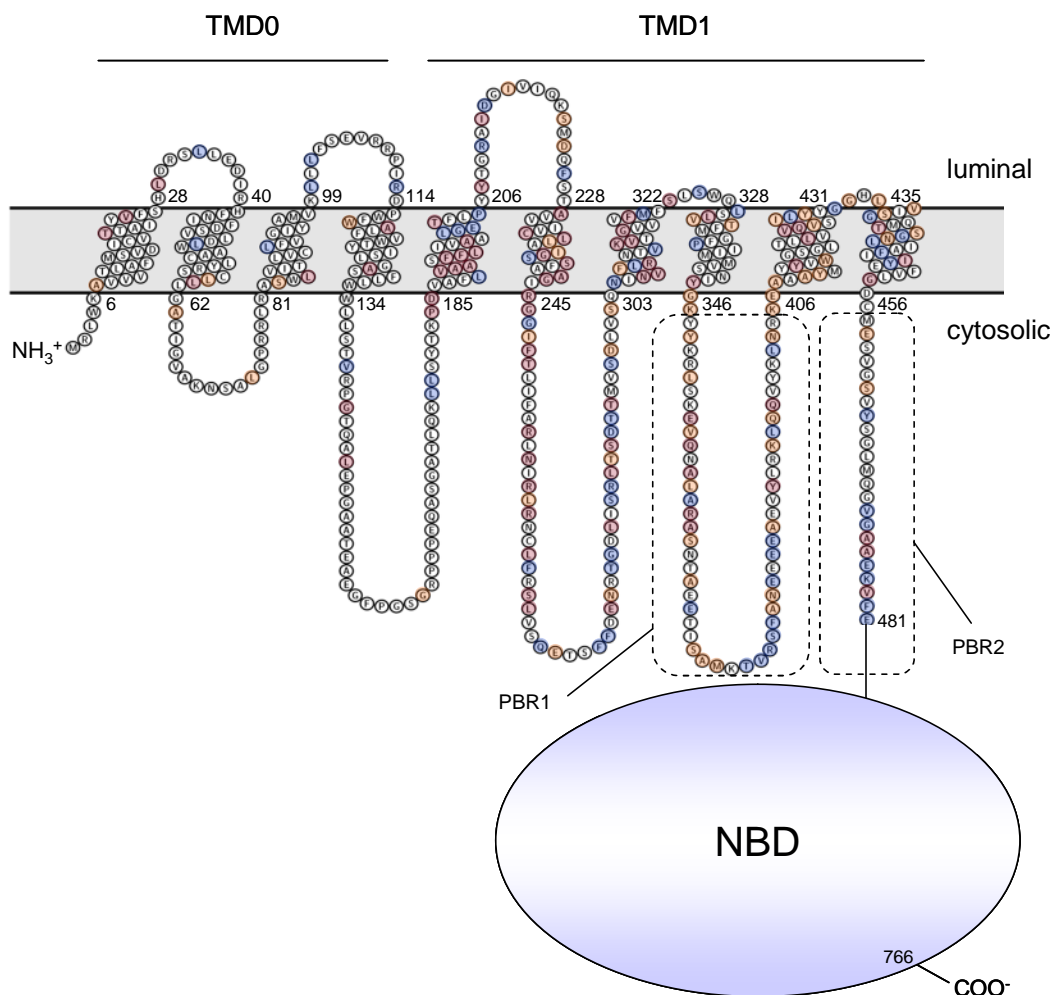


Figure 1-6. Topology model of TAPL. TAPL forms a half transporter composed of an N-terminal TMD (consists of TMD0 and TMD1) and a C-terminal, hydrophilic NBD localized in the cytosol. Based on hydrophobicity analysis and sequence alignments of TAPL with human TAP1 and TAP2, 10 transmembrane helices are predicted. The *numbers* resemble the N- and C-terminal residues of the membrane helices. To show the sequence identity between the transmembrane region of human TAPL and human TAP, residues—identical in the sequence alignment between TAPL and TAP1, TAP2 or both TAP subunits—are coloured in orange, red or blue, respectively. The putative peptide-binding regions (PBR1 and PBR2) are highlighted in *dashed boxes*. The topology model was created with the program Textopo (Beitz, 2000).

1.2.3 TAPL functions as a peptide transporter

The function of TAPL as a specific and ATP-dependent lysosomal peptide transporter was demonstrated by heterologous expression in *Sf9* insect cells and retroviral transduced Burkitt's lymphoma (Raji) cells (Wolters et al., 2005; Demirel et al., 2007). The transport activity of TAPL strictly requires ATP hydrolysis, since non-hydrolyzable ATP analogues, such as AMP-PNP and ATP γ S, do not energize peptide translocation. Similar to other ABC transporters, the transport could be inhibited by orthovanadate which can trap ABC transporters in a post-hydrolysis state. The half maximal inhibition concentration (IC₅₀) was

determined to be $11.5 \pm 1.0 \mu\text{M}$, similar to other ABC transporters (Ambudkar et al., 1992; Landmesser et al., 2002). The optimal temperature and pH value for TAPL transport activity are $37 \text{ }^\circ\text{C}$ and pH 7.0. Peptide transport follows a Michaelis-Menten kinetic with a $K_{M(\text{pep})}$ in the micromolar range ($6.8 \pm 2.8 \mu\text{M}$ for the peptide RRYQNSTC^fL, where f resembles the covalently bound labeled fluorescein). The turnover number of TAPL was calculated to 30 peptides/min, which is comparable to the transport activity of other ABC transporters (Eytan et al., 1996; Ambudkar et al., 1997; Patzlaff et al., 2003). Moreover, TAPL is an active transporter accumulating peptides more than 60 fold in the vesicle lumen.

In contrast to TAP, which is a high-affinity transporter (van Endert et al., 1994; Uebel et al., 1997; Neumann and Tampé, 1999), no peptide-binding activity was detected for TAPL by rapid filter assays, suggesting a low-affinity transporter (Wolters et al., 2005). Accordingly, TAPL seems to bind peptides in a different manner as TAP, although TAPL and TAP share a sequence identity of more than 49% with respect to the putative peptide-binding regions.

The recognition principle of TAPL and TAP is similar, since both transporters recognize peptides via their backbone, including the free N- and C-termini, and by side chain interactions (Uebel et al., 1997; Wolters et al., 2005). However, the peptide specificity of TAPL is very broad, ranging from 6-mer up to at least 59-mer peptides with a slight preference for 23-mers. TAPL appears to be highly promiscuous in peptide recognition since 10-fold longer peptides could be transported with the same efficiency as 6-mer peptides. In contrast, TAP most efficiently transports peptides from 8 to 12 amino acids in length optimized for peptide loading of MHC class I molecules (Koopmann et al., 1996). TAPL seems to work as a vacuum cleaner transporting a large variety of peptides with low affinity but high efficiency.

1.2.4 Nucleotide-dependent peptide transport

The peptide transport is energized by ATP hydrolysis. The transport follows Michaelis-Menten kinetics with a $K_{M(\text{ATP})}$ of $17.6 \pm 2.4 \mu\text{M}$ for ATP (Wolters et al., 2005), which is 4–20 fold lower than for TAP, P-glycoprotein, CFTR, and maltose permease from *E. coli* (Sarkadi et al., 1992; Li et al., 1996; Landmesser et al., 2002; Chen et al., 2003b). Based on the physiological ATP concentration, this $K_{M(\text{ATP})}$ value ensures that TAPL is always fully active. In order to determine the binding constant of ATP for TAPL, 8-azido[α -³²P]-ATP photocross-linking assays were performed, in which 8-azido[α -³²P]-ATP is a competitive substrate for ATP. An apparent dissociation constant of Mg•ATP of $90 \pm 12 \mu\text{M}$ for TAPL was derived. This value is in the same range as that of other ABC transporters (Horn et al., 2003; Qu et al., 2003). A

lower $K_{M(ATP)}$ value than the K_D for TAP indicates that the ATP-binding step is followed by intermediates before final hydrolysis occurs (Fersht, 1997). For such a multi-domain machinery, a multi-step process is conceivable, where peptide and ATP binding, ATP hydrolysis, and peptide transport occur in an ordered manner. As known from biochemical studies on isolated NBDs, ATP binding induces a conformational change of the NBD enabling the dimerization of the catalytic domain, which is the prerequisite for ATP hydrolysis and substrate transport (Moody et al., 2002b; Janas et al., 2003a; van der Does and Tampé, 2004; Zaitseva et al., 2005a).

In competition assays with 8-azido[α - 32 P]-ATP, and by transport studies, the nucleotide specificity of TAPL was disclosed and ranked into three categories (Wolters et al., 2005): ATP as the substrate with the highest affinity for TAPL; GTP, AMP-PNP, ADP, and UTP with an intermediate affinity; and CTP as well as AMP with a very low affinity. The similar nucleotide specificity was also observed in an ATP-agarose binding assay of solubilized rat TAPL (Ohara et al., 2008). The rTAPL binds to ATP-agarose, ADP-agarose, but not to AMP-agarose. The binding can be competed by free ATP, ADP, GTP or dATP, but not by AMP. Pyrimidine nucleotides such as UTP and CTP are less effective competitors. The binding of ATP requires Mg^{2+} , and was observed at neutral pH value. Furthermore, this nucleotide-binding preference is also reflected in the transport activity, where GTP shows 40%, UTP 20%, and CTP 10% of the ATP-driven transport activity (Wolters et al., 2005). Therefore, TAPL can be energized by different nucleotide triphosphates with a slight preselection for purine based nucleotides. This broad specificity is also found with other ABC transporters (Al-Shawi and Senior, 1993; Meyer et al., 1994; Muller et al., 1994) and results from a π - π interaction between the base of the nucleotide with the NBD (Hung et al., 1998).

1.2.5 Tissue distribution and cellular localization

Based on its mRNA level, TAPL is highly expressed in testis and moderately expressed in brain, spinal cord, and thyroid (Zhang et al., 2000). However, it was also found in other tissues such as intestine, kidney, lung and stomach (Yamaguchi et al., 1999; Mutch et al., 2004). Notably, the high expression of TAPL in Sertoli cells of mouse and rat testis was confirmed by immunostaining (Zhang et al., 2000), and these cells possess numerous lysosomes for phagocytosis. Moreover, TAPL expression is strongly upregulated during the maturation of monocytes to dendritic cells (Demirel et al., 2007). Dendritic cells are the most potent antigen processing cells, expressing MHC class II beside MHC class I on their cell surface.

In silico analysis did not detect a signal sequence for ER insertion and subcellular targeting. In double immunofluorescence staining of stable transfected SKOV3 using an anti-TAPL antibody and a panel of organelle markers, anti-TAPL-specific staining showed a pattern overlapping with the lysosomal markers LAMP-1 and LAMP-2 (LAMP, lysosome-associated membrane protein), and partially overlapping with the staining pattern of a marker for endosomes (Zhang et al., 2000). The lysosomal localization of TAPL was further confirmed by subcellular fractionation. More recently, the subcellular distribution of TAPL was addressed by quantitative immunofluorescence confocal laser scanning microscopy in HeLa cells, which transiently expressed TAPL C-terminal tagged with a Myc-epitope or eGFP. Both TAPL variants colocalized with LAMP-2 but not with calnexin as an ER marker or EEA1 as an early endosome marker (Demirel et al., 2007). Furthermore, indirect evidence for the localization of TAPL in a post-ER compartment results from peptide transport studies on crude membrane preparations derived from TAPL expressed in *Sf9* cells. Only a minor fraction of the transported peptide was found N-glycosylated and therefore transferred into the ER-lumen (Wolters et al., 2005).

The sorting signal for lysosomes is likely present within the amino-terminal transmembrane domain (Met¹–Arg¹⁴¹) of TAPL molecule. As visualized by means of fluorescent microscopy, both N-terminal domain and full-length transporter fused with GFP were targeted to lysosomal membranes in stable-transfected CHO-K1 cells, while the core domain was broadly distributed in intra-cellular membranes (Kamakura et al., 2008)

1.2.6 Physiological function

The adaptive immune system uses two sets of cells to protect hosts from various pathogens: B-cells and T-cells. T cells recognize antigenic peptides presented on the surface of host cells via two types of MHC molecules: MHC class I and II molecules. In general, MHC class I molecules present peptides of endogenous proteins to CD8⁺ cytotoxic T-cells and MHC class II molecules present peptides of exogenous proteins to CD4⁺ helper T-cells (Abele and Tampé, 2004). However, in professional antigen-presentation cells like macrophages, dendritic cells and B-cells, antigen cross-presenting also exists (Malnati et al., 1992; Cresswell et al., 2005). In these specialized cells, MHC class I molecules can present peptides from exogenous antigens in TAP-dependent and TAP-independent pathways (Cresswell et al., 2005; Shen and Rock, 2006). In the latter pathway, peptides were loaded onto MHC class I molecules in endolysosomes (Bachmann et al., 1995; Norbury et al., 2001; Lizée et al., 2003). Additionally,

MHC class II molecules have the ability to present endogenous peptides in a TAP-independent pathway (Rudensky et al., 1991; Chicz et al., 1993; Lich et al., 2000; Dani et al., 2004).

The physiological function of TAPL is still an open issue. However, it has been confirmed that TAPL shows no multidrug resistance, its gene regulation is different from TAP subunits, and it is not involved in MHC class I antigen presentation pathway (Kobayashi et al., 2000; Zhang et al., 2000; Demirel et al., 2007). Remarkably, TAPL expression is strongly upregulated during the maturation of monocytes to dendritic cells or macrophages (Demirel et al., 2007). Moreover, TAPL transports peptides into lysosomal compartments by hydrolyzing ATP (Demirel et al., 2007). Therefore, it was speculated that TAPL functions as a peptide transporter in the cross-presentation of endogenous antigens in the MHC class II pathway or delivers peptides of exogenous antigens into endolysosomes for MHC class I molecule loading (Demirel et al., 2007).

Nevertheless, a more general function should be considered, since TAPL is also found in MHC class II deficient Sertoli cells (Zhang et al., 2000) and still in lampreys which have no complicated immune system. Additionally, both TAPL orthologs Haf-4 and Haf-9 from *Caenorhabditis elegans* were reported to be localized in non-acidic intestinal but LAMP homologue (LMP-1)-positive granules and involved in the granule formation (Bauer, 2006; Kawai et al., 2009). In addition to granule defects, other phenotypes such as reduced brood size, slow growth and prolonged fecundation cycles were also observed in *haf-4* and *haf-9* deletion animals. The functions of Haf-4 and Haf-9 were proposed to be required for normal growth and spermatogenesis at the larval stage; in adult stage, their expressions may lead to the proper oogenesis (Kawai et al., 2009)

1.3 Objective

It is of utmost importance to decipher the substrate specificity of the lysosomal transporter TAPL, since it is connected to its physiological function. Previous work has demonstrated that TAPL has a broad length specificity for peptides, and peptides are recognized by the free termini and backbone (Wolters et al., 2005). However, detailed biochemical analysis of TAPL, especially, the detailed characterization of substrate specificity, is impossible to perform on crude membranes due to high background and side reactions. Therefore, a solubilization, purification and reconstitution procedure has to be developed for this ABC transporter individually since there is no common protocol for all membrane proteins. After optimization on many parameters in the solubilization, purification and reconstitution, the peptide specificity of TAPL on single residue level will be deciphered with combinatorial peptide libraries. First, the key peptide residues involved in TAPL recognition will be determined and, in a detailed screening, the amino acid preferences at these positions will be analyzed. Moreover, with the optimized purification and reconstitution procedure, it is planned to investigate whether the ATP hydrolysis of TAPL is coupled to substrate translocation. If so, the stoichiometry between substrate transport and ATP hydrolysis can be determined. This important mechanical question is always under debate in the field of ABC transporters (Davidson and Nikaido, 1990; Chen et al., 2001; Borths et al., 2005; Poolman, 2005).

To study the structure, dynamics and mechanism of TAPL, single cysteine mutations will be introduced into strategic positions for site-directed labeling. The prerequisite for introducing single cysteines to TAPL is the creation of the functional cysteine-less mutant. The functions of these mutants have to be characterized in a current project. The functional single cysteine mutants will be a good starting point for studying conformational changes by electron paramagnetic resonance, fluorescence energy transfer and/or chemical cross-linking.

TAPL orthologs Haf-4 and Haf-9 in *C. elegans* have about 40% sequence identity with TAPL. They are localized in lysosomal-related intestinal granules and are involved in these granules formation. In order to understand the function of Haf-4 and Haf-9 in more detail, both proteins will be expressed in *Sf9* insect cells as well as characterized for their interactions and peptide transport activities since their human ortholog TAPL was shown to be a lysosomal peptide transporter.

2 Materials

2.1 Chemicals

Table 2-1. Chemicals list

Chemical	Company
Acrylamide (fourth-crystallized)	Carl Roth
Acrylamide-bisacrylamide (37:1), Rotiphorese 30	Carl Roth
Adenosine-5'-triphosphate (ATP) disodium salt hydrate	Fluka
6-Aminohexanoic acid	Fluka
Ampicillin	Carl Roth
AmpLigase	Epicentre
Anti-His antibody	Qiagen
Anti-Myc antibody	Millipore
Anti-mouse IgG	Sigma
Anti-rabbit IgG	Sigma
Apyrase	Sigma
ATP-agarose	Sigma
Bac-to-Bac baculovirus expression system	Invitrogen
BD BaculoGold transfection buffers	BD Biosciences
Benzonase nuclease	Merck
Bio-Beads SM-2	Bio-Rad
Blue-Gal	Fermentas
Bradford assay kit	Pierce
Calf intestine alkine phosphatase (CIAP)	Fermentas
Chloramine T trihydrate	Sigma
Coomassie blue G-250	Serva
Coomassie blue R-250	Carl Roth
<i>n</i> -Decyl- β -D-maltoside (DM)	Glycon
Digitonin	Calbiochem/Carl Roth
Dimethylformamide (DMF)	Carl Roth

Chemical	Company
Dimethyl sulfoxide (DMSO)	Calbiochem
1,4-Dithiothreitol (DTT)	Fermentas
6×DNA loading dye	Fermentas
<i>n</i> -Dodecyl-β-D-maltoside (DDM)	Glycon
DOWEX 1×8 (200–400 mesh) analytical grade	Serva
Ethidium bromide solution (1 %)	Carl Roth
Ethylenediaminetetraacetic acid (EDTA)	Carl Roth
Fetal calf serum (FCS)	Biochrom
Foscholine-14 (<i>n</i> -Tetradecylphosphocholine)	Anatrace
Gel filtration molecular weight markers	Sigma
Gentamicin	Carl Roth
HIS-Select nickel affinity gel	Sigma
HiTrap chelating HP column	GE Healthcare
Imidazole	Merck
5-Iodoacetamidofluorescein (5-IAF)	Molecular Probes
Isopropyl-β-D-thiogalactopyranoside (IPTG)	Fermentas
Kanamycin	Carl Roth
Lipids	Avanti Polar Lipids
β-Mercaptoethanol	Carl Roth
Micro BCA protein assay reagent kit	Pierce
MultiScreen plates with glass fibre filter (PVDF membrane, pore size 0.65 μm)	Millipore
Na ¹²⁵ I	Hartmann Analytic
0.1% Neutral red solution	Sigma
Ni-NTA agarose	Qiagen
β-Nicotinamide adenine dinucleotide hydrate (NAD)	Sigma
Nitrocellulose membrane	Whatman
<i>n</i> -Octyl-β-D-glucopyranoside (OG)	Glycon
Penicillin/streptomycin (100×concentrated)	PAA
<i>Pfu</i> DNA polymerase	Fermentas

Chemical	Company
Phenylmethylsulphonyl fluoride (PMSF)	Carl Roth
Plasmid DNA purification kit (NucleoSpin Plasmid)	MACHEREY-NAGEL
Pluronic F-68	Invitrogen
Proteinase inhibitors (AEBSF, aprotinin, leupeptin, benzamidin, pepstatin A)	Calbiochem
PVDF membrane	Carl Roth
QIAquick gel extraction kit	Qiagen
QIAquick spin PCR purification kit	Qiagen
Restriction enzymes	Fermentas
SF-900 II serum free medium	Invitrogen
Solution master detergent kit (10% solution ampules)	Anatrace
SP Sepharose FF	GE Healthcare
Strep-Tactin HRP	IBA
Strep-Tactin matrices	IBA
Superdex 200 PC 3.2/30 column	GE Healthcare
Superose 6 PC 3.2/30 column	GE Healthcare
T4 DNA ligase	Fermentas
<i>Taq</i> polymerase	Fermentas
Tetracycline	Carl Roth
<i>N,N,N',N'</i> -Tetramethylethylenediamin (TEMED)	Carl Roth
Triton X-100	Supelco Analytical
Trypan blue solution (0.4%)	Sigma
Other chemicals	Carl Roth

2.2 Primers

Table 2-2. Primers designed for mutagenesis of hTAPL*

Primer	Sequence
Walker A	
hTAPL_K545A	CGGGCAGTGGGG <u>GCG</u> AGCTCCTGTGTC
H-loop	
hTAPL_H699A	CTCATCATCGCG <u>GCCCGG</u> CTGAGCAC
Cys-less	
hTAPL_C19A	GAGTGTGGACATCG <u>CC</u> GTGACCACGGCC
hTAPL_C54A	CTGGGCAGCC <u>GCC</u> CTGTACCGCAGC
hTAPL_C59A	CTGTACCGCAGCG <u>CC</u> CTGCTGCTGGG
hTAPL_C90A	GTCATCACCTCGTGG <u>CC</u> CTTTCGTGGGC
hTAPL_C233A	CGTCATCGTGG <u>CC</u> CTGCTGGCCATTGGC
hTAPL_C264A	CGCCTTCGAAAC <u>GCC</u> CTTCCGCTCACTGGTG
hTAPL_C458A	GTCCTGGGAGAT <u>GCC</u> ATGGAGTCCGTGGGC
hTAPL_C548V	GGGAAGAGCTCC <u>G</u> TGGTCAACATCCTGG
Single cysteine mutants	
hTAPL_S105C	GCTGCTCTTCT <u>GCG</u> AGGTGCGCAG
hTAPL_S170C	GAGCAGGCGT <u>GCGGG</u> CCAC
hTAPL_M222C	CATCCAGAAAAGCT <u>GCG</u> GATCAGTTCAGC
hTAPL_A264C	CCTTCGAAACT <u>GCC</u> CTTCCGC
hTAPL_Y409C	GCAGCTGCCT <u>G</u> CATGTACTACG
hTAPL_V465C	CGTGGGCTCCT <u>GCT</u> TACAGTGGCC
hTAPL_L701C	CGCGCACCGGT <u>G</u> CAGCACCGTGG

* The mutation sites are underlined.

Table 2-3. Primers designed for Haf-4 or Haf-9 cloning*

Primer	Sequence
haf-4_SacI_KpnI_for	CGATTAG <u>GAGCTCGGTACCATGAATTCGACGGTGGCTT</u> CC
haf-4_rev	AATTTATTCCGGCCGATGCG
haf-9_SacI_for	CGATTAG <u>GAGCTCATGAGTTCTTCTCTTTACACGGGTG</u> G
haf-9_His10_NotI_rev	ATAG <u>CGGCCGCTCAGTGATGGTGATGGTGATGGTGAT</u> GGTGGTGGCTCAAATAGCTGCTTGCAAATGAGG

* The restriction sites are underlined.

Table 2-4 Sequencing primers

Primer	Sequence
hTAPL_for2	ACCTTCACCTACCGCACTCG
hTAPL_for3	GGCCATTGGCAGCTCATTTG
hTAPL_revC	GAGCGGAAGAGACAGTTTCG
haf-4_for_1	GTATCTTCGTTCCCTATTAC
haf-4_for_2	CACTTGATGTCACCAGAACC
haf-4_for_3	GTTCGCTCGTTCTGTGATGG
haf-4-rev	CCTTGCGTAGGCGTACTCGAAGG
haf-9_for1	GCTCTCATTGGCTTCAACTG
haf-9_for2	TCACGTGGCGTTCAGTTATC
haf-9_revA	TTGTAGCGTGTGCATAGGTG
ME-774FW	CTTCTGCTCTAAAAGCTGCG

Table 2-5 M13 Primers

Primer	Sequence
M13 Forward (-40)	GTTTTCCCAGTCACGAC
M13 Reverse	CAGGAAACAGCTATGAC

2.3 Peptides

Table 2-6 Peptides list

Peptide	Sequence
C4F	RRYC ^f KSTEL; f: cysteine is labeled with fluorescein
R9LQK	RRYQKSTEL
X9 library	(X) ₉ , X represents any L-amino acid residue except L-cysteine
X6 library	(X) ₆ , X represents any L-amino acid residue except L-cysteine
D-library (9 mer)	(x) ₉ , x represents any D-amino acid residue except D-cysteine
OX8 sublibraries	O(X) ₈ , O reflects a defined amino acid residue at the N-terminal
X8O sublibraries	(X) ₈ O, O reflects a defined amino acid residue at the C-terminal

3 Methods

3.1 Molecular cloning

3.1.1 Plasmid DNA preparation

Single colonies of *Escherichia coli* (*E. coli*) strain DH5 α transformed with the pFastBacTM 1 plasmid were inoculated into 5 ml LB (Luria Bertani) medium (1% tryptone or peptone, 0.5% yeast extract, 1% NaCl) supplemented with 100 μ g/ml ampicillin using sterilized toothpicks and cultivated on a shaker at 200 rpm overnight at 37 °C. Plasmid DNA was prepared with the NucleoSpin[®] Plasmid kit (MACHEREY-NAGEL) according to the manufacturer's instructions. The plasmid DNA concentration was determined by measuring OD₂₆₀ on the NanoDrop[®] spectrophotometer (NanoDrop Technologies, Inc.)

3.1.2 Ligase chain reaction for site-directed *in vitro* mutagenesis

Single or multiple defined point mutations of TAPL were achieved by ligase chain reaction (LCR) using pFastBacTM1_tapl_his (containing the gene of TAPL wt with a C-terminal His₁₀-tag) as the template (Wolters et al., 2005). The primers were phosphorylated by T4 Polynucleotide Kinase (T4 PNK) before LCR reaction. The LCR product was purified via QIAquick PCR Purification Kit (Qiagen) and the parental plasmid DNA was digested by DpnI. The digestion products were transformed into DH5 α competent cells. Plasmid DNA was prepared from single colonies and sequenced by corresponding sequencing primers.

Primer phosphorylation

2 μ l primer (100 pmol/ μ l)

2 μ l 10 \times Kinase Buffer A

2 μ l ATP (10 mM)

1 μ l T4 Polynucleotide Kinase (10 U/ μ l)

13 μ l water

30 min incubation at 37 °C

10 min incubation at 70 °C

LCR reaction

1 μ l plasmid DNA (*ca.* 1 μ g)
10 μ l 10 \times *Pfu* Buffer with MgSO₄ (25 mM)
2 μ l phosphorylated mutagenic primer (10 pmol/ μ l)
10 μ l dNTP (2 mM)
1 μ l NAD (100 mM)
1 μ l *Pfu* DNA Polymerase (2.5 U/ μ l)
1 μ l AmpLigase (5 U/ μ l)
74 μ l water

LCR program

95 °C 3 min
95 °C 1 min
x °C 1 min } 30 cycles
65 °C 16 min
65 °C 16 min
4 °C pause

x represents the annealing temperature for defined primers

DpnI digestion

2 μ l 10 \times Buffer Tango
19 μ l purified LCR product
2 μ l DpnI (10 U/ μ l)
minimal 6 h or overnight incubation at 37 °C
20 min incubation at 80 °C

3.1.3 Plasmid DNA restriction analysis

Plasmid DNA restriction analysis was performed for 1 h at 37 °C. The reaction was stopped by addition of 6 \times DNA loading dye (10 mM Tris/HCl, pH 7.6, 0.03% bromophenol blue, 0.03% xylene cyanol FF, 60% (w/v) glycerol, 60 mM EDTA). The digested fragments were separated by 0.8% agarose gel electrophoresis in 1 \times TAE (Tris-Acetate-EDTA) buffer (40 mM Tris/acetate, pH 8.0, 1 mM EDTA). The electrophoresis was performed for around 1 h at 150 V.

The gel was stained with ethidium bromide solution (40 μ l of 1% ethidium bromide solution resolved in 400 ml deionized H₂O) for 10 min and subsequently visualized under UV light.

3.1.4 Subcloning the gene of interest by restriction digestion and ligation

For subcloning the genes of interest into different vectors, 6 μ g of plasmid DNA, containing gene inserts or target vectors, were digested with corresponding restriction enzymes for 3 h at 37 °C. The amount of enzymes in a total reaction volume of 100 μ l and the buffer system were chosen according to the instruction provided by the manufacturer (Fermantas Life Sciences). To prevent the vector from self ligation, 1 μ l (1 U/ μ l) of CIAP (calf intestine alkaline phosphatase) was added to dephosphorylate the vector after double digestion. The reactions were stopped by inactivating the enzymes for 20 min at 80 °C.

The restriction products were separated by electrophoresis using 0.8% agarose gel in 1 \times TAE buffer and purified via a gel purification kit (QIAquick Gel Extraction Kit, Qiagen). DNA concentration in the 50 μ l eluate was determined by OD₂₆₀. The purified insert and vector were mixed in different molar ratio (from 3:1 to 6:1) and ligated with T4 DNA ligase overnight at 16 °C. Subsequently, the ligation products were transformed into DH5 α competent cells (see 3.2.3) for further characterizations.

3.1.5 Subcloning the cDNAs of Haf-4 and Haf-9 by PCR

The cDNAs of human TAPL orthologs Haf-4 and Haf-9 from *Caenorhabditis elegans* were subcloned into the baculovirus expression system by PCR. The cDNA of Haf-4 with a C-terminal Myc-tag was subcloned from the construct pJG98_haf-4_myc (Bauer, 2006) into pFastBacTM1 using the forward primer haf-4_SacI_KpnI_for and reverse primer haf-4_rev. The PCR product and vector pFastBacTM1 were restricted by SacI and NotI followed by ligation as described above. The cDNA clone (yk1417f02) of Haf-9 (ORF name=ZK484.2a) was kindly provided by Prof. Dr. Yuji Kohara (National Institute of Genetics, Mishima/Japan). The Haf-9 cDNA was subcloned from the pME18-FL3 vector into pFastBacTM1 by PCR using the forward primer haf-9_SacI_for and reverse primer haf-9_His10_NotI_rev (introducing a C-terminal His₁₀-tag). The PCR products were purified via a gel purification kit and digested with SacI and NotI. The vector pFastBacTM1 was digested in the same way and ligated with PCR fragments as described above.

PCR reaction

1 μ l plasmid DNA (*ca.* 20 ng)
5 μ l 10 \times *Pfu* Buffer with MgSO₄
0.25 μ l primers (100 pmol/ μ l)
5 μ l dNTP (2 mM)
0.5 μ l *Pfu* DNA Polymerase (2.5 U/ μ l)
2.5 μ l DMSO
35 μ l water

PCR program

95 °C 4 min
95 °C 1 min
x °C 1 min } 35 cycles
72 °C 6 min
72 °C 10 min
4 °C pause

x represents the annealing temperature for defined pair of primers

3.1.6 Isolation of the recombinant Bacmid DNA

Transformation of DH10BacTM cells and isolation of recombinant Bacmid DNA were performed according to the manual for the Bac-to-Bac[®] Baculovirus Expression System (Invitrogen). This procedure was originally developed to isolate large plasmids (>100 kb) and has been adapted to allow isolation of Bacmid DNA. PCR analysis (using M13 primers) was used to verify the presence of the gene of interest in the recombinant Bacmid. DNA concentration was determined by OD₂₆₀.

3.2 Microbiological techniques

3.2.1 Bacterial culture

E. coli strain DH5 α and DH10Bac were routinely cultivated in either LB medium (1% tryptone or peptone, 0.5% yeast extract, 1% NaCl, pH 7.0) or on a LB agar plate (LB medium supplied with 1.5% agar). If not otherwise indicated, antibiotics were added to a certain concentration after autoclaving.

<u>Antibiotic stock solution (mg/ml)</u>	<u>Working concentration</u>
Ampicillin 100 mg/ml in water	100 µg/ml
Kanamycin 50 mg/ml in water	50 µg/ml
Tetracycline 10 mg/ml in water	10 µg/ml
Gentamicin 7 mg/ml in water	7 µg/ml

filter-sterilized, stored at -20 °C and protected from light

3.2.2 Preparation of competent cells

DH5 α cells were inoculated into 10 ml LB medium without any antibiotics and cultivated at 200 rpm overnight at 37 °C. Subsequently, the culture was scaled up into a shaker flask containing 200 ml LB medium with no antibiotics, and shaken at 200 rpm at 37 °C until OD₆₀₀ reaches 0.3–0.4. The culture was cooled down for 10 min on ice, and then centrifuged at 2000 \times g for 10 min at 4 °C. The cell pellet was resuspended in 40 ml ice cold TBF-I buffer (30 mM KAc, 100 mM RbCl, 50 mM MnCl₂, 10 mM CaCl₂, 15% (w/v) glycerol, adjusted to pH 5.8 with 1 M acetic acid, sterile filtered), incubated for 1 h on ice and centrifuged at 4000 \times g for 10 min at 4 °C. Finally, the cell pellet was resuspended in 8 ml ice cold TFB-II buffer (10 mM MOPS, 10 mM RbCl, 75 mM CaCl₂, 15% (w/v) glycerol, adjusted to pH 6.8 with 1 M KOH, sterile filtered), 100 µl aliquots were snap-frozen in liquid nitrogen and stored at -80 °C. To prepare DH10Bac competent cells, the same procedure was applied except that the cells were grown in LB medium supplied with 50 µg/ml kanamycin and 10 µg/ml tetracycline.

3.2.3 Transformation of plasmid DNA into chemical competent bacterial cells

For the transformation of DH5 α cells, 1 ng of the plasmid DNA was incubated with 100 µl of DH5 α competent cell suspension for 30 min on ice, if not otherwise mentioned. The mixture was heat shocked for 90 sec at 42 °C and then cooled down on ice for 1–2 min. 500 µl of LB medium without any antibiotic was added to the mixture and the cells were shaken on a thermomixer (Eppendorf) at 300 rpm for 45 min at 37 °C. After centrifugation at 19000 \times g for 1 min at room temperature, the cell pellets were resuspended in 100 µl LB medium without antibiotics and plated onto LB agar plates containing corresponding antibiotics. The plates were incubated overnight at 37 °C.

For the transformation of DH10Bac cells, 1 ng of the plasmid pFastBacTM1 containing the gene of interest was added to the cells (100 µl suspension) and mixed gently. After incubating

for 30 min on ice, the cells were heat shocked for 45 sec at 42 °C and immediately cooled down for 2 min on ice. 900 µl of S.O.C. medium (2% tryptone, 0.5% yeast extract, 0.05% NaCl, 2.5 mM KCl, 20 mM glucose, pH 7.0) was added to the cells and they were shaken on the thermomixer at 300 rpm for 4 h at 37 °C. An aliquot of 100 µl of suspension was plated on a LB agar plate supplied with 50 µg/ml kanamycin, 7 µg/ml gentamicin, 10 µg/ml tetracycline, 100 µg/ml Bluo-gal, and 40 µg/ml IPTG. The plates were incubated for 48 h at 37 °C. White colonies were picked and restreaked onto fresh LB agar plates containing the above additives and cultivated overnight at 37 °C. Single colonies confirmed to be white were inoculated into 2 ml LB liquid cultures supplied with 50 µg/ml kanamycin, 7 µg/ml gentamicin, 10 µg/ml tetracycline. The recombinant Bacmid DNA was prepared as described in 3.1.6.

3.3 Cell biology techniques

3.3.1 Thawing and freezing of *Sf9* insect cells

Before starting transfection and expression experiments, *Spodoptera frugiperda* (*Sf9*) insect cells had to be cultured. Normally, the cell culture started from an aliquot of cryo stock in liquid N₂. The cryo tube containing 1 ml *Sf9* cells (density $\geq 1.0 \times 10^7$ /ml) was thawed in a water bath at 27 °C. As soon as the cells were thawed, they were diluted with 4 ml ice cold modified Sf-900 II SFM medium (containing 5% fetal calf serum, 50 u/ml penicillin, 50 µg/ml streptomycin, 0.5 µg/ml Fungizone and 0.1% (v/v) Pluronic F-68) and incubated in a T₂₅ Roux flask for 20 min at 27 °C. Subsequently, the medium was changed to 5 ml prewarmed medium (27 °C) and the cells were cultivated for several days at 27 °C until they grew confluent. The medium was changed every second day. For long term storage, aliquots of cryo stocks can be prepared from either adherent culture (50–60% confluency) or suspension culture (cell density of $1.3\text{--}1.5 \times 10^6$ /ml). Cell viability should be higher than 99%. The cells were harvested by centrifugation at 1000×g for 5 min at room temperature and resuspended in a freezing mixture (Sf-900 II SFM medium containing 10% fetal calf serum, 10 u/ml penicillin, 10 µg/ml streptomycin and 10% DMSO) to a cell density of 1.0×10^7 /ml. Aliquots of 1 ml cell resuspension were frozen for 1 h at -20 °C, then for 24 h at -80 °C and finally stored in liquid N₂. The cell viability after such a treatment can be checked by thawing an aliquot of the cryo stocks.

3.3.2 *Sf9* insect cells culture

Sf9 cells were routinely maintained in adherent culture. When cells grew 80–90% confluent, the medium was discarded by aspiration. Then fresh, prewarmed medium was added to the flask (5 ml for T₂₅ flask and 15 ml for T₇₅ flask), and cells were resuspended by pipetting. Subsequently, the cells were inoculated into a new flask (2×10^4 for T₂₅ flask and 5×10^4 for T₇₅ flask) and cultured at 27 °C until 80–90% confluent.

In order to have large amounts of cells, the cell culture had to be adapted to suspension culture and scaled up in shaker flasks. The cells in a T₇₅ flask were cultured until 2-3 layers and dislodged by gentle patting on the bottom of the flask. Subsequently, the cells were diluted to 0.4×10^6 /ml (100 ml volume) and shaken in a 250-ml shaker flask at 110 rpm at 27 °C. When the cell density reached 2.0×10^6 /ml, the cells were subcultured in a 1.8 L-Fernbach flasks (Schott Duran) with up to 700 ml medium and shaken at 60 rpm at 27 °C.

3.3.3 Transfecting *Sf9* cells with recombinant Bacmid DNA

The transfection of *Sf9* insect cells was carried out using the calcium phosphate mediated transfection kit (BD BaculoGold™ Transfection kit containing buffer A and B) from BD Biosciences. 1.5×10^6 *Sf9* cells were seeded per well (of a 6-well tissue culture plate) and allowed to attach for at least 15 min at 27°C. In the mean time, 500 µl of buffer B with 10 µg Bacmid DNA were incubated for 10 min at room temperature. When the cells were attached, the medium was removed by aspiration and 500 µl of buffer A was added to the plate. Subsequently, the Bacmid DNA in buffer B was added drop by drop into buffer A. The suspension was mixed by gentle shaking and the plates were incubated for 4 h at 27 °C with gentle mixing every hour. After removing the suspension, the cells were washed once with medium and then incubated in 3 ml fresh medium for 6–7 days at 27 °C until harvesting the supernatant (corresponding to P₀ virus stock) by centrifugation at 500×g for 5 min at room temperature.

3.3.4 Amplification of the recombinant baculovirus

To obtain a high virus titer and an optimal expression, the virus stock had to be amplified several times. 0.8 ml of the P₀ stock was used to infect 4×10^6 cells seeded into a T₂₅ flask containing 5 ml medium. After 6–7 days, the virus was harvested by centrifugation and named P₁ virus stock. The P₂ virus stock was amplified by infecting 12×10^6 cells (in 12 ml medium) in a T₇₅ flask with 0.8 ml P₁ virus stock. Finally, 13 ml of the P₂ virus stock was used to

amplify 500 ml of the P₃ virus stock in a Fernbach flask with a cell density of 1.5×10^6 /ml. After 7 days, the P₃ virus stock was harvested (the cell death ratio should be around 95%) by centrifugation at $4000 \times g$ for 25 min at room temperature. All virus stocks were stored at 4 °C and protected from light.

3.3.5 Virus titer determination

In order to determine the virus titer or pick up single virus colonies which showed high expression levels, a plaque assay was performed. Before infection, 1.2×10^6 of *Sf9* cells were seeded in a well of 6-well plates. During attachment of the cells (15 min, 27 °C), 10-fold serial dilutions (10^{-3} to 10^{-8}) of the virus were prepared in Sf-900 II SFM medium without supplements. The medium was removed by aspiration and each well was inoculated with 1 ml of the virus dilutions (10^{-6} to 10^{-8}). The plates were incubated for 1 h at 27 °C. After removing the virus inoculums, 3 ml of 2% low melting agarose solution (1 g agarose in 50 ml medium, prewarmed at 40 °C) was added to the wells. After incubating the plates for 5 days at 27 °C, 0.5 ml of 0.1% neutral red solution (Sigma) was used to stain the agarose plates for 1 h at 27 °C. The supernatant was removed and the plates were incubated for another 24 h at 27 °C before counting the plaques. If necessary, single colonies were picked from the agarose plates with a Pasteur pipette to infect *Sf9* cells (0.1×10^6 cells in 1 medium) seeded into 24-well plates for virus amplifications. The following formula was used to calculate the titer (plaque forming units (pfu)/ml) of the viral stocks. Note that the optimal range to count is 3 to 20 plaques per well of a 6-well plate.

$$\text{titer (pfu/ml)} = \text{number of plaques} \times \text{dilution factor} \times \frac{1}{\text{ml of inoculum/well}}$$

3.3.6 Recombinant membrane protein expression

Once a recombinant pFastBac baculoviral stock with a suitable titre (around 1×10^8 pfu/ml) had been generated, *Sf9* insect cells were infected for expression of recombinant membrane proteins. *Sf9* cells were cultivated in shaker flasks in modified Sf-900 II SFM medium to a density of 2×10^6 /ml. Then the baculoviral stock was added to reach a MOI (multiplicity of infection, defined as the number of virus particles per cell) of 2. The expression was carried out for 48 h at 27 °C. The protein expression was detected by immunoblotting using specific antibodies. To prepare the immunodetection samples, 0.5 ml cell culture was harvested 48 h after infection by centrifugation at $1000 \times g$ for 5 min at 4 °C. The cell pellet was washed once

with phosphate-buffered saline (PBS) (137 mM NaCl, 2.7 mM KCl, 8.1 mM Na₂HPO₄, 1.8 mM KH₂PO₄, pH 7.4) and solubilized with 45 µl of 5×SDS sample buffer (313 mM Tris/HCl, pH 8.0, 10% SDS, 50% glycerol, 0.5% bromophenol blue) supplemented with 1 µl Benzonase[®] Nuclease (25 U/µl, Merck) and 100 mM DTT. The sample was incubated for 30 min at 37 °C before SDS-PAGE (10%) and immunoblotting. Alternatively, the cell pellets after virus harvesting could also be treated in the same way and analyzed for expression.

3.4 General biochemical methods

3.4.1 Protein concentration determination

The total protein concentration in the membranes or concentrations of synthetic peptides were determined by BCA assay using the Micro BCA[™] Protein Assay Kit (Pierce). The assay utilizes bicinchoninic acid (BCA) as the detection reagent for Cu¹⁺, which is formed when Cu²⁺ is reduced by the protein in an alkaline environment. A purple-colored reaction product is formed by the chelation of two molecules of BCA with one cuprous ion (Cu¹⁺). This water-soluble complex exhibits a strong absorbance at 562 nm that is linear with increasing protein concentrations. The macromolecular structure of the protein, the number of peptide bonds and the presence of four amino acids (cysteine, cystine, tryptophan and tyrosine) are reported to be responsible for the color formation with BCA (Wiechelman et al., 1988). A microplate procedure (linear working range of 2–40 µg/ml) was used in all membrane preparations. All of the samples and standard protein albumin were serially diluted in PBS. 150 µl of the sample or standard was mixed with 150 µl of freshly prepared working reagent in a 96-well microplate. The plate was incubated for 40 min at 37 °C before measuring the absorbance at 584 nm on a plate reader. The working reagent was prepared by mixing the following kit contents (25:24:1, reagent MA: MB: MC). The Micro BCA[™] Protein Assay Kit contents are the following: Micro BCA[™] Reagent A (MA) with sodium carbonate, sodium bicarbonate and sodium tartrate in 0.2 N NaOH; Micro BCA[™] Reagent B (MB) with 4% bicinchoninic acid in water; Micro BCA[™] Reagent C (MC) with 4% cupric sulfate and pentahydrate in water.

The concentration of the purified protein was determined via the modified Bradford method using Coomassie Plus—The Better Bradford[™] Assay Reagent (Pierce), which is compatible with glycerol and high concentrations of imidazole. When Coomassie dye binds the protein in an acidic surrounding, an immediate shift in absorbance maximum occurs from 465 nm to 595 nm. A standard microplate protocol (linear working range of 100–1500 µg/ml) was used

by mixing 10 μ l of the purified protein with 300 μ l assay reagent (Coomassie G-250 dye, methanol, phosphoric acid and solubilizing agents in water). After incubation of the plate for 10 min at room temperature, the absorbance at 584 nm was recorded on a plate reader.

3.4.2 SDS-PAGE

SDS-PAGE gels (8 \times 9 cm² size) were prepared with a home made gel casting system (8–9 gels at the same time). The separating gels and stacking gels were prepared with the components listed in Table 3-1. Normally, 10% SDS-PAGE gels were used.

Table 3-1. Components for the preparation of 10% SDS-PAGE gels (The amounts are for 8–9 gels)

Compound	Separating gel (10 %)	Stacking gel (4.5 %)
H ₂ O	31.25 ml	18.0 ml
Separating buffer ¹	18.75 ml	–
Stacking buffer ²	–	7.5 ml
Rotiphorese 30	25.0 ml	4.5 ml
10 % APS ³	300 μ l	180 μ l
TEMED	70 μ l	60 μ l

¹ Separating buffer: 1.5 M Tris/HCl, pH 8.8, 0.4 % SDS.

² Stacking buffer: 0.5 M Tris/HCl, pH 6.8, 0.4 % SDS.

³ 10% (w/v) ammonium persulfate solution (APS) must be made freshly or stored frozen.

The samples for the SDS-PAGE were prepared by mixing crude membranes or purified proteins with 5 \times SDS sample buffer (313 mM Tris/HCl, pH 8.0, 50% glycerol, 10% SDS and 0.5% bromophenol blue) and 100 mM DTT. The samples were incubated for 30 min at 37 °C. The gels were run for approximately 60 min at 175 V in 1 \times Tris-glycine electrophoresis buffer (25 mM Tris/HCl, pH 8.3, 192 mM glycine, 0.1% SDS). Prestained protein molecular weight marker (Fermentas) was used as a standard. The gels were either stained in Coomassie blue R-250 staining solution (40% methanol, 10% acetic acid, 0.25% Coomassie blue R-250) or electroblotted for immunodetection.

3.4.3 Immunoblotting

The proteins on SDS-PAGE were transferred onto a nitrocellulose (NC) membrane by electroblotting. Before blotting, the NC membrane and two layers of Whatman filter paper were soaked shortly in electroblotting buffer (192 mM glycine, 25 mM Tris, 20% (v/v) methanol). A sandwich of paper-membrane-gel-paper was placed on to a semi-dry blot apparatus (Bio-Rad) and blotted for 90 min under constant current (100 mA per gel). The NC

membrane was incubated for at least 1 h in blocking buffer and afterwards washed 3 times (5 min each) with TBS-T buffer (10 mM Tris/HCl, pH 8.0, 150 mM NaCl, 0.1% Triton X-100). Membranes were normally blocked in milk-containing blocking buffer (5% (w/v) skim milk powder, 0.1% NaN₃ in TBS-T buffer) except for Strep-Tactin HRP blotting, of which the membrane was blocked with α -strep blocking buffer (3% BSA in TBS-T buffer). The different antibodies used for various proteins are listed in Table 3-2. Subsequently, the NC membrane was incubated for 1 h with the primary antibody and washed 3 times (5 min each) with TBS-T buffer. Afterwards, it was incubated for another hour with the secondary antibody and washed again 3 times with TBS-T buffer. For development, the NC membrane was first incubated in ECL (Enhanced chemiluminescence) solution 1 (100 mM Tris/HCl, pH 8.5, 2.5 mM luminol sodium salt, 0.4 mM coumaric acid) for 1 min after which ECL solution 2 (100 mM Tris/HCl, pH 8.5, 0.02% H₂O₂) was added to the mixture. The chemiluminiscent signals on the membrane were documented after 1 min using a Lumi-ImagerTM F1 (Roche). The immunoblotting signal intensity could be quantified by LumiAnalysisTM image analysis software.

Table 3-2. The conditions for immunoblotting with antibodies for different proteins

Detected protein	Used detection					
	Primary antibody	Epitope	Dilution	Secondary antibody ¹	Dilution	Company/reference
TAPL	Purified α -TAPL ² (final bleeding)	17 a.a. at the C-terminus	1:500 in 2% milk/TBS-T	α -rabbit	1:10,000 in TBS-T	BioScience (Wolters et al., 2005)
His-tagged	α -His	His ₁₀ -tag	1:2,000 in TBS-T	α -mouse	1:10,000 in TBS-T	Qiagen
Strep-tagged	Strep-Tactin HRP	Strep-tag	1:10,000 in 1.5% BSA/TBS-T	–	–	IBA
Myc-tagged	α -Myc	Myc-tag	1:2,000 in TBS-T	α -mouse	1:10,000 in TBS-T	Millipore

¹ All secondary antibodies were purchased from Sigma.

² Purified using the epitope coupled to NHS (*N*-hydroxyl succinimide) activated agarose.

If the NC membrane had to be redeveloped with the second primary and secondary antibodies, membrane stripping was applied to remove the original primary and secondary antibodies. The membrane was incubated in stripping buffer (62.5 mM Tris/HCl, pH 6.8, 2% SDS and 100 mM β -mercaptoethanol) for 30 min at 50 °C. The stripped membrane was washed twice with TBS-T buffer, blocked in blocking buffer followed by development with the new primary and secondary antibodies as described in the normal protocol.

3.5 Biochemical assays for TAPL

3.5.1 Peptide labeling with 5-iodoacetamidofluorescein

All peptides were synthesized by solid phase technique applying conventional Fmoc-chemistry. Peptides containing cysteine residues at various positions were coupled to fluorescein by incubating 2.5 mg of peptides with a 1.2 molar excess of 5-iodoacetamidofluorescein (5-IAF, Molecular Probes) in PBS (pH 6.5), 20% (v/v) dimethylformamide (DMF) for 2 h at room temperature in the dark. Labeled peptides were purified by reversed-phase C18 analytical column (column size 4.6 mm×250 mm, particle size 5 μm , pore size 300 \AA , Vydac) on a Jasco HPLC system. The elution was monitored with the absorbance detector (280/450 nm). A gradient of water/acetonitrile (0.1% trifluoroacetic acid (TFA)) was used to separate labeled peptide from free dyes as well as unlabeled peptides. The fractions from the HPLC were pooled, snap-frozen in liquid N_2 and lyophilized. Finally, the labeled peptides were resolved in water and stored at $-20\text{ }^\circ\text{C}$. The identity and purity of labeled peptides were verified by MALDI-TOF (Matrix-assisted laser desorption/ionisation-time of flight) mass spectrometry. The peptide concentration was determined by OD_{492} in 100 mM Tricine buffer, pH 9.0 (molar extinction coefficient (ϵ): $75000\text{ cm}^{-1}\text{ M}^{-1}$).

3.5.2 Peptide labeling with Na^{125}I

Peptides were iodinated using the chloramine T-method (Hunter and Greenwood, 1962). Before start, 15 μl of 8.8 μM peptides were diluted with 35 μl PBS (pH 7.4). The reaction was initiated by addition of 10 μl 1% (w/v) chloramine T/PBS and 10 μl (100 μCi) Na^{125}I . After a 5-min incubation at room temperature, the reaction was stopped by addition of 120 μl sodium disulfite ($\text{Na}_2\text{S}_2\text{O}_5$) solution (0.17 mg/ml in PBS). To remove free iodine, 220 μl Dowex 1X8 resin (stored in 100 mg/ml in PBS/0.2% dialyzed BSA/0.1% NaN_3 ; washed 3 times with PBS before use) were added to the radiolabeled reaction mixture, vortexed and incubated for 5 min at room temperature. The suspension was applied to an empty spin column (Bio-Rad) and centrifuged at $750\times g$ for 30 sec at room temperature. The flow-through containing radiolabeled peptides was collected and complemented with 500 μM unlabeled peptides to the final concentration of 10 μM . The specific activity of the peptides was measured on a γ -counter (Beckman Coulter). Normally 2 μl of the iodinated peptides has about 400,000 CPM (counts per minute). For the labeling of peptide libraries, a peptide concentration of 40 μM instead of 8.8 μM was used in the reaction. Correspondingly, 200 μCi of Na^{125}I were added to achieve high labeling efficiency.

3.5.3 Membrane preparation

Membranes containing the target protein were prepared from *Sf9* insect cells infected with recombinant baculovirus. After 48 h of infection, 10 μ l aliquot of cell culture was incubated with 10 μ l of 0.4% trypan blue solution (Sigma) for several minutes at room temperature. The numbers of total cells and dead cells were counted on a cell counting chamber (Roth), and the cell density as well as the viability was calculated. From a standard 500 ml expression, the cells were harvested by centrifugation at 1000 \times g for 10 min at 4 °C. Afterwards, the pellet was washed with ice cold PBS and centrifuged again at 1000 \times g for 5 min at 4 °C. The pellet was frozen at -20 °C before preparing membranes. For membrane preparation, the cell pellet was thawed on ice in the presence of 50 ml of ice cold 10 mM Tris/HCl (pH 7.4) supplemented with 1% PI-Mix (5 mg/ml AEBSF hydrochloride, 0.1 mg/ml aprotinin, 1 mg/ml leupeptin, 0.5 mg/ml pepstatin A and 15.6 mg/ml benzamidine). As an alternative, a mixture of 1 mM phenylmethylsulfonyl fluoride (PMSF) and 2.5 mM benzamidine was used instead of 1% PI-Mix. The cells were disrupted by dounce homogenization (30 times) with a dounce tissue grinder (Wheaton). To remove the cell debris and nuclei, samples were centrifuged at 200 \times g for 4 min followed by another centrifugation at 700 \times g for 8 min at 4 °C. Subsequently, the supernatant was pelleted by centrifugation at 20,000 \times g for 30 min at 4 °C. Crude membranes were resuspended in HEPES buffer (20 mM HEPES, 140 mM NaCl, pH 7.5), and aliquots were snap-frozen in liquid nitrogen and stored at -80 °C. The total protein concentration was determined by BCA assay.

3.5.4 Membrane solubilization

To find the optimal detergent for solubilization, crude membranes were pelleted and resuspended in solubilization buffer (20 mM HEPES, 140 mM NaCl, 15% (w/v) glycerol, pH 7.5) supplemented with 1 mM PMSF, 2.5 mM benzamidine to end up with a protein concentration of 5 mg/ml. Detergents were added to reach a ρ value of 2, where ρ is given as follows (Rivnay and Metzger, 1982),

$$\rho = \frac{[\text{detergent}] - \text{CMC}}{[\text{lipid}]}$$

where CMC represents the critical micelle concentration of the detergent. The lipid-to-protein ratio (w/w) was assumed to be 1, and the average molecular mass of phospholipids was taken as 700 Da. After incubation with detergent for 30 min on ice, the solubilized samples were centrifuged at 100,000 \times g for 30 min at 4 °C. To determine the solubilization efficiency, the

supernatant was analyzed by SDS-PAGE (10%) followed by immunoblotting using an epitope-purified anti-TAPL polyclonal antibody (see 3.4.3) and quantified by chemiluminescence using Lumi-ImagerTM F1. The signals were normalized to the solubilization efficiency of crude membranes observed with 1% SDS.

3.5.5 Determination of critical micelle concentration

The critical micelle concentration of digitonin and dodecylmaltoside (DDM) in the purification solutions was determined by a fluorimetric method (De Vendittis et al., 1981). The anionic dye, 8-anilidonaphthalene-1-sulfonic acid (ANS), is almost nonfluorescent in water but becomes highly fluorescent in organic solvents or in the interior of a micelle. In brief, 1.26 ml of ANS solutions (30 μ M ANS in IMAC (Immobilized Metal Affinity Chromatography) binding buffer or elution buffer (20 mM HEPES, 140 mM NaCl, 15% (w/v) glycerol, pH 7.5, with 20 mM or 250 mM imidazole, respectively)) were titrated in 5 μ l steps with detergent solutions (20 mM HEPES, pH 7.5, 0.5% detergent, 30 μ M ANS, 140 mM NaCl, 15% (w/v) glycerol, 20 mM or 250 mM imidazole) in the Fluorolog-3 fluorescence spectrometer (Horiba). The excitation wave length was set to 410 nm, and emission intensity was recorded at a wave length range of 450–520 nm. The excitation and emission slit widths were at 5/5 nm. The integration interval was set to 1 nm and the sample was stirred constantly at 5 °C. The intensity at maximal emission (493 nm) was plotted against the detergent concentrations. The CMC was given by the intercept of two extrapolated lines with low and high slopes.

3.5.6 Purification

Crude membranes containing TAPL (5 mg/ml) prepared from *Sf9* insect cells were solubilized in solubilization buffer supplemented with 20 mM imidazole, 1 mM PMSF, 2.5 mM benzamidine, and 1% digitonin. After 30-min incubation on ice and centrifugation (30 min at 100,000 \times g at 4 °C), the supernatant was applied to a SP SepharoseTM Fast Flow column equilibrated with binding buffer (20 mM HEPES, 140 mM NaCl, 20 mM imidazole, 15% (w/v) glycerol, pH 7.5) supplemented with 0.1% digitonin. The flow-through was loaded onto a Zn²⁺-iminodiacetate (Zn-IDA) column (SepharoseTM) equilibrated with binding buffer supplemented with 0.1% digitonin. After stringent washing with up to 100 mM imidazole, the specifically bound protein was finally eluted with elution buffer (20 mM HEPES, 140 mM NaCl, 250 mM imidazole, 15% (w/v) glycerol, pH 7.5) supplemented with 0.1% digitonin.

The eluate was concentrated in a 100 kDa cut-off AmiconTM concentrator (Millipore). When DDM instead of digitonin was used for purification, a concentration of 0.3–0.5% was used for solubilization, and 0.05% for washing and elution. When Triton X-100 was used for the purification, the detergent concentration for solubilization and purification were 1% and 0.1%, respectively.

3.5.7 Gel filtration

TAPL with a concentration of 1 mg/ml was centrifuged at 100,000× g for 30 min at 4 °C and subjected to gel filtration (size exclusion chromatography (SEC)). A 50 µl aliquot of TAPL was applied to a SuperoseTM 6 PC 3.2/30 column on Ettan LC system (GE Healthcare). The protein was eluted with elution buffer (20 mM HEPES, pH 7.5, 150 mM NaCl, 250 mM imidazole, 15% (w/v) glycerol) supplemented with 0.1% digitonin or 0.05% DDM, at a flow rate of 50 µl/min. The absorbances at 254 nm and 280 nm were recorded. Fractions of 100 µl were collected and analyzed by SDS-PAGE (10%) and immunodetection. For column calibration, soluble protein standards from Sigma were used. To determine the size (hydrodynamic radius) and oligomeric status of TAPL, V_e/V_o of TAPL was compared to V_e/V_o of the protein standards (V_e is the elution volume and V_o is the void volume). The V_o was determined by the elution volume of blue dextran (molecular weight approx. 2,000,000 Da). The logarithms of the molecular mass of standard proteins versus their respective V_e/V_o values were plotted and fitted by a linear regression.

3.5.8 Blue native PAGE

For Blue native PAGE (BN-PAGE), a 4–13% gradient gel was used, which covers protein mass range of 10 kDa to 3 MDa. The amount of each reagent used to cast 9 mini gels (0.1×9×7 cm) are given in Table 3-3. The separation gels were casted in the cold (4 °C) using a gradient mixer. Before casting the separation gels, 1-cm height of water was loaded into the gel-casting device and, subsequently, the acrylamide solution was pumped in through a hole from the bottom. The sample gels were casted after the separation gels were polymerized at room temperature. For storage, the sample combs were removed and gels were covered with 1×gel buffer (25 mM imidazole, 0.5 M 6-aminohexanoic acid, pH 7.0). The gels were stored at 4 °C for up to 4 weeks if the overlaid 1×gel buffer was changed at three days intervals.

Table 3-3. Solutions for preparing 9 BN-PAGE gels (0.1×9×7 cm)

	Sample gel	Gradient separation gel	
	3.5% acrylamide	4% acrylamide	13% acrylamide
Acrylamide-bisacrylamide mixture ¹	2.64 ml	3 ml	7.8 ml
3×gel buffer	12 ml	12 ml	10 ml
Glycerol (86%)	–	–	6.2 ml
Water	20.4 ml	20.8 ml	6 ml
Total volume	36 ml	36 ml	30 ml
10% APS ²	300 µl	200 µl	150 µl
TEMED	30 µl	20 µl	15 µl

¹ Acrylamide-bisacrylamide mixture: 48 g acrylamide and 1.5 g bisacrylamide per 100 ml. Stored at 4 °C.

² 10% (w/v) ammonium persulfate solution (APS) must be made freshly or stored frozen.

The crude membranes used for BN-PAGE were suspended in BN-PAGE solubilization buffer (50 mM imidazole/HCl, pH 7.0, 50 mM NaCl, 1 mM EDTA, 2 mM 6-aminohexanoic acid), snap-frozen in liquid N₂ and stored at -80 °C. For sample preparation, 500 µg membranes were solubilized in BN-PAGE solubilization buffer supplemented with detergent. The detergent was added to a given detergent/protein ratio of 6 g/g for digitonin and 2.5 g/g for DDM, respectively. The membranes were solubilized for 30 min on ice, and the insoluble parts were pelleted by centrifugation at 20,000×g for 15 min at 4 °C. Subsequently, glycerol (86%, w/v) and 5% (w/v) Coomassie blue G-250 (Serva) (suspended in 500 mM 6-aminohexanoic acid, stored at 4 °C) were added to the supernatant to give an end glycerol concentration of 5% (w/v) and detergent/dye ratio of 8 g/g, respectively. If the purified protein was analyzed in BN-PAGE, 5% (w/v) glycerol and 0.01% Ponceau S from a Ponceau S/glycerol stock solution (0.1% Ponceau S, 50% glycerol, (w/v)) was added instead of Coomassie blue dye to avoid dissociation of the detergent-labile subunits. As a molecular mass standard, bovine heart mitochondria (400 µg protein, as a generous gift from Prof. Dr. Hermann Schägger and Dr. Ilka Wittig, Uni-Frankfurt) were solubilized and treated as described in the original protocol (Wittig et al., 2006). 7.5 µg of purified TAPL was loaded onto the BN-PAGE.

The electrophoresis was performed at 4 °C using the buffers listed in Table 3-4. The power supply was set at 100 V until the samples had entered the gel. Then, the electrophoresis was continued with a constant voltage of 300 V (current limited to 10 mA). After the blue running front had moved about one third of the desired total running distance, the cathode buffer B was changed to slightly blue cathode buffer B/10 for better detection of faint protein bands, and to improve native blotting (Wittig et al., 2006). The gel was stained in Coomassie blue R-250

(40% (v/v) methanol, 10% (v/v) acetic acid, 0.25% (w/v) Coomassie blue R-250) and destained with destaining solution (40% (v/v) methanol, 10% (v/v) acetic acid).

Table 3-4. Electrode and gel buffers for BN-PAGE*

	Cathode buffer B	Cathode buffer B/10	Anode buffer	3×gel buffer
Tricine (mM)	50	50	–	–
Imidazole (mM)	7.5	7.5	25	75
Coomassie blue G-250 (%)	0.02	0.002	–	–
6-Aminohexanoic acid (M)	–	–	–	1.5
pH	7.0	7.0	7.0	7.0

*Adapted from the original protocol (Wittig et al., 2006).

Electroblotting was carried out on a semi-dry electronic blotter (Bio-Rad). Before blotting, PVDF (Polyvinylidene difluoride) membrane was first soaked in methanol and BN-PAGE electroblotting buffer (50 mM Tricine, 7.5 mM imidazole, pH 7.0) together with two pieces of 3-mm Whatman chromatographic papers. The transfer was performed for 3 h at room temperature with current limited to 0.5 mA/cm² gel area. The membrane was destained in destaining solution (40% (v/v) methanol, 10% (v/v) acetic acid) to record the protein standards. Afterwards, the membrane was further destained by methanol and sequentially developed for immunoblotting (3.4.3).

3.5.9 Reconstitution

To remove all kinds of contaminations, the *E. coli* total lipid extract (Avanti) was washed by acetone/ether. The crude lipid extract was dissolved in chloroform (2.5 ml per 0.5 g lipid). Resolved lipids were dropped slowly into 100 ml cold (-20 °C) acetone containing 1 mM DTT. The suspension was stirred vigorously for 4 h (or overnight) at 4 °C and protected from light. Importantly, a clamp was added on the stopper, otherwise, the increased pressure upon stirring would blow it away. The insoluble part was precipitated by centrifugation in a glass tube at 2500×g for 15 min at room temperature. The pellet was washed once with 100 ml cold acetone containing 1 mM DTT, and dried thoroughly by a N₂ stream. Lipids were dissolved in 200 ml of diethyl ether with 10 mg of DTT under stirrer mixing for 1 h at room temperature. The suspension was centrifuged again at 2500×g for 15 min at room temperature to remove the insoluble material. The supernatant was carefully transferred to a preweighed round bottom flask, and diethyl ether was evaporated on a rotary evaporator at 40 °C. Finally, the lipid film

was weighed and resolved in chloroform to a concentration of 20 mg/ml. The washed lipid was named as the *E. coli* polar lipid extract and stored at -20 °C under N₂ gas.

For liposome preparation, lipids were dissolved in chloroform at 20 mg/ml and mixed in defined ratios (w/w). Chloroform was removed under reduced pressure on a rotary evaporator. The remaining lipid film was rehydrated in reconstitution buffer (20 mM HEPES, 140 mM NaCl, 5% (w/v) glycerol, pH 7.5) by bath sonification for 5 min at room temperature. To prepare homogenous large unilamellar vesicles, liposomes (10 mg/ml) were frozen in liquid N₂ and thawed at room temperature for five times, followed by extruding 11 times through a 400-nm polycarbonate filter (Avestin) with an Avestin mini-extruder. The liposomes were diluted to 2.5 mg/ml in reconstitution buffer and titrated with Triton X-100 until light scattering at 540 nm reached maximum and started to decrease. The Triton X-100-destabilized liposomes were mixed with the purified protein in a mass ratio of 40:1 (the volume ratio of 9:1), and incubated for 30 min at 4 °C under gentle agitation. For detergent removal, 40 mg/ml (wet weight) polystyrene beads (Bio-Beads SM-2; Bio-Rad) washed with methanol and water and equilibrated with reconstitution buffer were added successively four times (1 h, O/N, 2 times 2 h at 4 °C). A Bio-spin column (Bio-Rad) was used to remove Bio-Beads, and proteoliposomes were pelleted by centrifugation (300,000×g, 45 min, 4 °C). Finally, proteoliposomes (5 mg/ml lipids) were resuspended in reconstitution buffer.

3.5.10 Freeze fracture electron microscopy

Proteoliposome preparations were placed between two small copper disks and rapidly frozen in liquid ethane. Replicas were prepared in a freeze fracture unit (BAF 400T; Balzers) and shadowed with platinum/carbon at an angle of 45°. Replicas reinforced by pure carbon were cleaned from organic material in chromosulfuric acid and analyzed by a Philips EM208S electron microscope. The experiment was performed by Dr. Winfried Haase (MPI of Biophysics, Frankfurt)

3.5.11 ATPase activity assay

For measuring ATP hydrolysis, 1.25 µg of the digitonin-purified or reconstituted TAPL were incubated in 25 µl elution (supplemented with 0.1% digitonin) or reconstitution buffer supplemented with 2 mM ATP, 5 mM MgCl₂, and inhibitors for other types of ATPases (1 mM ouabain, 5 mM NaN₃ and 50 µM EGTA) for 1 h at 37 °C. The reaction was started by adding MgCl₂ and terminated with 175 µl of 20 mM sulfuric acid (H₂SO₄). The concentration of

inorganic phosphate (Pi) was determined by a colorimetric method (Baykov et al., 1988). 15 min after the addition of 50 μ l of freshly prepared malachite green solution (0.096% (w/v) malachite green, 1.48% (w/v) ammonium molybdate, and 0.173% (w/v) Tween-20 in 2.9 M H_2SO_4), the absorbance was measured at 620 nm in 96-well plates. All measurements were performed under conditions giving a linear rate of product formation (Pi). Calibration of free phosphate concentration was carried out with Na_2HPO_4 (5–80 μ M) in 200 μ l of 20 mM H_2SO_4 .

3.5.12 Peptide transport assay

The peptide transport was performed either with fluorescein-labeled (Neumann and Tampé, 1999) or ^{125}I -labeled peptides. For peptide transport, proteoliposomes (1.25 μ g TAPL, 50 μ g phospholipids) were preincubated with 5 mM $MgCl_2$ and 1 μ M ^{125}I -labeled or 3 μ M fluorescein-labeled peptides in PBS on ice. The transport was initiated by adding 3 mM ATP. After incubation for 10 min at 37 °C, the transport was stopped by the addition of 200 μ l of ice-cold stop buffer (10 mM EDTA/PBS). Subsequently, the samples were transferred to a microfilter plate (MultiScreen plates, Durapore PVDF membrane, 0.65- μ m pore size; Millipore) preincubated with 0.3% polyethyleneimine. Filters were washed twice with 250 μ l of ice-cold stop buffer. The amount of radiolabeled peptide was quantified by a γ -counter (Beckman Coulter). If the fluorescent peptides were used, the washed filters were incubated with 250 μ l of 1% SDS/PBS for 5 min at room temperature. Fluorescent peptides were quantified by a fluorescence plate reader ($\lambda_{ex/em}$ =485/520 nm; Polarstar Galaxy, BMG Labtech). Background transport activity was measured in the absence of ATP.

When crude membranes were used for transport assay, the membranes (25 μ g total protein) containing TAPL were incubated with 5 mM $MgCl_2$ and radiolabeled or fluorescence labeled peptide in 50 μ l PBS for 3 min at 37 °C, in the presence or absence of 3 mM ATP. The rest of experimental steps were as described above.

3.5.13 Peptide transport assay (glycosylation assay)

To investigate peptide transport into the endoplasmic reticulum (ER), a glycosylation based assay was used. Crude membranes (100 μ g of total protein) were incubated with 5 mM $MgCl_2$ and 3 μ M of fluorescence labeled peptide (RRYQNSTC^fL, where f indicates iodoacetamidofluorescein coupled via a cysteine residue) in 50 μ l PBS for 3 min at 37 °C, in the presence or absence of 3 mM ATP. The reaction was stopped by adding 1 ml of ice-cold

stop buffer. After centrifugation at 20,000×g for 8 min at 4 °C, the membrane pellets were solubilized in 850 µl of lysis buffer (50 mM Tris/HCl, pH 7.5, 150 mM NaCl, 5 mM KCl, 1 mM CaCl₂, 1 mM MnCl₂ and 1% NP-40) for 15 min at room temperature. The insoluble material was removed by centrifugation, and the supernatant was incubated with 50 µl Concanavalin A (ConA)-Sepharose (50% (w/v), Sigma-Aldrich; washed twice with 500 µl lysis buffer) for 1 h at 4 °C. The ConA beads were pelleted by centrifugation at 1500×g for 2 min at 4 °C and washed twice with 500 µl of lysis buffer. Finally, the glycosylated peptides were eluted with freshly prepared 200 mM methyl- α -D-mannopyranoside/lysis buffer and quantified with a fluorescence plate reader ($\lambda_{\text{ex/em}}=485/520$ nm).

3.5.14 Co-immunoprecipitation

Membranes prepared from *Sf9* cells (5 mg of total protein) containing Haf-Myc/Haf-9-His₁₀ were solubilized in 1 ml of IP solubilization buffer (20 mM Tris/HCl, pH 7.4, 150 mM NaCl, 5 mM MgCl₂, 1% proteinase inhibitor mix HP (Serva), 1% digitonin) for 60 min on ice. Insoluble proteins were removed by centrifugation at 100,000×g for 45 min at 4 °C. An aliquot of the solubilizate (500 µl) was incubated for 2 h at 4 °C with Dynabeads[®] M-280 sheep anti-mouse IgG (DynaL Biotech), which were preloaded with a mouse anti-Myc monoclonal antibody (Millipore). As a negative control, Dynabeads[®] loaded with a monoclonal MHC class I-specific antibody (HC10) were used. Afterwards, the beads were washed three times with 1 ml washing buffer (20 mM Tris/HCl, pH 7.4, 150 mM NaCl, 0.1% digitonin), and finally the precipitated protein was eluted with 30 µl of 1×SDS sample buffer (62.5 mM Tris/HCl, pH 8.0, 2% SDS, 10% glycerol, 0.1% bromphenol blue) for 20 min at 65 °C. Fractions from the co-immunoprecipitation procedure were analyzed by immunoblotting using anti-His and anti-Myc antibodies, respectively.

To prepare the antibody-coupled magnetobeads, 150 µl of the beads slurry were first washed two times with 1 ml IP buffer (20 mM Tris/HCl, pH 7.4, 0.5% BSA, 150 mM NaCl, 5 mM MgCl₂), and then incubated with 10 µg anti-Myc antibody (in 500 µl IP buffer) or 500 µl of HC10 for 2 h at 4 °C. After washing three times with 1 ml IP buffer, the beads were ready to use.

4 Results

4.1 Functional expression of TAPL

For the functional characterization and structural studies, human TAPL wild-type with a C-terminal His₁₀-tag or a Strep-tag II was heterologously expressed by baculovirus infection (with a MOI of 2). The *Sf9* cells were harvested 48 h after infection and crude membranes were prepared. By BCA assay, around 150 mg of crude membrane proteins could be prepared from 1 L of cell culture. The protein expression was detected by immunoblotting using a TAPL-specific antibody. As a negative control, membranes from insect cells infected with baculovirus encoding for tapasin had no cross-reaction (Figure 4-1A). Tapasin is a co-factor of the MHC class I peptide-loading complex and does not bind or transport peptides (Koch et al., 2004). Membranes containing TAPL showed an ATP-specific transport of fluorescence-labeled peptide RRYC^fKSTEL (Figure 4-1B), indicating that the expressed TAPL was functional. As expected, tapasin-containing membranes did not show peptide transport.

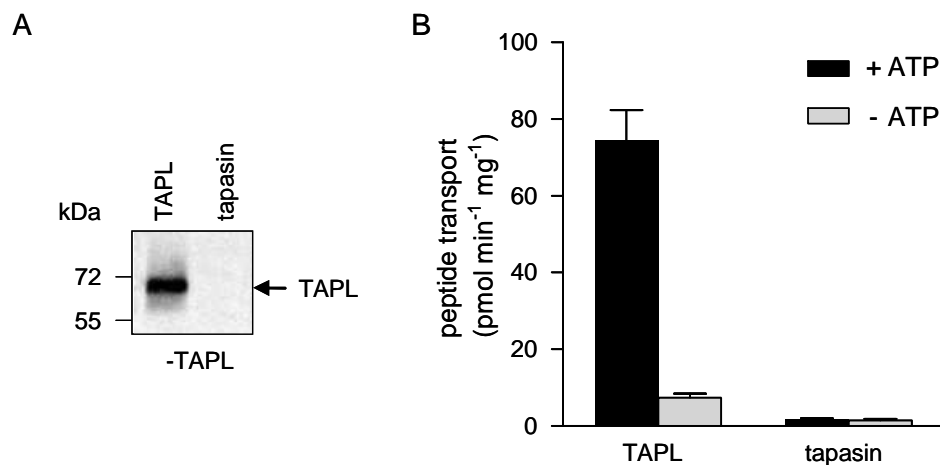


Figure 4-1. Functional expression of TAPL. *A*, expression of TAPL. Membranes (7.5 μ g of total protein) derived from insect cells infected with baculovirus-TAPL-His₁₀ or baculovirus-tapasin were analyzed by immunoblotting with an epitope-purified anti-TAPL polyclonal antibody. *B*, TAPL-specific transport. Membranes (25 μ g of total protein) were incubated with 3 μ M fluorescein-labeled RRYC^fKSTEL (where f represents fluorescein coupled to cysteine) and 5 mM MgCl₂ in PBS for 3 min at 37 °C, in the presence or absence of 3 mM ATP. After stopping the reaction and washing, membranes were solubilized by 1% SDS, and fluorescent peptides were quantified with a fluorescence plate reader ($\lambda_{\text{ex/em}}=485/520$ nm). The experiments were performed in triplicate. Error bars, S.D.

4.2 Solubilization of TAPL

Since biological membranes are very complex, detailed functional analysis of membrane proteins and intracellular transport processes are extremely difficult. Therefore, purification and reconstitution of membrane proteins are required and form a challenging task. It is of utmost importance to decipher the substrate specificity of the lysosomal transporter TAPL, since it is connected to its physiological function. Due to the high background and side reactions, it was impossible to resolve the substrate specificity in crude membranes. Therefore, a solubilization and reconstitution procedure was developed for this ABC transporter.

Since solubilization by detergent is a critical step in membrane protein purification, we first screened for the optimal detergent for TAPL by comparing the solubilization efficiency of the mild nonionic detergents digitonin, DDM, DM, OG, and Triton X-100 as well as the zwitterionic detergents Fos-14, CHAPS, and Zwittergent 3-12. TAPL was extracted from crude membranes with a detergent concentration equivalent to a ρ value of 2. After 30-min incubation on ice, insoluble material was removed by centrifugation. Solubilization efficiencies of different detergents were analyzed by SDS-PAGE and immunoblotting using a TAPL-specific antibody. The solubilization was normalized by the TAPL signal derived from SDS-treated crude membranes (Figure 4-2). Fos-14 showed the highest solubilization efficiency (112%), followed by Zwittergent 3-12 (65%), Triton X-100 (65%), digitonin (56%), DDM (52%), CHAPS (40%), DM (34%), and finally OG (13%). Since detergent-solubilized membrane proteins can denature and aggregate over time, I tested the stability of TAPL after 60 h of storage at 4 °C in the detergent containing buffers. After removing the aggregates by centrifugation, soluble TAPL was analyzed by SDS-PAGE and immunoblotting (Figure 4-2). TAPL stored for 60 h in digitonin, DDM, DM, Triton X-100, and Fos-14 did not precipitate, since the immunoblotting signal stayed constant over time. However, in the presence of OG, CHAPS, and Zwittergent 3-12, roughly 50% of the solubilized TAPL precipitated and could not be detected in the soluble fraction over the same period.

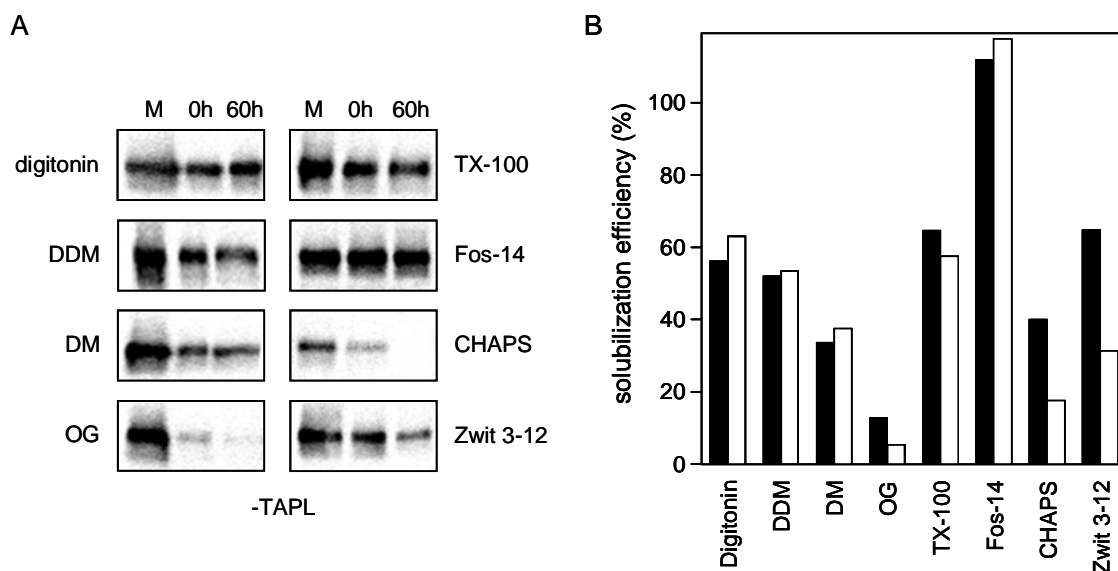


Figure 4-2. Solubilization and stability of TAPL. *A*, crude membranes (*M*) from insect cells (1.0 mg of total protein) were solubilized in 200 μ l of solubilization buffer supplemented with detergents ($\rho=2$) and proteinase inhibitors. After solubilization for 30 min on ice, the supernatant (0h) was collected after centrifugation (1 h; 100,000 $\times g$), stored for 60 h at 4 $^{\circ}$ C, and centrifuged again, resulting in the second supernatant (60h). Equal amounts of crude membranes solubilized in 1% SDS and both supernatants were analyzed by SDS-PAGE (10%) and subsequent immunoblotting using a TAPL-specific antibody. *B*, immunoblotting signals were quantified by chemiluminescence. The signals were normalized to the solubilization efficiency of crude membrane with 1% SDS. *Filled* and *open bars* symbolize TAPL in the supernatant after 0 and 60 h of solubilization. TX-100, Triton X-100; Fos-14, Foscholine-14; Zwit 3-12, Zwittergent 3-12.

Previously, some detergents were reported to disrupt membrane protein complexes (Herget et al., 2007); therefore, the existence of TAPL homologous complex in the presence of the stability-preserving detergents was analyzed by co-expression of TAPL with a C-terminal His₁₀-tag (TAPL-His) and TAPL with a C-terminal Strep-tag II (TAPL-Strep) in *Sf9* insect cells. TAPL was then solubilized using different detergents and isolated via the His₁₀-tag. Due to the low affinity of His₁₀-tag to Ni-NTA agarose beads (Qiagen), high amount of TAPL was lost in the flow-through and washing steps. Importantly, TAPL-Strep could be co-precipitated with TAPL-His in the presence of Triton X-100, DDM, DM and digitonin, whereas Foscholine-14 appeared to disrupt the TAPL complex (Figure 4-3). For further studies, digitonin and DDM were used to extract TAPL from *Sf9* crude membranes, because it had high solubilization efficiency, preserved the homologous complex, and in particular, restored peptide transport activity after reconstitution (see below). Triton X-100 solubilized TAPL did not show any activity, but was used to mediate the reconstitution procedure as described later. Besides that, Triton X-100 had high absorbance at 280 nm, which is problematic for purification with FPLCTM system, therefore, no detailed trails was made for this detergent.

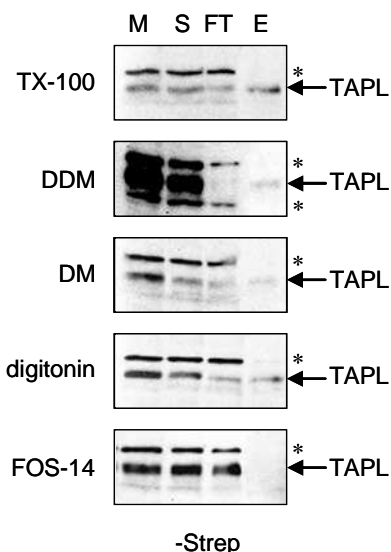


Figure 4-3. Pull down assay via His₁₀-tag. Membranes (1 mg of total protein) containing TAPL-His/TAPL-Strep were solubilized with different detergents (ρ value of 2) and purified with Ni-NTA agarose (Qiagen) or Zn-IDA (GE-healthcare) in the case of DDM. Fractions (1:100 aliquot) of the membrane (M), the solubilize (S), the flow-through and the eluate (E) were separated by SDS-PAGE (10%) and analyzed by immunoblotting against the Strep-tag II using Strep-Tactin HRP. * represents cross reactivity.

4.3 Purification of TAPL

Multistep protein purifications suffer from the drop of protein recovery with each step and, in addition, the protein can be inactivated by surface interactions. Therefore, I established a gentle two-step method. First, impurities were removed by a cation exchange chromatography without binding TAPL. Second, the flow-through from this step was loaded onto a Zn²⁺-iminodiacetate matrix, in which TAPL is specifically bound via its C-terminal His₁₀-tag. After stringent washing with up to 100 mM imidazole, TAPL was eluted with 250 mM imidazole (Figure 4-4). By this procedure, a yield of about 500 μ g/L cell culture of highly purified TAPL was obtained.

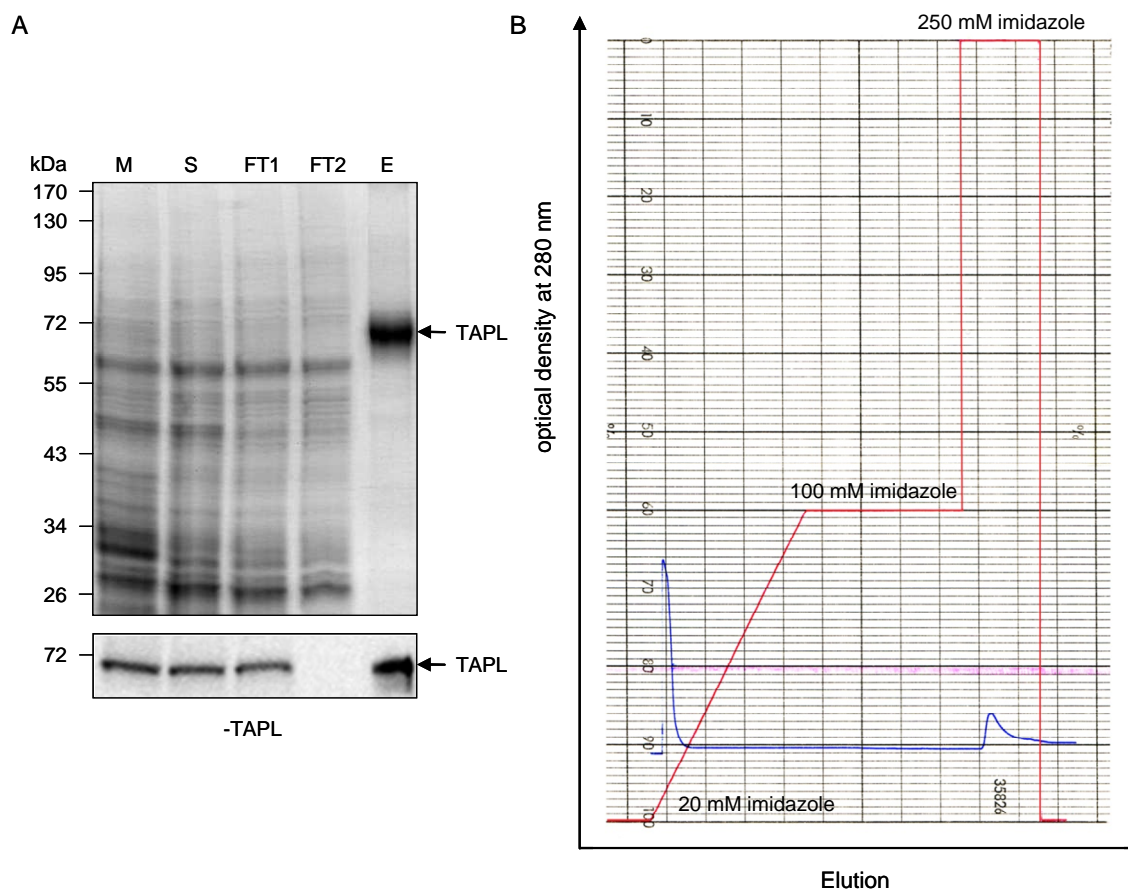


Figure 4-4. Purification of TAPL. *A*, Coomassie staining and immunoblotting. Crude membranes (M) from insect cells (5 mg/ml) were solubilized in 1% digitonin. After centrifugation, the supernatant (S) was cleared from contaminations by a cation exchange chromatography (SP Sepharose™ Fast Flow), whereas TAPL was recovered (80–90%) in the flow-through (FT1) as determined from immunoblotting signal quantification. In the second step, FT1 was applied to a Zn²⁺-iminodiacetate affinity chromatography. TAPL was not detected by immunoblotting in the flow-through (FT2) but rather in the eluate (E) with a recovery of ~50% from the solubilized TAPL. From fractions M, S, FT1 and FT2, 5 µl sample (aliquot of 1:6,000) was loaded for SDS-PAGE separation and immunoblotting, whereas 10 µl sample (aliquot of 1:1,000) from the eluate was loaded. For Coomassie staining, 3 µg purified TAPL was loaded. *B*, FPLC™ chromatogram of affinity purification via His₁₀-tag. The 1 ml HiTrap™ Chelating HP column was first washed by a linear imidazole gradient (20–100 mM) of 20 column volumes, followed by another 20 column volumes of washing with constant 100 mM imidazole. Finally, TAPL was eluted by 10 column volumes of 250 mM imidazole. The flow rate for loading was 0.5 ml/min, and 1 ml/min for washing and eluting. The imidazole gradient is depicted in red and the chromatogram at 280 nm in blue.

4.4 Oligomeric status

Some ABC transporters seem to form also higher oligomers. For example, the full transporter CFTR was reported to form monomeric (Marshall et al., 1994; Chen et al., 2002; Haggie and Verkman, 2008), dimeric (Eskandari et al., 1998; Li et al., 2004) or larger complexes (Ramjeesingh et al., 2003) in the membranes even though its minimal functional unit is a monomer (Ramjeesingh et al., 2001). Moreover, the multidrug resistance-associated transporter ABCG2 which is considered to be a half transporter and forms a homodimer, can be detected also in higher oligomeric states (McDevitt et al., 2006; Xu et al., 2007). To investigate the oligomeric status of TAPL, two strategies were employed: gel filtration and blue native PAGE. The gel filtration was performed in elution buffer supplemented with 0.1% digitonin. On SuperoseTM 6 PC gel filtration column, the slightly concentrated TAPL (0.3 mg/ml) showed one peak which is almost monodisperse at 1.53 ml (Figure 4-5A). This peak was correlated with TAPL as shown by immunodetection (Figure 4-5B). The peak at 1.75 ml could be small amounts of impurities and digitonin micelles which are supposed to have slight light scattering at 260 nm as well as 280 nm. The soluble protein standards were applied in the same conditions and used to compare the hydrodynamic radius with TAPL as described in the method parts (3.5.7). The void volume (V_o) of the column was determined by blue dextran (around 2,000 kDa) to be 0.85 ml, whereas the protein standard thyroglobulin (669 kDa) was eluted at 1.28 ml, apoferritin (443 kDa) at 1.45 ml, β -amylase (200 kDa) at 1.56 ml and BSA (66 kDa) at 1.69 ml. Based on these soluble standard proteins (Figure 4-5A *inset*), the size of TAPL was determined to be similar as the size of a soluble protein of 200 kDa, which was ~20% higher than the theoretical molecular weight of homodimeric TAPL calculated from the amino acid sequence, *i.e.* 172 kDa. When TAPL was further concentrated to 3 mg/ml, the main peak was still at 1.53 ml, but two additional small peaks at 0.89 (void volume) and 1.15 ml (>1700 kDa) appeared (Figure 4-5C). On Coomassie stained SDS-PAGE gel (Figure 4-5D), TAPL showed very high purity in every gel filtration fraction. Therefore, these two additional peaks indicated the formation of aggregates or higher oligomers.

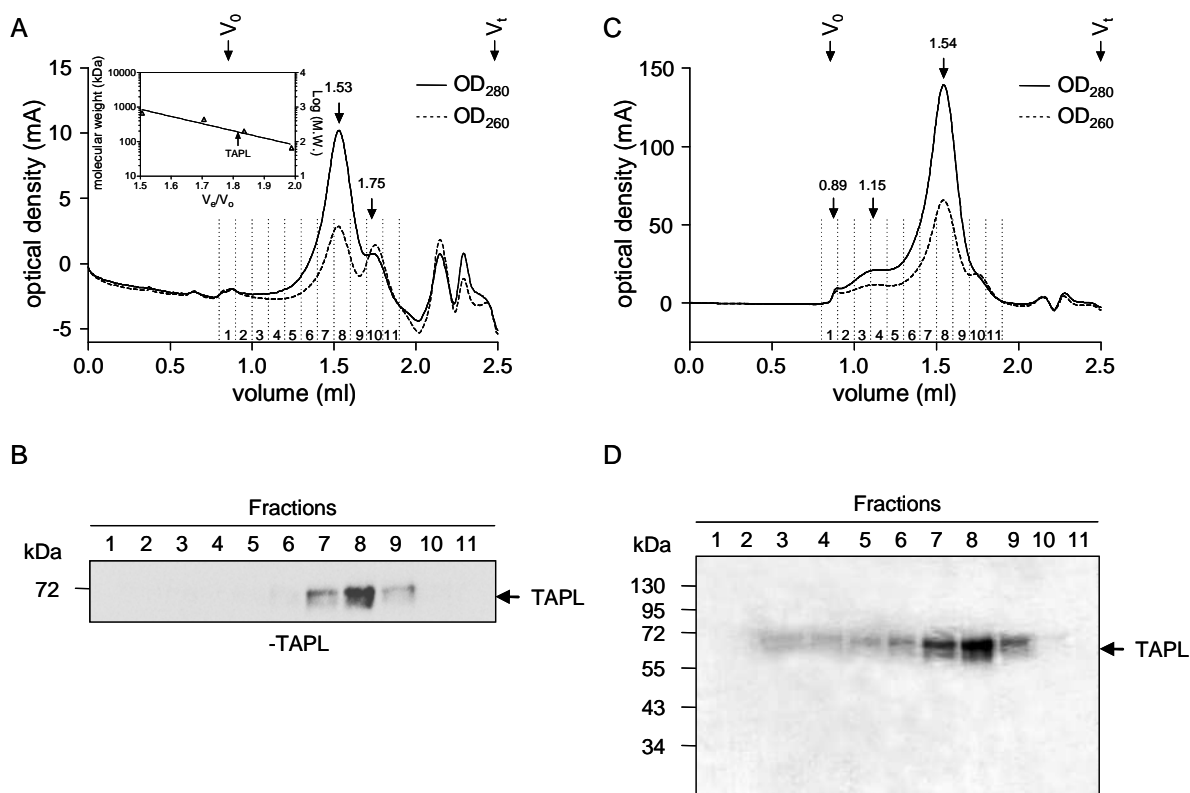


Figure 4-5. Oligomeric state of TAPL analyzed by gel filtration chromatography. *A*, gel filtration chromatogram of TAPL purified via IMAC. The eluate (15 μ g, 0.3 mg/ml) from Zn-IDA column was applied on SuperoseTM 6 PC 3.2/30 column, and eluted with elution buffer (20 mM HEPES, 140 mM NaCl, 250 mM imidazole, 15% (w/v) glycerol, pH 7.5) supplemented with 0.1% digitonin. The flow rate was set to 50 μ l/min. Fractions of 100 μ l were collected. The *inset*, protein standard curve was made as described in the *methods* part. The marker proteins (20 μ g for each protein) in use were thyroglobulin (669 kDa), apoferritin (443 kDa), β -amylase (200 kDa) and BSA (66 kDa). The size of TAPL (indicated by the *arrow*) was estimated based on the linear regression of the retention of the markers. V_0 and V_t indicate the void volume and total column volume. *B*, immunodetection. Aliquots (30 μ l) from each fraction were analyzed by SDS-PAGE (10%) and immunoblotting using an anti-TAPL antibody. *C*, gel filtration of concentrated TAPL. TAPL was concentrated to 3 mg/ml and 150 μ g of protein was applied to gel filtration as described above. *D*, Coomassie blue staining. An aliquot (25 μ l) from each fraction was subjected to SDS-PAGE (10%) followed by staining with Coomassie blue R-250.

The oligomeric status of TAPL was also studied by blue native PAGE (BN-PAGE), which can be used for one-step isolation of protein complexes from biological membranes, total cells or tissue homogenates, as well as for determining native protein masses, oligomeric states and identifying physiological protein-protein interactions (Wittig et al., 2006). TAPL wild-type purified in the presence of 0.1% digitonin was analyzed by BN-PAGE and stained with Coomassie blue R-250. As a standard, bovine heart mitochondria (a kind gift from Prof. Dr. Hermann Schägger and Dr. Ilka Wittig, Uni-Frankfurt) were solubilized with digitonin, and loaded side by side with TAPL. Purified TAPL migrated roughly monodisperse with the

similar migration rate as mitochondrial respiratory chain complex IV (200 kDa). The apparent molecular weights were consistently determined to be 200 kDa in both gel filtration and BN-PAGE. Together with the pull down data about TAPL forming complexes in the presence of digitonin (Figure 4-3), the existence of monomeric TAPL can be ruled out. Therefore, it is rational that digitonin-purified TAPL is a dimeric complex, although the micellar weight of digitonin, the number of bound dyes and lipids are unknown. (Figure 4-6).

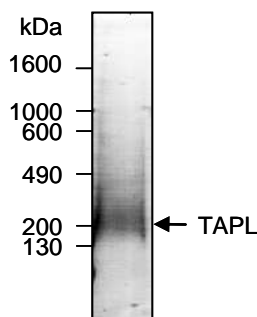


Figure 4-6. Oligomerization of TAPL studied by BN-PAGE. Purified TAPL (7.5 μ g) in the presence of 0.1% digitonin was mixed with 5% Ponceau S solution and applied on BN-PAGE (4–13%). As markers, the respiratory chain complexes of bovine heart mitochondria (100 μ g, a kind gift from Prof. Dr. Hermann Schägger and Dr. Ilka Wittig, Uni-Frankfurt) were used. The size and components of each complex were described in the original protocol (Wittig et al., 2006).

4.5 Functional reconstitution of TAPL

Functional reconstitution of membrane proteins is a critical step depending on different parameters. Therefore, I optimized TAPL reconstitution into liposomes composed of *Escherichia coli* lipids for the highest transport activity with respect to the liposome preparation, destabilization of liposomes, lipid-to-protein ratio, and detergent removal. The substrate transport was determined with fluorescein-labeled peptide RRYC^fKSTEL (where f represents fluorescein coupled to cysteine) in the presence or absence of 3 mM ATP at 37 °C (Figure 4-7A). The highest transport activity was obtained using large unilamellar liposomes (diameter \leq 400 nm), destabilized by Triton X-100 to the point slightly beyond the maximal light scattering (R_{sat}) (Figure 4-7B), a lipid-to-protein ratio of 40:1 (w/w), and removal of detergents by serial addition of polystyrene beads. The membrane insertion of TAPL was confirmed by freeze-fracture transmission electron microscopy (performed by Dr. Winfried Haase, MPI of Biophysics, Frankfurt), by which membrane incorporated particles are visible only after reconstitution of TAPL (Figure 4-7C).

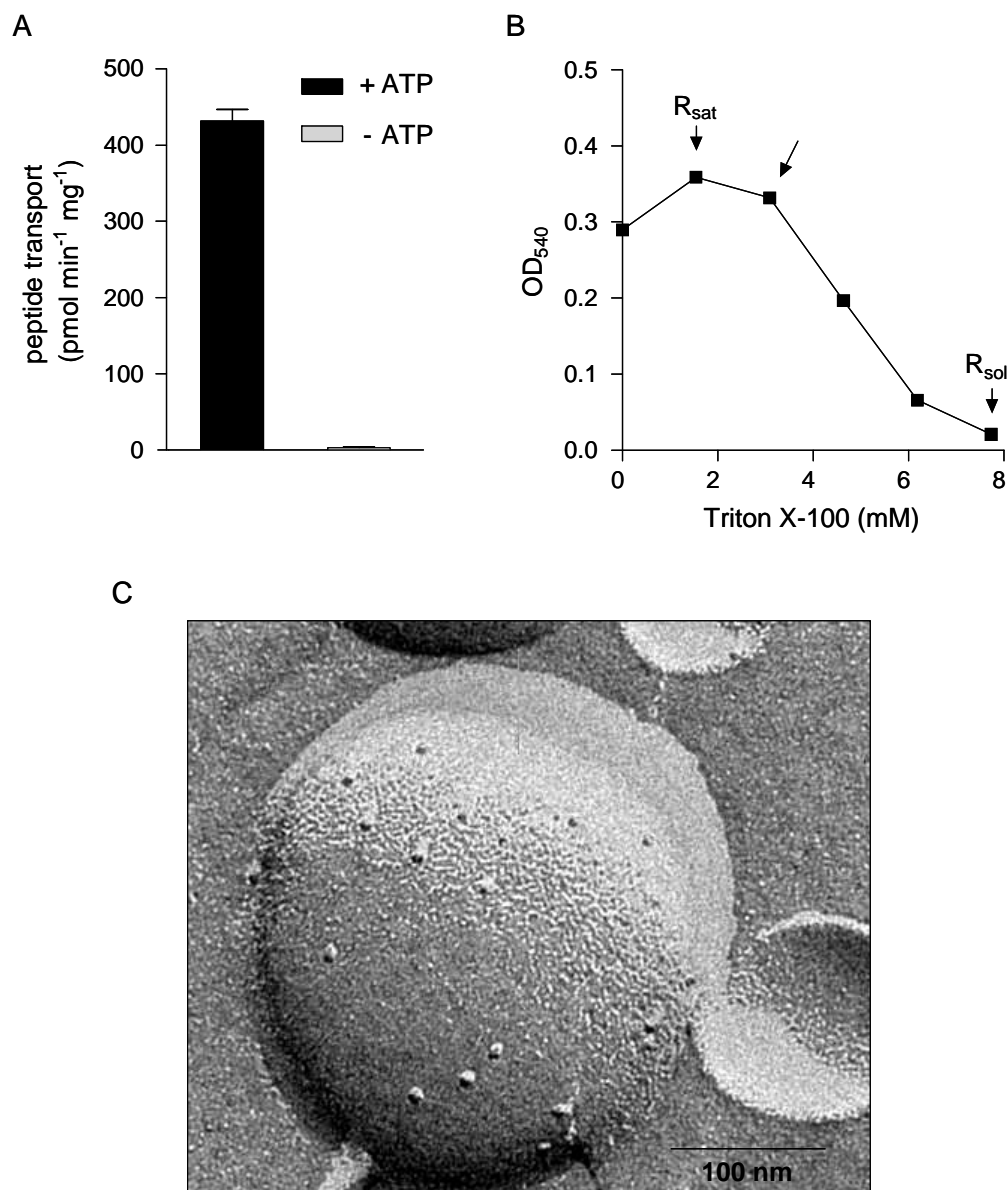


Figure 4-7. Functional reconstitution of TAPL. *A*, ATP-dependent peptide transport of reconstituted TAPL. 50 μ l of proteoliposomes (1.25 μ g of TAPL in *E. coli* lipids) in PBS were incubated with 3 μ M fluorescein-labeled peptide RRYC^fKSTEL and 5 mM MgCl₂ in the presence or absence of 3 mM ATP for 10 min at 37 °C. After washing, the proteoliposomes were solubilized by 1% SDS, and the fluorescent peptides were quantified by a fluorescence plate reader ($\lambda_{\text{ex/em}}=485/520$ nm). The experiments were performed in triplicate. *Error bars*, S.D. *B*, Titration of preformed liposomes with Triton X-100. Liposomes (10 mg/ml) composed of *E. coli* lipids were extruded through a 400 nm polycarbonate filter, diluted to 2.5 mg/ml with reconstitution buffer and exposed to increasing Triton X-100 concentrations at room temperature. The turbidity of liposomes was measured by absorbance at 540 nm. R_{sat} and R_{sol} indicate detergent concentrations at which liposomes were saturated and solubilized. The *arrow* indicates the Triton X-100 concentration which was used to destabilize liposomes. *C*, reconstitution of TAPL. After reconstitution via polystyrene beads, proteoliposomes were analyzed by freeze-fracture electron microscopy (Dr. Winfried Haase, MPI of Biophysics, Frankfurt). The particles indicate the incorporation of protein into the membranes.

After reconstitution into proteoliposomes, TAPL showed almost the same transport activity as in crude membranes, since the Michaelis-Menten constants (Figure 4-8) for the fluorescein-labeled nonapeptide RRYC^fKSTEL ($K_{M(pep)}=10.5 \pm 2.3 \mu\text{M}$) and ATP ($K_{M(ATP)}=97.6 \pm 27.5 \mu\text{M}$) were in a good agreement with those determined from crude membranes ($K_{M(pep)}=6.8 \pm 2.8 \mu\text{M}$, $K_{M(ATP)}=17.6 \pm 2.4 \mu\text{M}$) (Wolters et al., 2005). The maximal transport activity (V_{max}) was determined to be $286.2 \pm 18.3 \text{ pmol min}^{-1} \text{ mg}^{-1}$.

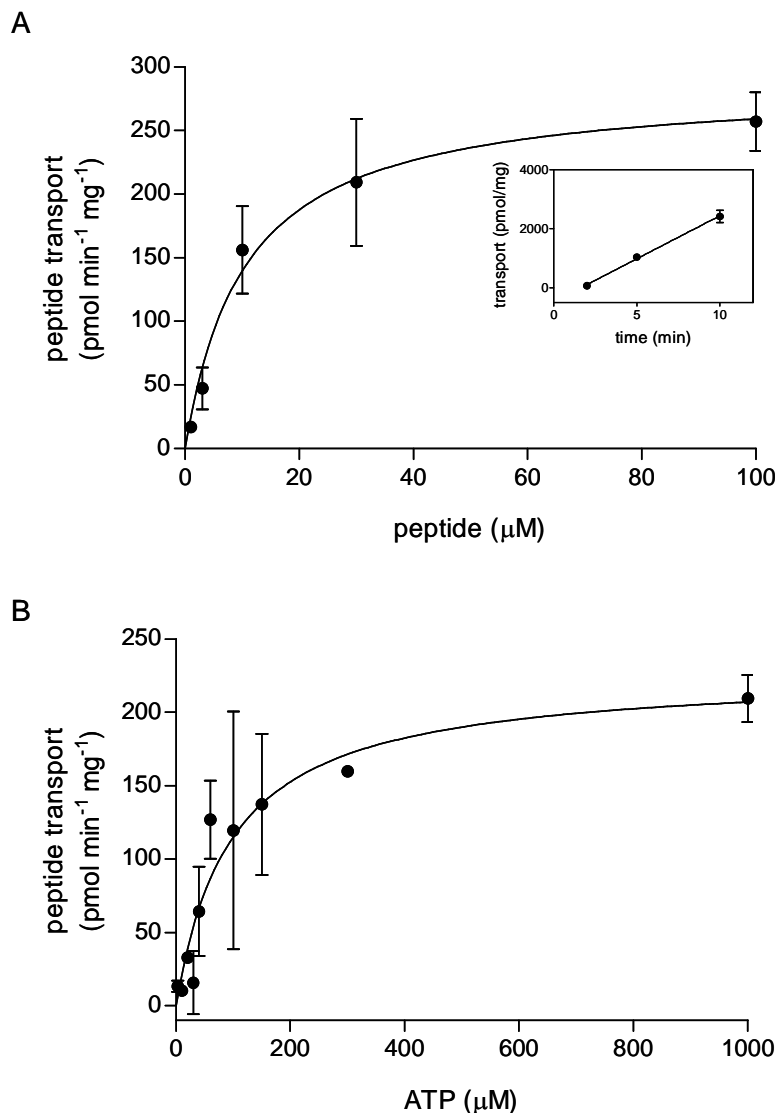


Figure 4-8. Michaelis-Menten kinetics of reconstituted TAPL. *A*, peptide dependent transport activity. The reconstituted TAPL (1.25 μg protein in 50 μg lipids) was incubated in PBS for 10 min at 37 $^{\circ}\text{C}$ with 5 mM MgCl_2 and increasing concentrations of fluorescein-labeled peptide RRYC^fKSTEL, in the presence or absence of 3 mM ATP. By fitting the ATP-dependent transport with the Michaelis-Menten equation, a $K_{M(pep)}$ of $10.5 \pm 2.3 \mu\text{M}$ was determined. A linear peptide uptake within the first 10 min at 30 μM peptide concentration is illustrated in the *inset*. *B*, ATP-dependent transport activity. Peptide transport was followed under saturating peptide concentration (20 μM), and a $K_{M(ATP)}$ of $97.6 \pm 27.5 \mu\text{M}$ was determined. The data were fitted by the Michaelis-Menten equation. The experiments were performed in triplicate. *Error bars*, S.D.

4.6 Lipid activation of TAPL

The lipid composition is a critical parameter for the activity of reconstituted membrane proteins. Therefore, I screened different lipid compositions. Since TAPL is expressed in mammalian cells, I first compared the transport activity of TAPL reconstituted in liposomes derived from lipid extracts of bovine heart, brain, and liver with *E. coli* lipids. Surprisingly, TAPL was only active in *E. coli* lipids and not in any of the bovine lipid extracts (Figure 4-9A).

Since the *E. coli* lipid composition differs drastically from the phospholipid repertoire in mammalian cells, I checked whether phosphatidylcholine, the most abundant phospholipids in eukaryotic cells, was suitable for the functional TAPL reconstitution (DiRusso and Nystrom, 1998; van Meer et al., 2008). By mixing *E. coli* lipids with increasing concentrations of synthetic DOPC, a bell-shaped curve for transport activity was detected with a maximal 3-fold increase at 30% of DOPC compared with pure *E. coli* lipids. At DOPC concentrations higher than 50%, the transport activity of TAPL was strongly decreased, whereas proteoliposomes of pure DOPC were inactive in peptide transport (Figure 4-9B).

For two-dimensional crystallization as well as functional studies on the single-molecule level, it will be beneficial to work with a defined lipid mixture of pure phospholipids. Therefore, I reconstituted TAPL in liposomes containing a mixture of DOPC and either egg PG, DOPA, DOPS, or DOPE at a fixed ratio of 9:1 (w/w). Peptide transport was detected in liposomes containing DOPS or DOPA with a preference for DOPS (Figure 4-9C). Proteoliposomes containing DOPE or PG were inactive in peptide transport. Next, TAPL activity in proteoliposomes composed of different ratios of DOPS and DOPC was analyzed to find the optimal phospholipid mixture (Figure 4-9D). TAPL activity showed a bell-shaped dependence on the DOPS concentration with maximal transport at a DOPS/DOPC ratio of 1:1. These results demonstrate that TAPL activity is dependent not only on the charge but also on the specific head group of phospholipids.

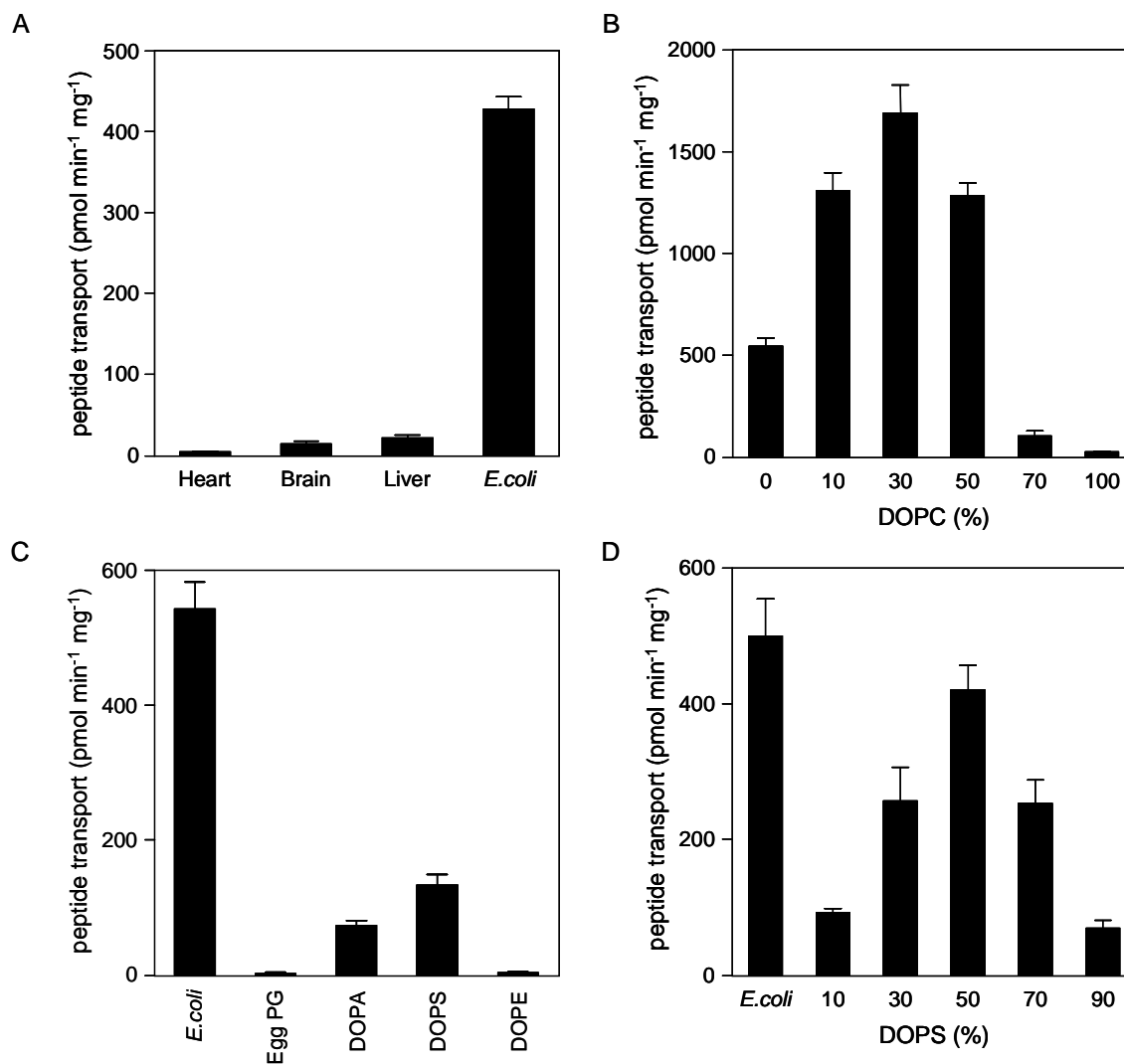


Figure 4-9. Lipid activation of TAPL. *A*, TAPL reconstituted in lipid extracts. The transport activity of TAPL reconstituted in liposomes prepared from bovine heart, brain, or liver lipids or *E. coli* lipids. *B*, phosphatidylcholine-dependent transport. TAPL was reconstituted in liposomes of *E. coli* lipids containing increasing concentrations of DOPC, and the transport activity was quantified. *C*, reconstitution of TAPL in liposomes of defined lipid composition. The transport activity of TAPL reconstituted in liposomes composed of DOPC and either DOPA, DOPE, DOPS, or egg PG in a fixed ratio of 9:1 (w/w) was determined. For comparison, the activity of TAPL reconstituted in *E. coli* liposomes is given. *D*, phosphatidylserine-dependent transport. TAPL was reconstituted in liposomes composed of DOPC and increasing concentrations of DOPS, and the transport activity was quantified. For comparison, the activity of TAPL reconstituted in *E. coli* liposomes is given. The peptide transport was analyzed with 3 μ M fluorescein-labeled peptide RRYC^fKSTEL for 10 min at 37°C. For ATP-dependent transport, the background signal obtained in the absence of ATP was subtracted from the fluorescence signal of peptide transport in the presence of 3 mM ATP. The experiments were performed in triplicate. Error bars, S.D.

4.7 Key positions for substrate recognition

TAPL has a broad peptide length specificity, ranging from 6-mer peptides up to at least 59-mer peptides (Wolters et al., 2005). Peptides are recognized via their backbone, the free N- and C-terminus, and side chain interactions. To investigate the peptide specificity on the single-residue level, I first focused on deciphering the key positions of the transported peptides. Thus, single cysteine-containing derivatives of the antigenic peptide RRYQKSTEL were labeled with 5-iodoacetamidofluorescein, which due to its size is expected to interfere with peptide transport. The position-dependent effects of this bulky fluorophore on ATP-dependent peptide transport can be grouped in four classes (Figure 4-10A): (i) peptides labeled on the N- or C-terminal residue are not transported; (ii) the fluorophore at positions 2 and 3 interferes with peptide transport, in comparison with (iii) positions 4–7, and (iv) fluorescein at position 8 shows no reduction of the transport rate compared with radioactive labeled peptide and does not interfere with peptide transport.

In order to further investigate residues critical for substrate recognition by TAPL, peptide transport was analyzed using ^{125}I -labeled, totally randomized nonameric peptide libraries (X9), which uncouples the studies from a specific peptide sequence context. In this combinatorial peptide library, all naturally occurring amino acids except cysteine are equally distributed at each position, as demonstrated by pool sequencing and mass spectrometry (Stevanovic and Jung, 1993; Metzger et al., 1994; Wiesmuller et al., 1996). First, peptide transport of peptide libraries with one D-amino acid at a given position was examined (Figure 4-10B). These peptides differ only in the conformation of the side chain of this one residue in comparison with all of the L-peptide libraries, allowing us to detect the influence of a single position on transport. Peptide translocation was strongly impaired for peptide libraries with a D-amino acid at the N- or C-terminal position. However, randomized peptides with D-amino acids on all other positions except the N- and C-terminus showed transport rates comparable with the all L-peptide library (X9). Notably, peptides with all D-amino acids are not transported by TAPL (Wolters et al., 2005). Taken together, the data show that the N- and C-terminal residues are crucial for peptide recognition by TAPL, whereas the internal amino acids form only minor contacts with TAPL. Moreover, a bulky side chain at position 2 or 3 interferes with peptide transport most likely by steric hindrance.

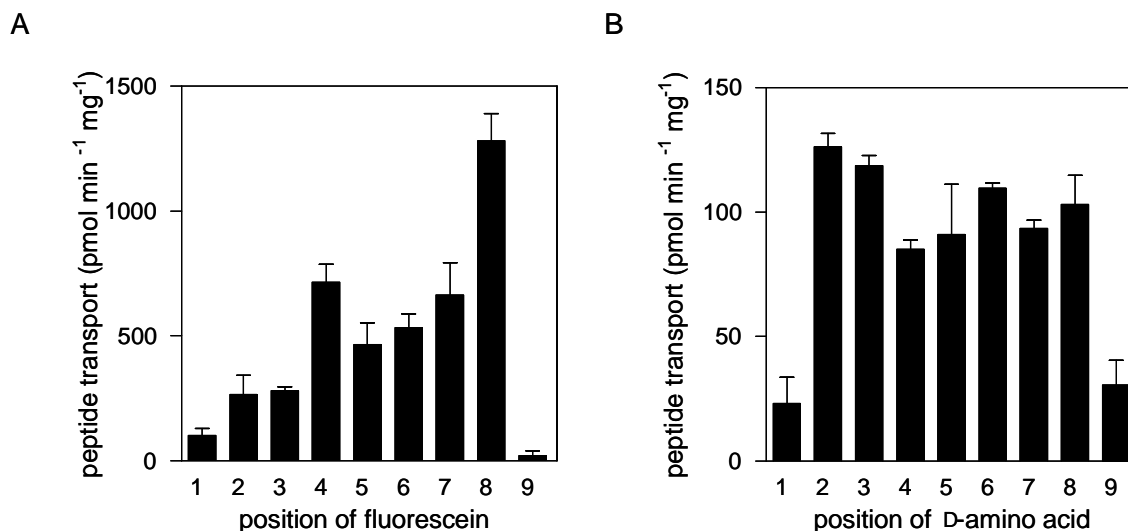


Figure 4-10. Key position for peptide transport. *A*, peptide transport of fluorescein-labeled peptides. Proteoliposomes containing TAPL (1.25 μg) were incubated in the presence or absence of 3 mM ATP with 3 μM derivatives of the nonapeptide RRYQKSTEL, in which each position was subsequently substituted with cysteine and labeled by iodoacetamidofluorescein. After 10 min incubation at 37 $^{\circ}\text{C}$, transport was stopped, and the ATP-dependent peptide transport was quantified by fluorescence intensity. *B*, peptide transport of combinatorial nonapeptide libraries. TAPL-dependent transport was determined in the presence of 1 μM radiolabeled, randomized peptide libraries containing one D-amino acid at a given position for 10 min at 37 $^{\circ}\text{C}$. The ATP-dependent transport was quantified by γ -counting. The experiments were performed in triplicate, and the error bars show the S.D.

4.8 Sequence specificity of TAPL

To determine the amino acid preferences of the N- and C-terminal residues, we determined the transport rates of randomized peptide libraries with a defined amino acid at either the N or C terminus of the peptide (Figure 4-11). Importantly, in this analysis, all observed transport rates were in the linear range and could be normalized to the transport of the totally randomized peptide library (X9). In general, TAPL showed similar preferences for each of the termini. Positively charged, long hydrophobic residues and the aromatic side chains of Phe and Tyr at both positions are favored, whereas negatively charged residues as well as Asn and Met are disfavored. The differences in transport rates of favored and disfavored amino acid residues cover 2 orders of magnitude, and the differences are more pronounced for the C-terminal than the N-terminal position.

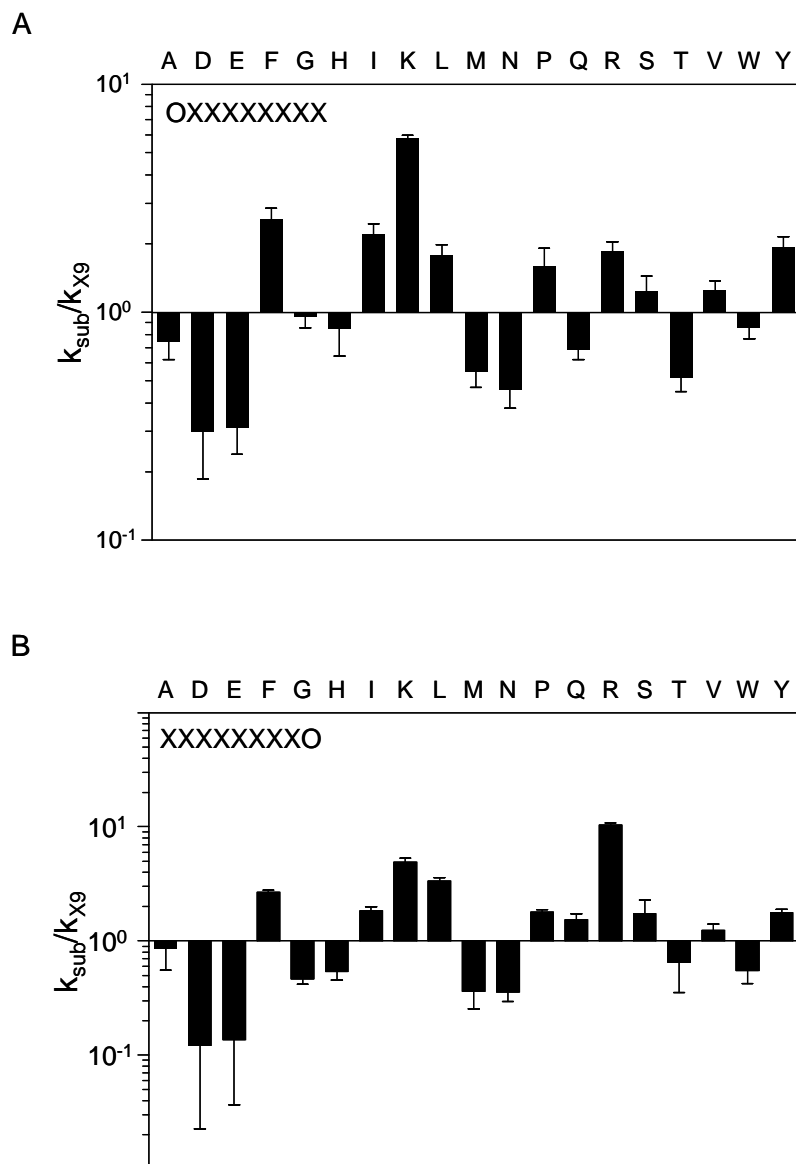


Figure 4-11. Transport activity of N- and C-terminal randomized nonameric peptide sublibraries. ^{125}I -Labeled, randomized nonapeptide sublibraries (1 μM) with defined N-terminal (A) or C-terminal (B) residues were incubated with proteoliposomes containing TAPL (1.25 μg) in the presence or absence of 3 mM ATP for 10 min at 37 $^{\circ}\text{C}$. The ATP-dependent transport rates (k_{sub}) were normalized by the transport rate (k_{X9}) obtained with the totally randomized peptide library X9. The experiments were performed in triplicate, and the *error bars* show the S.D.

Since TAPL shows a broad length specificity ranging from 6-mer to at least 59-mer peptides, I tested whether this recognition pattern is length-independent. To do so, I determined peptide transport of a subset of randomized 6-mer peptide libraries with defined amino acids on the N- or C-terminal end resembling favored, disfavored, or intermediate amino acids (Figure 4-12). Strikingly, the pattern of preference in transport rates normalized by X6 library was very

similar to the 9-mer libraries. Again, positively charged and aromatic residues at both ends are preferred, whereas negatively charged residues and Asn are disfavored. Moreover, as reflected by the higher variation, the C-terminal residue of the *X6* library has a stronger impact on transport than the N-terminal residue, also agreeing with the results from the *X9* library. However, the polar Ser residue at either end is disfavored in the *X6* library while favored in the *X9* libraries. In conclusion, the N- and C-terminal residues of the peptide constitute the key residues independent of the peptide size with a distinct preference for positively charged and aromatic amino acids.

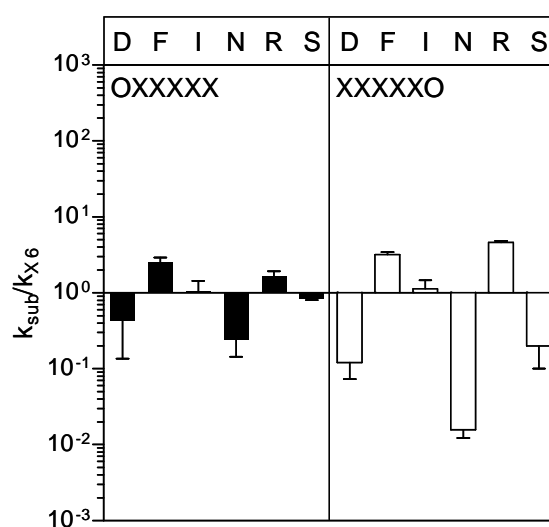


Figure 4-12. Transport of randomized hexameric peptide sublibraries. ^{125}I -Labeled, randomized hexameric peptide sublibraries ($1\ \mu\text{M}$) with defined N-terminal or C-terminal residues were incubated with proteoliposomes containing TAPL ($1.25\ \mu\text{g}$) in the presence or absence of $3\ \text{mM}$ ATP for $10\ \text{min}$ at $37\ ^\circ\text{C}$. The ATP-dependent transport rates (k_{sub}) were normalized by the transport rate (k_{X6}) obtained with the totally randomized peptide library *X6*. The experiments were performed in triplicate, and the *error bars* show the S.D.

To investigate the influence of a single amino acid on each residue of a nonameric peptide, I screened the transport efficiency of nonameric peptide libraries containing Arg or Asp at a defined position, since these residues showed the strongest influence on transport selectivity when present at either end (Figure 4-13). All peptide libraries containing Arg showed a higher transport rate than the total randomized peptide library *X9* (Figure 4-13A). Libraries with Arg at positions 1–8 were similarly efficient, whereas Arg at the C-terminal position doubled the transport rate in comparison with all other positions. The transport pattern of libraries containing Asp was very different from the Arg-containing libraries. Asp at positions 1–3 and especially position 9 disfavored transport (Figure 4-13B). A negative charge at the remaining

positions had only minor influence on peptide transport. The libraries containing Asp at position 4 or 8 exceeded slightly the transport rate of the X9 library. The peptide transport of libraries containing Asp is reminiscent of the transport with the fluorescein-labeled peptides. In conclusion, TAPL prefers positively charged amino acids with the strongest effect on the C-terminal position, whereas negative charges at the three N-terminal positions or the C-terminal position are disfavored.

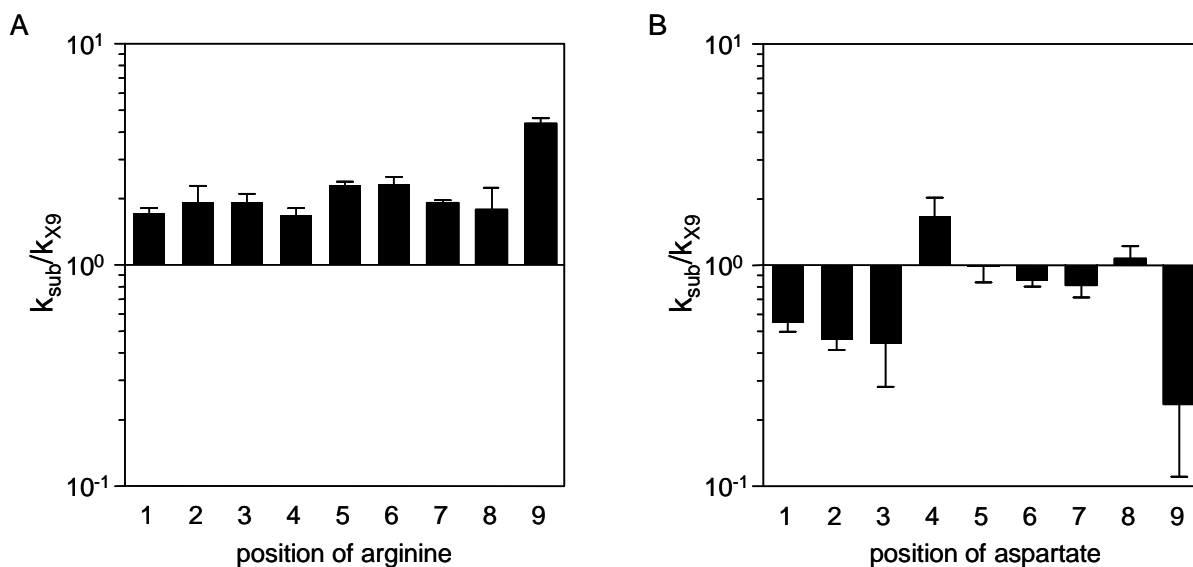


Figure 4-13. Transport of nonameric sublibraries containing Arg or Asp at defined positions. ^{125}I -Labeled, randomized peptide sublibraries (1 μM) containing Arg (A) or Asp (B) at a defined position were incubated with proteoliposomes containing TAPL (1.25 μg) in the presence or absence of 3 mM ATP for 10 min at 37 $^{\circ}\text{C}$. The ATP-dependent transport rates (k_{sub}) were normalized by the transport rate (k_{X9}) obtained with the totally randomized peptide library X9. The experiments were performed in triplicate, and the *error bars* show the S.D.

4.9 ATPase activity

An important mechanistic issue of ABC transporters concerns the stoichiometry between ATP hydrolysis and substrate translocation, and whether both processes are strictly coupled under physiological conditions. To specify the activity of purified or reconstituted TAPL, ATP hydrolysis was measured. The ATPase activity was assayed by the release of the inorganic phosphate from ATP, which was in a linear range for at least 1 h at 37 $^{\circ}\text{C}$ (Figure 4-14B *inset*). In the assay, saturating ATP (2 mM) and peptide RRYQKSTEL (30 μM) concentrations were used. No ATP regeneration system was included in the ATP hydrolysis assay to remove the inhibitory product ADP since maximal 10% of total ATP was hydrolyzed. TAPL showed a basal ATPase activity in both digitonin-solubilized and reconstituted states (Figure 4-14A,B),

but no peptide stimulation was detected. It seems that the peptide transport activity and ATP hydrolysis are not coupled. Importantly, the ATPase activity could be inhibited by 500 μM sodium orthovanadate (inhibitor for ABC transporters and P-type ATPases). Vanadate is a valid inhibitor of TAPL peptide transport with an IC_{50} value of $11.5 \pm 1.0 \mu\text{M}$. (Wolters et al., 2005). The initial ATP hydrolysis rate for digitonin-solubilized TAPL was determined to be $45 \pm 6 \text{ nmol min}^{-1} \text{ mg}^{-1}$, which was around six times lower than TAPL in the proteoliposomes ($v=268 \pm 29 \text{ nmol min}^{-1} \text{ mg}^{-1}$). In order to ensure that the basal ATPase activity was TAPL specific and did not refer to a copurified ATPase, the Walker A/H-loop mutant TAPL-K545A/H699A (KAHA) was generated. Mutations of these conserved motifs abolish the ATP hydrolysis and reduce ATP binding in ABC transporters (Holland and Blight, 1999; Matsuo et al., 1999; Zaitseva et al., 2005a). This mutant showed no peptide translocation activity (Figure 4-14C) and no ATPase activity when purified and reconstituted. Hence, the ATP hydrolysis for the purified and reconstituted TAPL wt was TAPL specific. However, ATP hydrolysis is not coupled with peptide transport. Therefore, determining the stoichiometry between these two reactions is not meaningful.

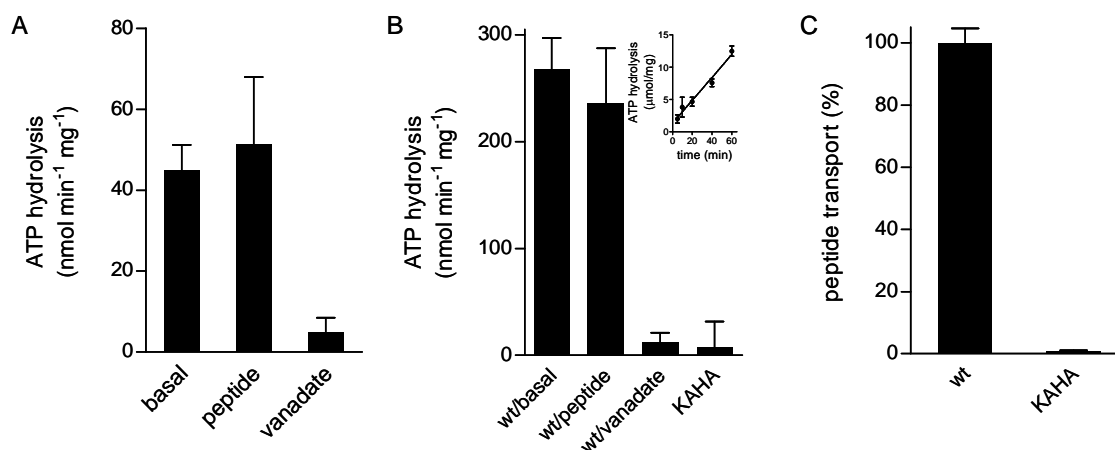


Figure 4-14. ATPase activity of TAPL. **A**, ATP hydrolysis of purified TAPL. Purified TAPL (1.25 μg) was incubated with 2 mM ATP and 5 mM MgCl_2 for 1 h at 37 $^\circ\text{C}$ in the presence of elution buffer supplemented with 0.1% digitonin and ATPase inhibitors (1 mM ouabain, 5 mM NaN_3 and 0.05 mM EGTA). The ATP autohydrolysis was subtracted as background. The working concentration for sodium orthovanadate and peptide RRYQKSTEL were 0.5 mM and 30 μM , respectively. **B**, the ATP hydrolysis of 1.25 μg reconstituted TAPL wild-type (wt) or TAPL-K545A/H699A (KAHA) mutant was measured for 1 h at 37 $^\circ\text{C}$, in the presence of reconstitution buffer (20 mM HEPES, 5% (w/v) glycerol, 140 mM NaCl, pH 7.5) supplemented with 2 mM ATP, 5 mM MgCl_2 , and inhibitors for other ATPases. The same amount of liposomes incubated with ATP was used as background control. The concentration of inorganic phosphate (Pi) was determined by a colorimetric method. **C**, the reconstituted TAPL wt or KAHA mutant (0.625 μg protein) were tested for ATP-specific peptide transport. Proteoliposomes were incubated with 3 μM of fluorescent-labeled peptide RRYC[†]KSTEL and 5 mM MgCl_2 in PBS for 10 min at 37 $^\circ\text{C}$, in the presence or absence of 3 mM ATP. The transport activity was normalized to TAPL wt. The experiments were performed in triplicate, and the *error bars* show the S.D.

4.10 Functional solubilization and purification of TAPL by dodecylmaltoside

For structural studies, the digitonin extract from *Digitalis purpurea* is not suitable due to its heterogeneity, aggregation even at 4 °C and high price. From the solubilization screen studies, dodecylmaltoside (DDM) turned out to be a suitable detergent for TAPL solubilization. However, when 1% DDM was used to solubilize and purify TAPL from *Sf9* cell membranes, no transport activity was observed after reconstitution. Therefore, the solubilization by DDM was optimized in order to purify functional TAPL. The high detergent concentration usually causes delipidation of membrane proteins. In order to reduce detergent amounts but still keep relatively high solubilization efficiency, various concentrations (up to ρ value of 2) of DDM were used to extract TAPL from crude membranes. The extracted TAPL was quantified by immunoblotting signal and compared with the membranes solubilized by 1% SDS (Figure 4-15). The solubilization of TAPL by DDM was concentration dependent. The maximum solubilization was reached at 0.5% DDM ($\rho=1.4$). Interestingly, the solubilization efficiency decreased at higher DDM concentrations. To prevent delipidation, 0.3% DDM ($\rho=0.8$) was used for further solubilization tests since relative high amount (~40%) of TAPL could already be solubilized at this concentration.

The solubilization efficiency of membrane proteins is also influenced by factors such as pH value, protein concentration, ionic strength, and the presence or absence of chemical ‘chaperons’ such as glycerol and sucrose (Hunte et al., 2002). To analyze the influence of the ionic strength on TAPL solubilization, membranes containing TAPL were solubilized with 0.3% DDM in the presence of increasing concentrations of NaCl. As indicated by immunoblotting using an anti-TAPL antibody, the amounts of solubilized TAPL were NaCl concentration dependent. The solubilization efficiency increased strongly at NaCl concentration of 150 mM. The solubilization reached maximum at 150 mM NaCl, but reduced slightly at higher NaCl concentrations (Figure 4-16).

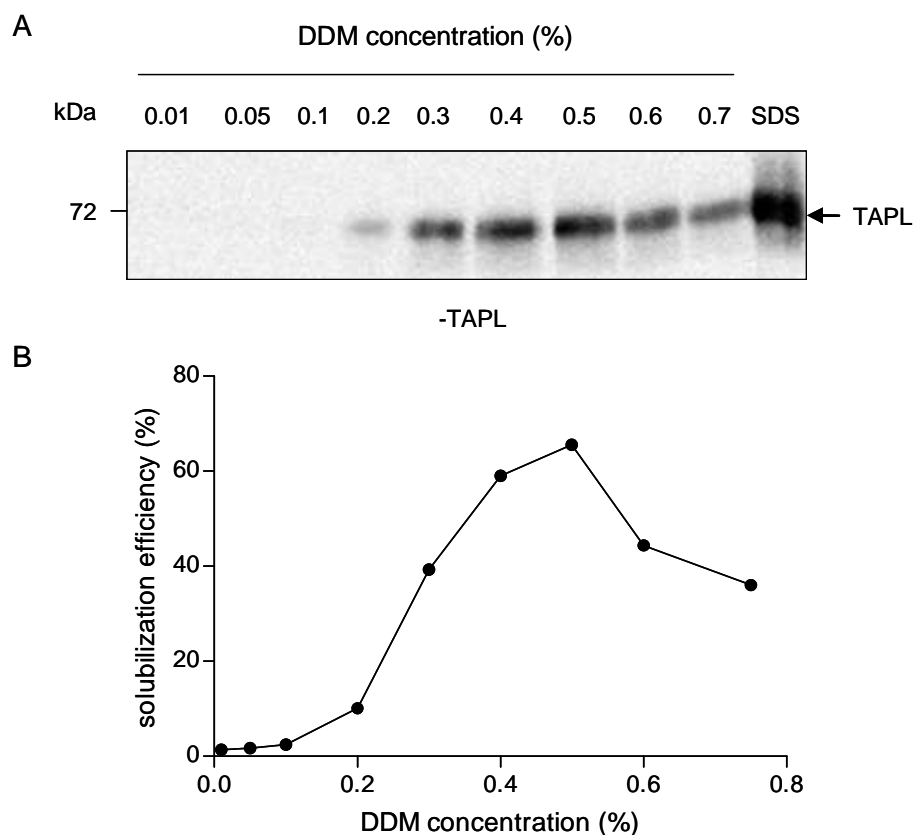


Figure 4-15. Solubilization of TAPL by various concentrations of DDM. *A*, the extraction of TAPL from *Sf9* cell membranes with DDM. TAPL-containing membranes (5 mg/ml total protein) were solubilized in solubilization buffer supplemented with 1 mM PMSF, 2.5 mM benzamide and increasing concentrations of DDM (up to $\rho=2$) for 30 min on ice. After removing the insoluble proteins by centrifugation (100,000 \times g; 30 min), 3 μ l aliquots of supernatant were analyzed by 10% SDS-PAGE and immunoblotting using an anti-TAPL antibody. The membranes solubilized with 1 \times SDS sample buffer (containing 1% SDS) served as reference. *B*, quantification of immunoblotting signals normalized to the SDS solubilize.

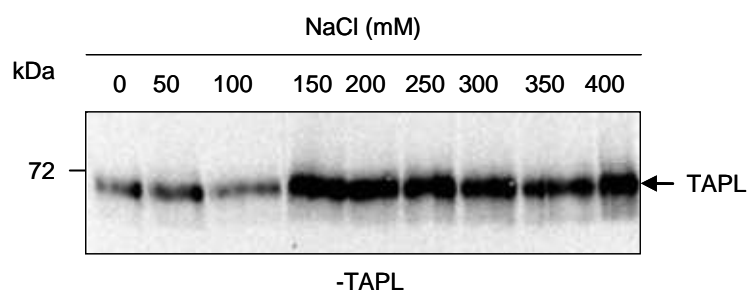


Figure 4-16. Ionic strength-dependent solubilization of TAPL. The TAPL-containing membranes (5 mg/ml total protein) were solubilized in solubilization buffer supplemented with 1 mM PMSF, 2.5 mM benzamide, 0.3% DDM, and increasing concentrations of NaCl. Subsequently, the insoluble proteins were removed by centrifugation (100,000 \times g; 30 min), and 3 μ l aliquots of supernatant were analyzed by SDS-PAGE (10%) and immunoblotting using an anti-TAPL antibody.

After obtaining the optimized solubilization conditions (0.3–0.5% DDM and 150 mM NaCl), TAPL was solubilized in the presence of 0.3% DDM and purified in two steps similar to the

purification with digitonin. The presence of TAPL in each purification fraction was analyzed by immunodetection using the anti-TAPL antibody. Around 50–75% (differs from batch to batch) of TAPL could be recovered from the solubilizate. However, the purity of the eluate was not as high as digitonin-purified TAPL as indicated in the Coomassie staining (Figure 4-17).

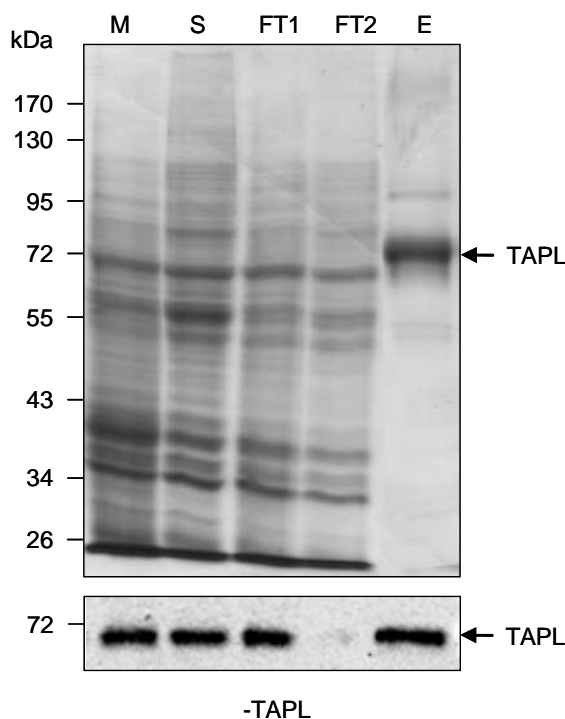


Figure 4-17. Purification of TAPL by DDM. Crude membranes (M) from insect cells (5 mg/ml total protein) were solubilized in 0.3% DDM. After centrifugation, the supernatant (S) was cleared from contaminations by a cation exchange chromatography (SP Sepharose™ Fast Flow), whereas TAPL was left in the flow-through (FT1). In the second step, FT1 was applied to a Zn²⁺-iminodiacetate affinity chromatography. Only small fraction of TAPL (~10%) was detected by immunoblotting against TAPL in the flow-through (FT2). The purity of the eluate (E) was indicated by Coomassie staining.

To investigate the oligomeric status of DDM-purified TAPL, gel filtration and BN-PAGE were carried out. Comparing with the monodisperse peak of the digitonin-purified TAPL, the DDM-purified TAPL showed two peaks on the gel filtration chromatogram (Figure 4-18A). The first peak was in the void volume (V_0) of Superose™ 6 column and might contain lipids or impurities such as DNA since the signal at 260 nm was slightly higher than 280 nm. A small amount of aggregated TAPL was also present in the peak as indicated by Coomassie stained elution fractions (Figure 4-18B). The second peak eluted at 1.53 ml was very broad and asymmetric, containing mainly TAPL and impurities co-eluted. Similar as the digitonin-purified TAPL, there was a shoulder peak at 1.74 ml, which could be light scattering of DDM micelles and contaminated proteins. From the elution profile of soluble protein

standards, DDM-purified TAPL was estimated to have the same hydrodynamic radius as a soluble protein of 200 kDa, which is slightly bigger (~20%) than the theoretical molecular weight (172 kDa) of dimeric TAPL. Since the amount of bound DDM is not clear, the DDM-purified TAPL could still be a dimeric complex considering the complex formation in the presence of DDM (Figure 4-3).

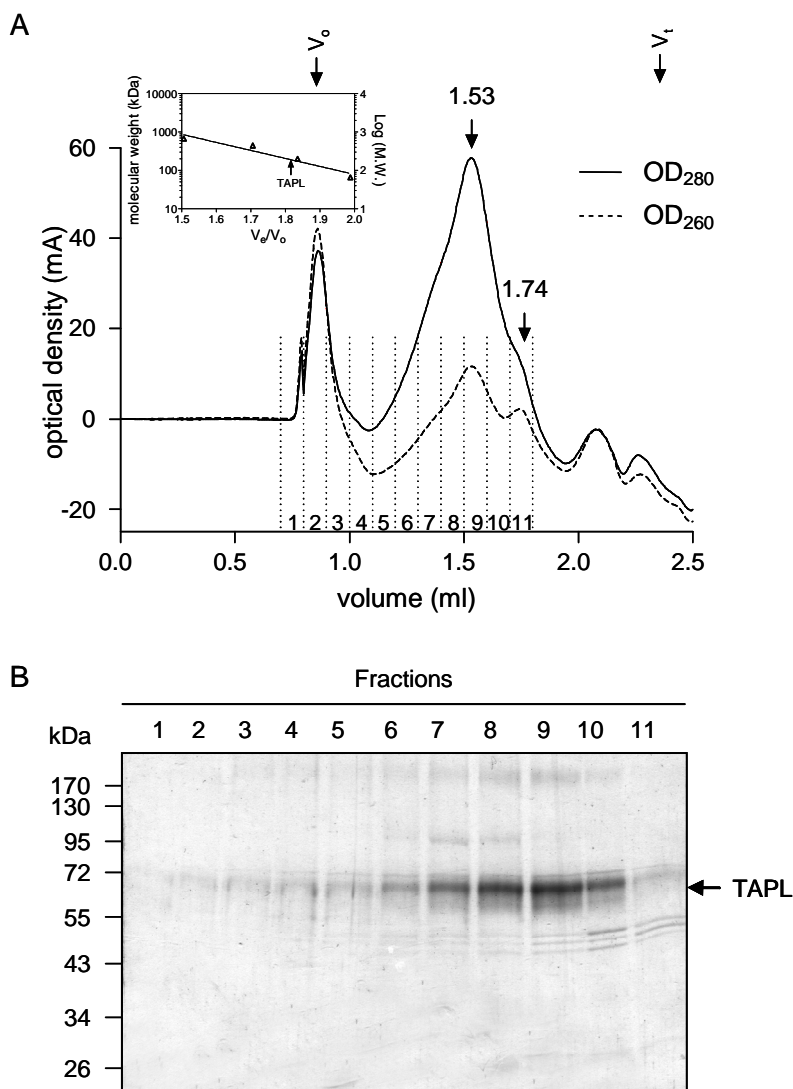


Figure 4-18. Oligomeric state of DDM-purified TAPL analyzed by gel filtration chromatography. *A*, gel filtration chromatogram. TAPL (35 μ g) was applied on a SuperoseTM 6 PC 3.2/30 column, and eluted with elution buffer supplemented with 0.05% DDM. The flow rate was 50 μ l/min. Fractions of 100 μ l were collected. The protein standards from Sigma were applied according to the manufacturer's instruction. V_0 and V_t indicate the void volume and total volume of the column. *B*, Coomassie blue staining. 25 μ l aliquots from each fraction were subjected to SDS-PAGE (10%) followed by staining with Coomassie blue R-250.

On BN-PAGE, DDM-purified TAPL showed almost monodispersity and migrated similarly as respiratory chain complex IV (200 kDa), which was the same as the digitonin-purified TAPL

(Figure 4-19). Taken together, TAPL forms homodimeric complex when purified in the presence of DDM.

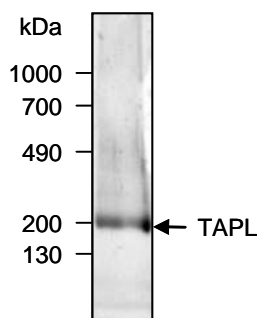


Figure 4-19. Oligomerization of DDM-purified TAPL studied by BN-PAGE. Purified TAPL (7.5 μg) in the presence of 0.05% DDM was mixed with 5% (w/v) Ponceau S solution and applied on BN-PAGE (4–13%). As markers, the respiratory chain complexes of bovine heart mitochondria (100 μg , a kind gift from Prof. Dr. Hermann Schägger and Dr. Ilka Wittig) solubilized with DDM were used. The size and components for each complex was described in the original protocol (Wittig et al., 2006).

To confirm the function of DDM-purified TAPL, the same reconstitution procedure for digitonin-purified TAPL was applied for ease of comparison, and the transport activity of the reconstituted TAPL was tested. DDM-purified TAPL showed almost identical transport activity ($551.1 \pm 16.4 \text{ pmol min}^{-1} \text{ mg}^{-1}$) as digitonin-purified one ($431.3 \pm 15.2 \text{ pmol min}^{-1} \text{ mg}^{-1}$) (Figure 4-20 and Figure 4-7A). Collectively, DDM is a suitable detergent for functional solubilization and purification of TAPL from *Sf9* cell membranes. Comparing with digitonin, DDM is cheaper and more stable in solution, therefore, will facilitate crystallization and many biophysical applications.

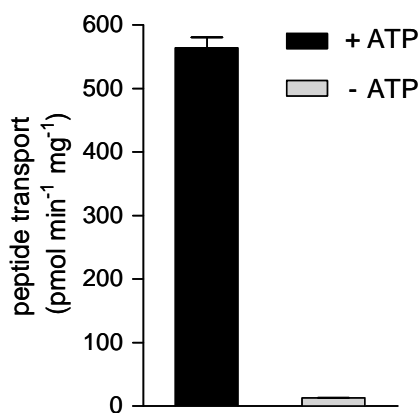


Figure 4-20. Functional reconstitution of DDM-purified TAPL. The ATP-dependent peptide transport of reconstituted TAPL. 50 μl of proteoliposomes (0.625 μg of TAPL in DOPC/*E. coli* lipids (3/7, w/w)) in PBS were incubated with 3 μM fluorescein-labeled peptide RRYC^fKSTEL and 5 mM MgCl_2 in the presence or absence of 3 mM ATP for 10 min at 37 $^\circ\text{C}$. After washing on a filter plate, proteoliposomes were solubilized by 1% SDS, and the transported fluorescent peptides were quantified with a fluorescence plate reader ($\lambda_{\text{ex/em}}=485/520 \text{ nm}$). The experiments were performed in triplicate. Error bars, S.D.

4.11 Functional expression of TAPL cysteine-less mutant and single cysteine mutants

An important tool to investigate the structure, dynamics and transport mechanism of TAPL is to construct a functional cysteine-less (cys-less, C-less) mutant. TAPL contains 8 cysteines (C19, C54, C59, C90, C233, C264, C458, and C548) which are localized in the putative transmembrane helices (C19, C54, C59, C90 and C233), intracellular loops or stretches of the TMD (C264 and C458) and the NBD (C548) (Figure 4-21). If residues were conserved in mouse, rat and human, cysteines were replaced by alanines. Instead of alanine, residue C548 was replaced by valine because valine is found in mouse, rat and human TAP1 as well as TAP2 at this position. TAPL cys-less was expressed with the baculovirus expression system. After membrane preparation, the presence of TAPL cys-less was detected by immunoblotting using the TAPL-specific antibody (Figure 4-23A, *left panel*), and the signals were quantified (Table 4-1). The TAPL cys-less mutant had 65% expression level of TAPL wt. The function of expressed TAPL cys-less was confirmed by the peptide transport assay using fluorescein-labeled nonapeptide RRYC^fKSTEL (Figure 4-23B). TAPL cys-less showed 3-fold higher transport activity than the wild-type in crude membranes. The Michaelis-Menten constants of reconstituted (in *E. coli* lipids/DOPC (7/3, w/w)) TAPL cys-less for ATP ($K_{M(ATP)}=224.8 \pm 24.9 \mu\text{M}$) and the fluorescein-labeled peptide RRYC^fKSTEL ($K_{M(pep)}=5.2 \pm 0.6 \mu\text{M}$) were in good agreements with those determined for TAPL wt. The maximal transport rate ($V_{\max}=2.7 \pm 0.1 \text{ nmol min}^{-1} \text{ mg}^{-1}$) was found to be 10-fold higher than TAPL wt in *E. coli* lipids which might be due to the optimized lipid composition too.

With the fully functional TAPL cys-less in hand, single cysteine residues were introduced in strategic positions (Figure 4-22). Based on the topology model of TAPL, the mutated residue S105C is in the luminal loop of TMD0-TAPL; S170C is in the cytosolic connection loop between TMD0- and TMD1-TAPL (core-TAPL); M222C is in the luminal loop 1 of core-TAPL; A264C is in the cytosolic loop 1 of core-TAPL; Y409C is in the putative transmembrane helix 9; V465C is in the cytosolic stretch following transmembrane helix 10, which belongs to the putative peptide-binding region; and L701C is close to the conserved H-loop motif within the NBD. These residues are in the α -helical structures to have less mobility.

TAPL single cysteine mutants were also expressed in *Sf9* insect cells. The amounts of TAPL single cysteine mutants in crude membranes were detected and quantified by immunoblotting (Figure 4-23A, *right panel*), and the expression levels were compared with TAPL wt (Table 4-1). The expression level ranges from 20% (L701C) to 160% (S170C).

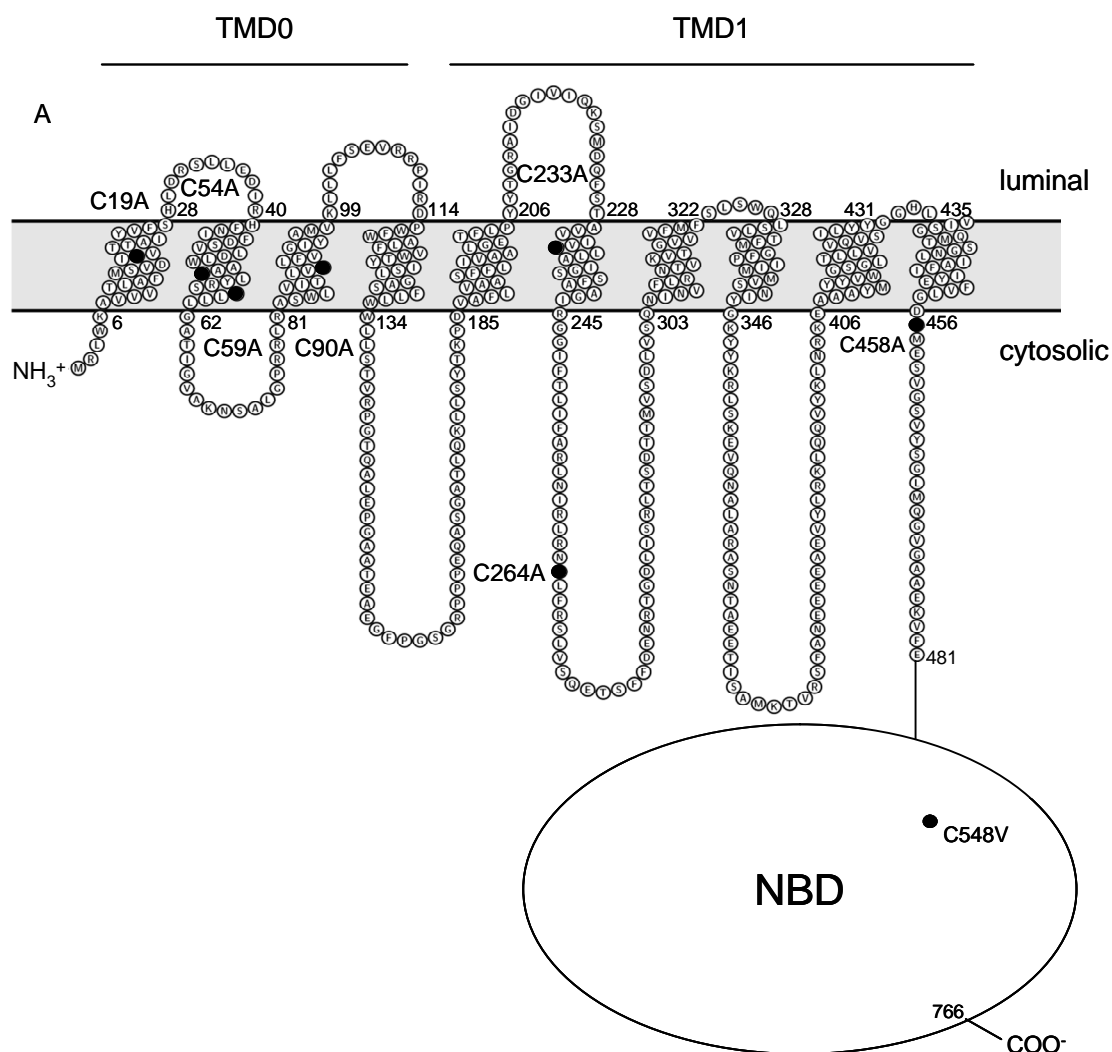


Figure 4-21. Positions of intrinsic cysteines in TAPL wt. To generate TAPL cys-less, 8 intrinsic cysteines were replaced by LCR based mutagenesis into alanines (C19A, C54A, C59A, C90A, C233A, C264A and C458A) or valine (C548V). The cysteines are depicted with *filled circles* in the topology model.

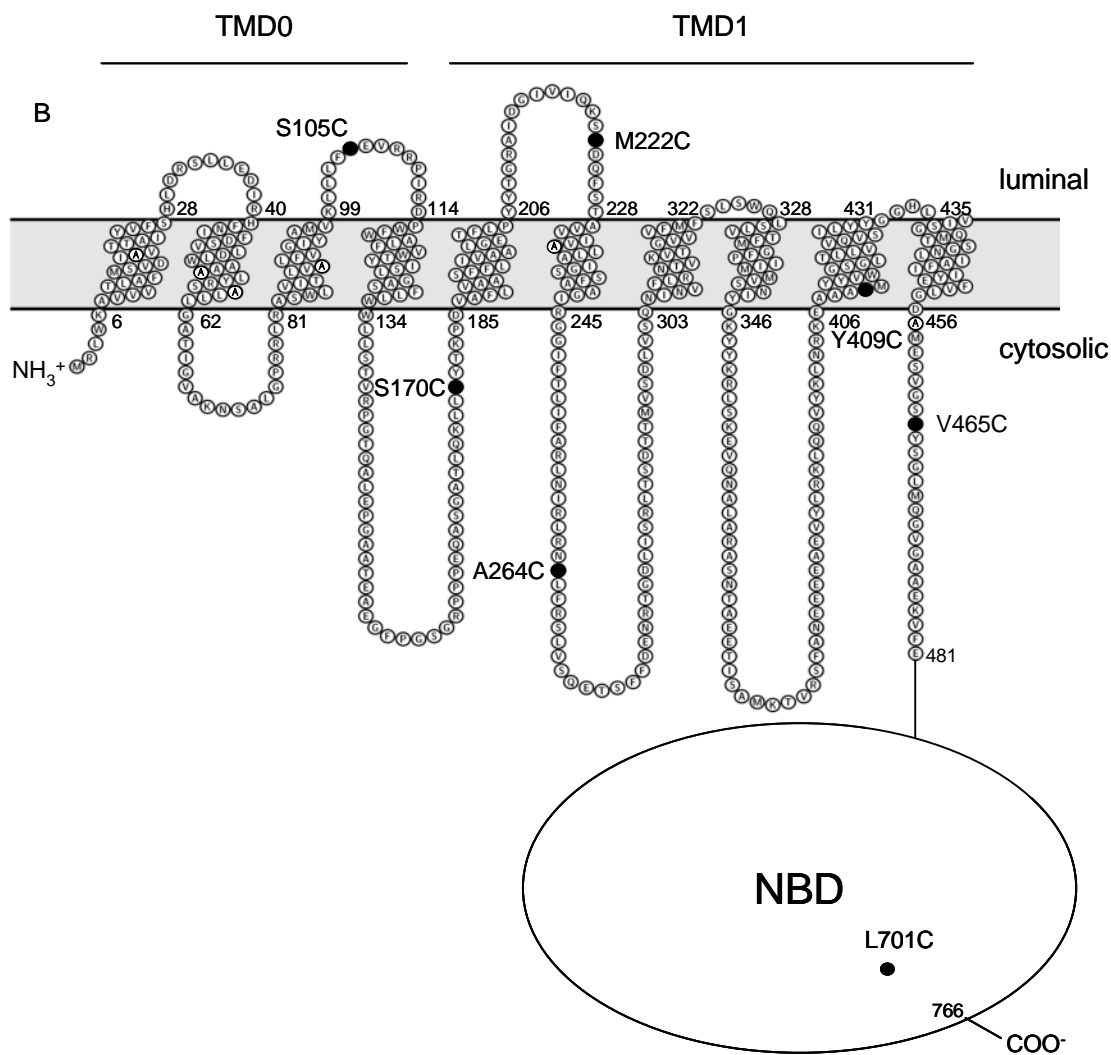


Figure 4-22. Positions of single cysteines introduced in TAPL *cys*-less mutant. 7 single cysteine mutants (S105C, S170C, M222C, A264C, Y409C, V465C and L701C) were produced by LCR. The cysteines are depicted with *filled circles* in the topological model.

In the peptide transport assay, most of the single cysteine mutants had the similar transport activity as the wild-type, except for the mutant L701C which showed impaired transport (Figure 4-23B). This mutant is close to H699 in the H-loop, and perhaps changes the local structure of the H-loop. Collectively, TAPL *cys*-less mutant is active in peptide transport. The generation of active single cysteine mutants is a starting point for site-directed labeling.

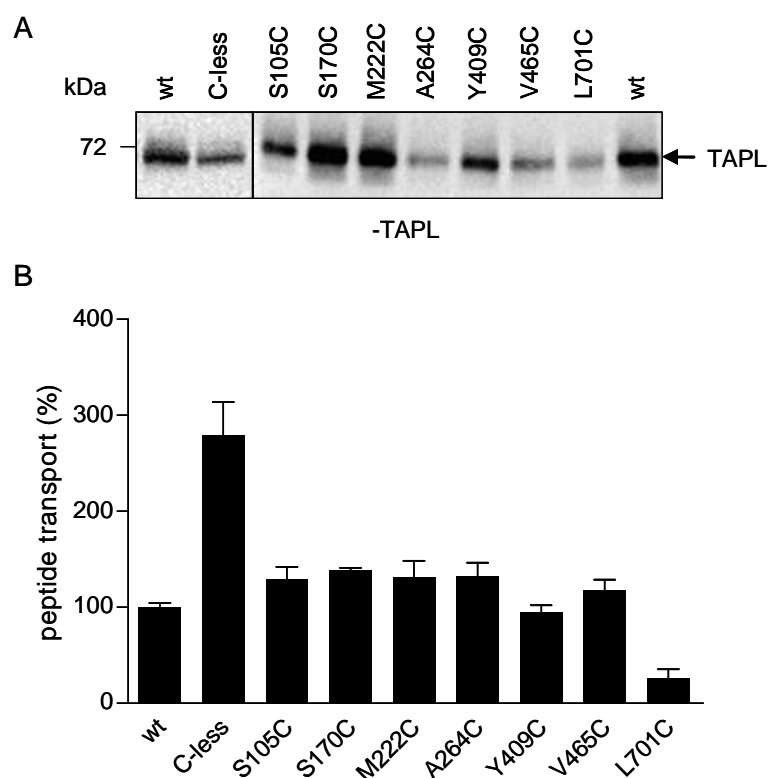


Figure 4-23. Expression analysis and peptide transport activity of TAPL mutants. *A*, expression level of TAPL wt and its mutants. Crude membranes (50 μ g of total protein) containing TAPL wt or its mutants were solubilized in 1 \times SDS sample buffer and analyzed by SDS-PAGE (10%) and immunoblotting by an anti-TAPL antibody. The immunoblotting signals were quantified by Lumi-ImagerTM F1 and normalized to TAPL wt. The expression levels were listed in *Table 4-1*. *B*, peptide transport of TAPL and its mutants. The peptide transport was performed with a filter assay. Membranes (25 μ g of total protein) were incubated with 3 μ M fluorescein-labeled peptide RRYC^fKSTEL and 5 mM MgCl₂ in PBS for 3 min at 37 °C, in the presence or absence of 3 mM ATP. The ATP-specific transport for each mutant was normalized by TAPL expression level and the transport activity of TAPL wt. The experiments were performed in triplicate. *Error bars*, S.D.

Table 4-1 Expression of TAPL wt and its mutants

Constructs	Expression level (%)
TAPL wt	100
TAPL C-less	65
S105C	42
S170C	160
M222C	133
A264C	25
Y409C	36
V465C	27
L701C	20

4.12 Characterization of TAPL orthologs from *Caenorhabditis elegans*

There are three TAPL orthologs (Haf-2, Haf-4 and Haf-9) in *C. elegans*, among which Haf-4 and Haf-9 have the closest sequence identity (~38%) with TAPL. Both proteins were identified as half ABC transporters with a similar architecture of N-terminal 8 putative transmembrane helices followed by the NBD domain (Sheps et al., 2004), and reported to be involved in intestinal granules formation (Bauer, 2006; Kawai et al., 2009). To further understand the physiological role and interactions of Haf-4 and Haf-9, both half transporters were expressed in *Sf9* insect cells and characterized in terms of peptide transport and interaction.

4.12.1 Expression of Haf-4 and Haf-9 in *Sf9* insect cells

The genes of Haf-4 and Haf-9 were cloned by PCR into pFastBac1 vector. For interaction studies and detection, Haf-4 had a C-terminal Myc-tag, and Haf-9 had a His₁₀-tag on its C-terminus. Both proteins were expressed with the baculovirus expression system under the control of the polyhedrin promoter. The *Sf9* cells were harvested 48 h after infection (with a MOI of 2) and crude membranes were prepared. The protein expression was identified using immunoblotting against the terminal tags (Figure 4-24A). The apparent molecular masses for both Myc-tagged Haf-4 (85 kDa) and His₁₀-tagged Haf-9 (82 kDa) were slightly smaller than the theoretical molecular weight (Haf-4-Myc, 90 kDa; Haf-9-His₁₀, 92 kDa) on 10% SDS-PAGE. Beside that, Haf-9-His migrates a little faster than Haf-4-Myc. Actually, similar phenomena were observed for other membrane proteins, for example, TAPL migrates at around 70 kDa, which is much smaller than its theoretical molecular weight (85 kDa). This phenomenon is reasonable for membrane proteins since incomplete denaturation by SDS might occur (Rath et al., 2009).

For co-expression, an equal amount of virus stock (MOI of 2 for each virus) was used for both constructs. Interestingly, the co-expression of Haf-4 and Haf-9 caused significant increase of expression for both proteins, suggesting that these two half transporters might stabilize and interact with each other. When equal amounts of membranes from single expression and co-expression were analyzed by immunoblotting against the C-terminal tags, Haf-4 expression level was two-fold higher when co-expressed with Haf-9, whereas Haf-9 expressed five-fold higher in the co-expression experiment (Figure 4-24B).

To compare the expression level of Haf-9 and TAPL, an anti-His antibody was used in the immunoblotting since both proteins have His₁₀-tags. From the quantitative immunoblotting, TAPL and Haf-9 from *Sf9* crude membranes had an immunoblotting signal ratio of 4:1

(Figure 4-24C). The expression of Haf-4 and TAPL as well as Haf-4 and Haf-9 cannot be compared directly due to different tags. Therefore, MRJ cells stably expressing Myc-tagged TAPL KAHA mutant (generated by Irina Bangert) were used as a reference to compare the relative expression of Myc-tagged Haf-4 and TAPL wt (Figure 4-24D). The same amounts of *Sf9* and MRJ cells were analyzed by immunoblotting. Haf-4 and TAPL KAHA had an immunoblotting signal ratio of 1:1 analyzed by an anti-Myc antibody (Figure 4-24D, *upper panel*). TAPL wt in *Sf9* cells and TAPL KAHA in MRJ cells also had an immunoblotting signal ratio of 1:1 determined by the TAPL-specific antibody (Figure 4-24D, *lower panel*). By comparing the relative expression of different tagged proteins, I concluded that Haf-4 and TAPL had the same expression in *Sf9* cells, and both proteins expressed 4-fold higher than Haf-9.

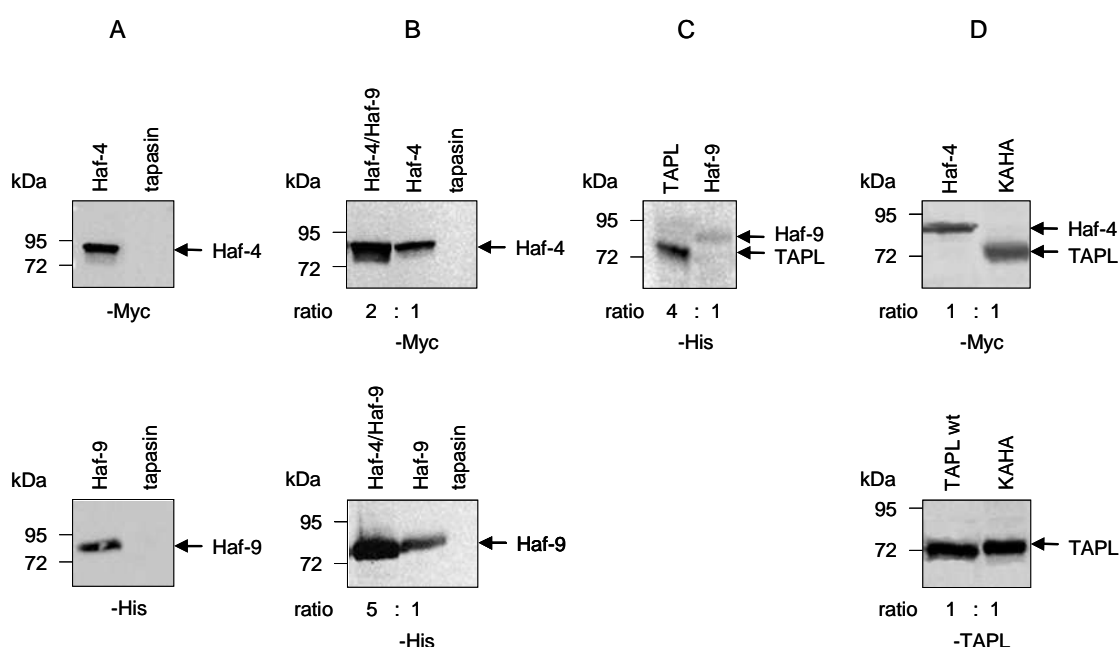


Figure 4-24. Expression analysis of Haf-4 and Haf-9. *A*, single expression of Haf-4 or Haf-9. Crude membranes containing Haf-4-Myc or Haf-9-His were analyzed by SDS-PAGE (10%) and immunoblotting against different tags. Membranes containing tapasin were used as a negative control. *B*, co-expression of Haf-4 and Haf-9. Membranes containing Haf-4-Myc, Haf-9-His or Haf-4-Myc/Haf-9-His were analyzed by SDS-PAGE (10%) and immunoblotting against Myc-tag or His-tag. Due to sensitivity reason, membranes containing 50 μ g total membrane protein was used for the anti-Myc blot, whereas 250 μ g total protein was analyzed in the anti-His blot. *C*, comparison of TAPL and Haf-9 expression. Membranes (50 μ g of total protein) containing His₁₀-tagged TAPL and Haf-9 were analyzed by SDS-PAGE (10%) and immunoblotting against His-tag. *D*, comparison of TAPL and Haf-4 expression. *Sf9* cells and MRJ cells (7×10^5 cells) expressing Haf-4-Myc, TAPL wt and its KAHA mutant were lysed in 1 \times SDS sample buffer and proteins were separated by SDS-PAGE (10%) followed by immunoblotting against the indicated antibodies. The immunoblotting signal ratios were listed.

4.12.2 Haf-4 and Haf-9 are ATP-dependent peptide transporters

To understand the physiological functions of Haf-4 and Haf-9, it is essential to look for their substrates. Since their human ortholog TAPL functions as a specific and ATP-dependent

peptide transporter, I investigated whether Haf-4 and Haf-9 could also transport peptide. The crude membranes derived from insect cells infected with baculovirus coding for various proteins were tested for transport by incubating with 3 mM ATP, 5 mM MgCl₂ and 3 μM of fluorescein-labeled peptide RRYC^fKSTEL for 3 min at 37 °C (Figure 4-25A). Haf-4, Haf-9 and co-expressed Haf-4/Haf-9 showed ATP-dependent transport as TAPL, however, the transport (+ ATP) to background (- ATP) ratio was much smaller than for TAPL, indicating a low transport activity for the given peptide. The membranes containing TAPL showed an ATP-dependent transport rate of $145.2 \pm 0.6 \text{ pmol min}^{-1} \text{ mg}^{-1}$ and a signal-to-background ratio (SBR) of 19.6; Haf-4 membranes had a transport rate of $7.4 \pm 1.0 \text{ pmol min}^{-1} \text{ mg}^{-1}$ and a SBR of 3.6; Haf-9 membranes showed a transport rate of $4.1 \pm 1.0 \text{ pmol min}^{-1} \text{ mg}^{-1}$ and a SBR of 1.7; membranes containing Haf-4 and Haf-9 had a transport rate of $7.5 \pm 2.5 \text{ pmol min}^{-1} \text{ mg}^{-1}$ and a SBR of 2.5; membranes containing tapasin were not active in transport as expected. Based on the expression level quantified by immunoblotting (Figure 4-24C,D), Haf-4 and Haf-9 have 20- and 9-fold lower transport activities than TAPL, respectively. Haf-4 is 2-fold more active than Haf-9. Besides that, the co-expressed Haf-4 and Haf-9 show a decrease in transport (4- and 5-fold lower than Haf-4 and Haf-9, respectively) when they exclusively form heteromers (see below).

Since *C. elegans* is normally cultivated at 20–25 °C, I tested whether the transport activity of Haf-4 and Haf-9 shows a temperature dependence distinct from TAPL (Wolters et al., 2005). Therefore, the transport activities of TAPL, Haf-4 and Haf-9 at 37 °C and 25 °C were compared (Figure 4-25B). Similar to TAPL which showed 60% reduced peptide transport at 25 °C compared to 37 °C, Haf-4 and Haf-9 also showed reduced transport (~25%) at 25 °C, suggesting that physiological temperature of nematode is not optimal temperature for the transport activity of Haf-4 and Haf-9 expressed in *Sf9* insect cells.

In contrast to TAPL, of which transport is saturated after 3–4 min (Wolters et al., 2005), the transport rates for Haf-4 and Haf-9 were still in the linear range within at least 10 and 20 min, respectively (Figure 4-25C,D *inset*). Therefore, the following transport experiments were performed for 10 min and 20 min for Haf-4 and Haf-9, respectively, to get a better signal-to-background ratio.

The specificity of ATP-dependent transport was studied in detail using several nucleotides as controls. The peptide transport of Haf-4 and Haf-9 was specifically driven by ATP hydrolysis because the addition of ADP as well as non-hydrolyzable ATP analogues AMP-PNP and ATPγS showed the similar background fluorescence as controls with apyrase or no nucleotide

(Figure 4-25C,D). The peptide specificity of Haf-4 and Haf-9 dependent transport was demonstrated by the competition of transport with a 200-fold excess of unlabeled competitor peptide RRYQKSTEL (Figure 4-25E). In conclusion, Haf-4 and Haf-9 show ATP- and peptide-specific transport.

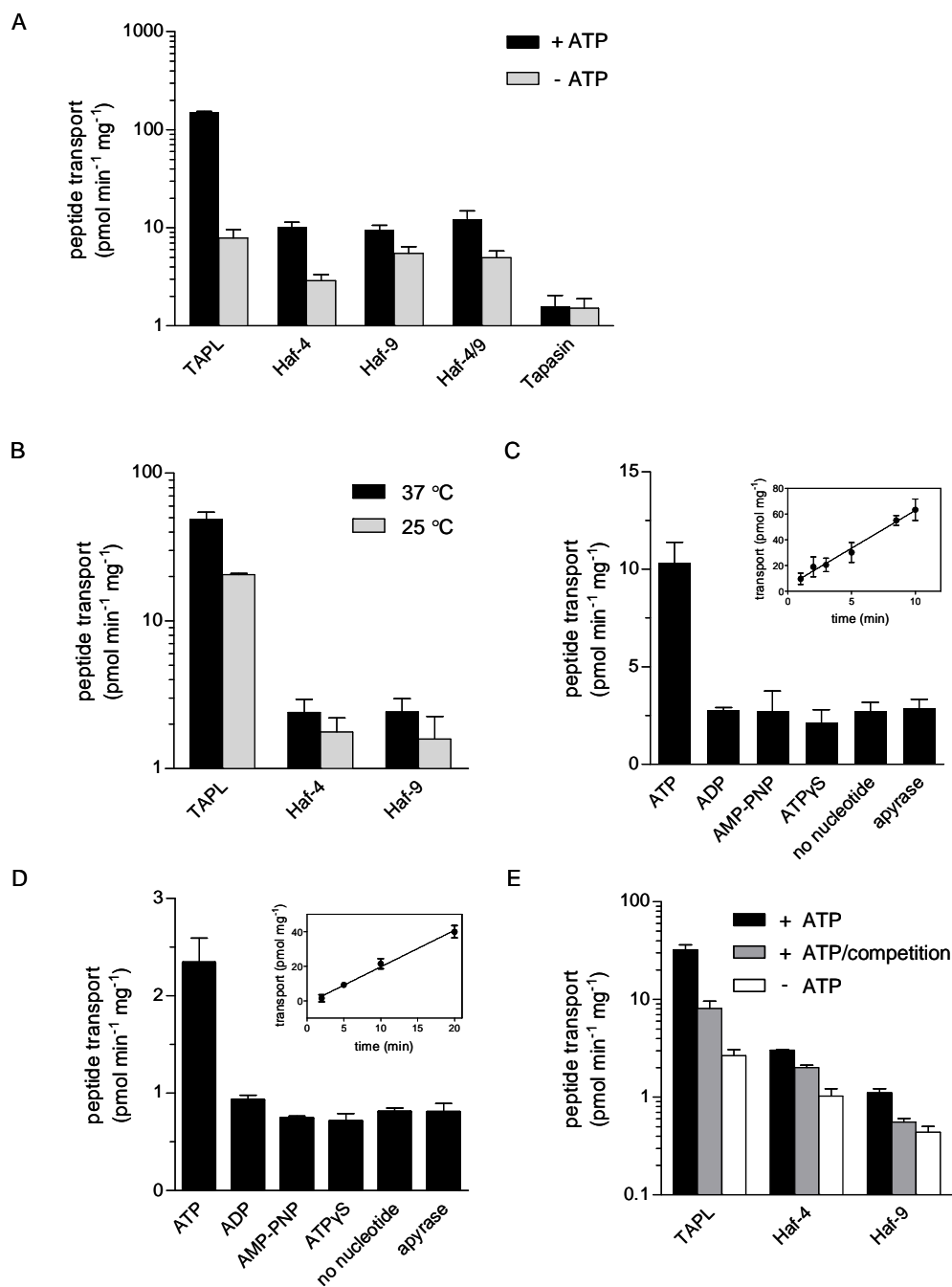


Figure 4-25. Peptide transports of Haf-4 and Haf-9. **A**, Haf-4 and Haf-9 specific transport. Membranes derived from *Sf9* cells (25 μ g of total protein) containing TAPL, Haf-4, Haf-9, Haf-4/Haf-9 or tapasin were incubated with 3 μ M fluorescein-labeled peptide RRYC^FKSTEL and 5 mM MgCl₂ in PBS for 3 min at 37 °C, in the presence or absence of 3 mM ATP. **B**, temperature-dependent peptide transport. Two temperatures were tested for peptide transport (37 °C and 25 °C). The transport was performed as described above, but the transport time

for TAPL, Haf-4 and Haf-9 were 3 min, 10 min and 20 min, respectively, to get better signal to background ratios (also for the following experiments). *C* and *D*, ATP-dependent transport of Haf-4 (*C*) and Haf-9 (*D*). All kinds of nucleotides or nucleotide analogues in the transport assay had a concentration of 3 mM, whereas the background transport activity was measured in the presence of apyrase (1 unit) or no nucleotide. *E*, peptide-dependent transport. Transport was performed with 1 μ M of fluorescein-labeled peptide RRYC^fKSTEL in the presence or absence of 200 μ M unlabeled competitor peptide RRYQKSTEL, and in the presence or absence of 3 mM ATP. The experiments were performed in triplicate. *Error bars*, S.D. The *insets* indicate that the transport was measured in the linear range.

The weak transport of Haf-4 and Haf-9 could be caused by the retention of both transporters in the ER and the resulting peptide export from microsomes. However, glycosylation traps peptides in the ER (Koopmann et al., 2000). In order to get a hint of Haf-4 and Haf-9 localization, a glycosylation transport assay was performed for Haf-4, Haf-9 or both proteins co-expressed, and TAPL served as control. The peptide used in the glycosylation assay was RRYQNSTC^fL (NST is a glycosylation sequence) which could be purified via the ConA beads after glycosylation in the ER lumen. Haf-4, Haf-9 or co-expressed proteins had weak transport in this assay. In comparison with transport rates in the direct transport assay, Haf-4, Haf-9 and co-expressed proteins showed 30-, 110- and 30-fold decreased transport, respectively, which is similar to the lysosomal transporter TAPL (50-fold decreased transport in the glycosylation assay). Since peptide glycosylation only happens in the ER compartment, the results indicate that most of Haf-4, Haf-9 and co-expressed proteins are not localized in the ER of *Sf9* cells (Figure 4-26). The slight transport activities might come from transporters which are synthesized in the ER but haven't trafficked to the other subcellular compartments.

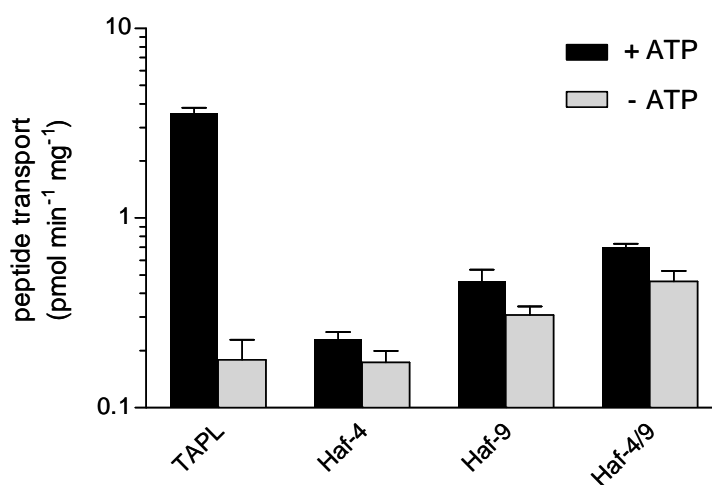


Figure 4-26. ER-specific transport. Membranes (100 μ g of total protein) containing Haf-4, Haf-9 or both proteins co-expressed were incubated with 5 mM MgCl₂ and 3 μ M fluorescein-labeled peptide RRYQNSTC^fL for 3 min at 37 °C, in the presence or absence of 3 mM ATP. The glycosylated peptides were pulled down by 50 μ l ConA beads as described in the *Methods* part. For a negative control, membranes containing TAPL were treated in the same way. The data represent the average of triplicate measurements and the *error bars* show S.D.

4.12.3 Interaction between Haf-4 and Haf-9

Since Haf-4 and Haf-9 were predicted half transporters and found in the same cells and the same compartment, the question whether they form homo- and/or heterodimers was raised. The single expressed Haf-4 and Haf-9 were active in peptide transport, which could be an indication for the homodimerization of these two half transporters. The interaction between Haf-4 and Haf-9 was investigated by co-immunoprecipitation. *Sf9* cell membranes containing co-expressed Haf-4-Myc/Haf-9-His were solubilized with 1% digitonin and applied to anti-mouse IgG magnetobeads coupled with a mouse monoclonal anti-Myc antibody. The specific interaction between Haf-4 and Haf-9 was clearly proved by co-immunoprecipitation of His₁₀-tagged Haf-9 with the anti-Myc antibody coupled magnetobeads. The precipitation was antibody specific since an unrelated antibody (monoclonal antibody HC10 against MHC class I molecule) could precipitate neither Haf-4 nor Haf-9 (Figure 4-27). From signal quantification on both anti-Myc and anti-His immunoblots, the signal ratios between the input (the solubilizate) and eluate were identical (10:1). In conclusion, Haf-4 and Haf-9 seem to form heteromers (likely heterodimers) exclusively when co-expressed.

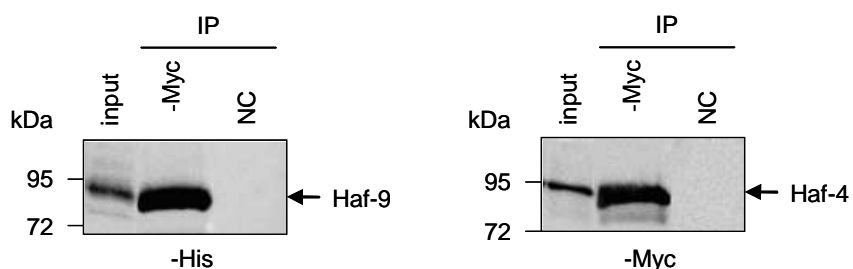


Figure 4-27. Co-immunoprecipitation of co-expressed Haf-4/Haf-9. *Sf9* cell membranes (2.5 mg of total protein) containing co-expressed Haf-4-Myc and Haf-9-His were solubilized with 1% digitonin and applied onto magnetobeads coupled with an anti-Myc antibody. The beads were washed and eluted as described in the *Methods* part. Fractions from the solubilizate (input, aliquot of 1/50) and eluate were analyzed by SDS-PAGE (10%) and immunoblotting using antibodies against different tags. The magnetobeads coupled with a monoclonal antibody against MHC class I (HC10) were used as a negative control (NC).

5 Discussions

Based on systematic screens of various detergents for the solubilization as well as the optimization of the purification and reconstitution procedures, I succeeded in the functional reconstitution of the human lysosomal transport complex TAPL, a milestone for the research on eukaryotic ABC transporters. In contrast to the multidrug transporters as well as the lipid/cholesterol transporters reconstituted so far, TAPL transports hydrophilic peptides, which are easily quantified and are also good targets for systematic modifications.

The functional reconstitution enabled me to decipher the substrate specificity of TAPL with the help of combinatorial peptide libraries. The key residues are restricted to the N- and C-terminal positions, of which the positively charged, aromatic and large hydrophobic amino acids are preferred and the negatively charged residues as well as Asn and Met are disfavored. Moreover, peptides with a positive net charge are favored in contrast to the negatively charged peptides.

For studying the structure, mechanism and dynamics of TAPL during peptide transport cycle, using biophysical methods such as EPR or FRET, TAPL cys-less and single cysteine mutants were generated and characterized. Most of them are fully functional in terms of peptide transport, therefore, could be subjected to spin or fluorescence labeling for further projects.

To understand the physiological functions of TAPL orthologs Haf-4 and Haf-9 from *C. elegans*, both proteins were expressed in insect cells and characterized as ATP-dependent peptide transporters. Moreover, for the first time, it was shown that both half transporters form heteromers.

5.1 Solubilization, purification and reconstitution

5.1.1 Solubilization

A prerequisite for the analysis of substrate specificity was the solubilization, purification, and reconstitution of TAPL. From the solubilization screen, digitonin and DDM were the most powerful detergents with respect to efficiency, stability, and function of TAPL. OG, CHAPS, and Zwittergent 3-12 showed low solubilization efficiency paired with strong destabilization of TAPL. Short alkyl chain detergents and also zwitterionic detergents are beneficial for the reconstitution because of their high critical micelle concentration. However, they often suffer from the low solubilization efficiency as well as low long term stability of membrane proteins (Seddon et al., 2004). Fos-14 was acceptable as regards to solubilization and stability but

disrupted the homodimeric peptide transport complex. This also has been reported for other membrane proteins (Herget et al., 2007). A similar solubilization pattern was derived from TAPL expressed in Schneider cells (Ohara et al., 2008).

Digitonin was used for most of the substrate specificity studies, however, DDM was also found to preserve TAPL function after proper optimization of the detergent concentration and ion strength in the solubilization trials. Solubilization by DDM was concentration dependent, the solubilization efficiency reached maximum at 0.5% DDM and decreased upon increasing DDM concentrations. The observation was different from digitonin, of which the solubilization efficiency stayed constant after reaching maximum at 1% digitonin (data not shown). Moreover, the effects of NaCl concentration on solubilization were significant. Solubilization efficiency was maximal at 150 mM NaCl, but reduced at higher concentrations. The same was true for LacS, of which the reduced solubilization efficiency at high salt concentration was due to protein aggregation (Knol et al., 1996). Remarkably, the activity of reconstituted TAPL was strongly dependent on the DDM concentration used for solubilization. Using 0.3–0.5% DDM for the solubilization of membranes, reconstituted TAPL showed the same activity as TAPL purified in the presence of digitonin. However, TAPL solubilized with 1% DDM was inactive after reconstitution. Lower DDM concentrations might prevent the strong delipidation by mimicing the effect of digitonin, which is believed to be less delipidating during the solubilization of membranes (Wittig et al., 2006).

5.1.2 Purification

To obtain high purity of the transport complex required for biochemical and biophysical studies with few purification steps, TAPL containing a C-terminal Strep-tag II or His₁₀-tag was generated (Wolters et al., 2005) to facilitate purification in one step. However, the Strep-tagged TAPL did not bind to the Strep-Tactin Superflow matrix (IBA) tightly and the purity was very low. For the His-tag affinity chromatography, different column resins from various companies were tested and compared. TAPL did not show high affinity for the Ni-NTA agarose from Qiagen, but bound tightly with the HIS-Select[®] Nickel Affinity Gel (agarose beads, Sigma) and Hitrap[™] Chelating HP column (IDA(iminodiacetic acid)-agarose beads, GE healthcare) loaded with Zn²⁺. Zn²⁺ is preferred for IDA column over Ni²⁺ because it significantly increases the affinity of TAPL on IDA column (data not shown). This might be explained by the accessibility of His₁₀-tag in the presence of detergent micelle since two vincinal histidines are enough to bind Zn²⁺, whereas Ni²⁺ binds specifically to His-tag

(manufacturer's instruction of IDA columns from GE healthcare). For ease of handling with the FPLCTM system, the prepacked HitrapTM Chelating HP column was used for purification. After many trials on the optimization of single-step purification via the His₁₀-tag, especially, varying the imidazole concentration in the binding step and stringent washing with a high concentration of imidazole, it was still difficult to achieve high purity. Therefore, the combination of IMAC followed by anion exchange or affinity chromatography with ATP-agarose was tested. However, the purity was still not improved by either of these strategies. Moreover, TAPL was eluted at high salt concentration (500 mM NaCl) on strong anion exchanger Q SepharoseTM matrix (GE healthcare), which obviously was not a suitable condition for the protein activity. TAPL did not bind to ATP-agarose tightly and ~85% of the protein was lost in the flow-through and washing steps (data not shown).

Since TAPL tightly binds to the strong anion exchanger, I established a gentle two-step method. First, impurities were removed by cation exchange chromatography because TAPL does not bind to the cation exchange matrix, hence, the denaturation of TAPL by surface contacts as well as its loss was minimized. In the second step, TAPL was isolated to more than 95% purity via IMAC. The cation exchange step was essential to remove background ATPase activity for the precise quantification of TAPL-specific ATP hydrolysis. The purifications with digitonin and DDM were performed in the same procedure but ended up with different purities. Digitonin gave higher purity than DDM, and this difference might reside in the solubilization of more contaminant proteins by DDM.

5.1.3 Reconstitution

The functional reconstitution of membrane proteins is a critical step depending on different parameters. Therefore, I optimized TAPL reconstitution into liposomes for the highest transport activity with respect to the detergent used in destabilization of liposomes, lipid-to-protein ratio (LPR), detergent removal and temperatures.

The reconstitution procedure started with preparing large unilamellar liposomes by extruding lipid suspension through a 400-nm filter. The preformed liposomes were then destabilized by increasing concentrations of detergents. The destabilization process could be followed by determining the turbidity of the suspension (Figure 4-7B). The solubilization of liposomes can be subdivided into three distinct phases. In the first phase, the light scattering increases due to the enlargement of liposomes by the incorporation of detergents into the phospholipid bilayer until a saturated detergent concentration (R_{sat}) is reached. In the second phase, the lamellar

structures are disrupted and the mixed micelles of lipids and detergents start to form, resulting in a drastic decrease of turbidity by increasing detergent concentrations. In the third phase, the liposomes are completely solubilized and, consequently, the solution becomes optical transparent. The detergent concentration at which liposomes are completely solubilized is called R_{sol} (Paternostre et al., 1988). Liposome destabilization was essential for efficient reconstitution of TAPL since a drastic reduction in the transport activity was shown when the preformed liposomes were not destabilized. However, no significant difference in TAPL activity was observed for Triton X-100 concentrations between R_{sat} and R_{sol} , indicating that the total solubilization of liposomes was not beneficial. Similar observations were also made for other membrane proteins including F_0F_1 -ATPase from chloroplasts (Richard et al., 1990), the glutamate carrier from *B. stearothermophilus* (Gaillard et al., 1996), the lactose transport protein from *S. thermophilus* (Knol et al., 1996), and the erythrocyte membrane anion exchanger, band 3 (Boulter et al., 1996). It is likely that Triton X-100 mediated the unidirectional incorporation of TAPL into liposomes as for other membrane proteins.

For liposome destabilization, the mild detergents are preferred to prevent membrane protein denaturation (Geertsma et al., 2008). It was also true for TAPL, when the digitonin-purified protein was mixed with the OG-destabilized liposomes, no transport activity was observed, which may be due to a reduced protein stability in OG. The peptide transport activities of the reconstituted TAPL were preserved when Triton X-100, DDM or DM were used to destabilize liposomes at a concentration slightly above R_{sat} . However, Triton X-100 gives the highest activity among these detergents followed by DDM and then DM (data not shown). The distinct activity of reconstituted TAPL mediated by different detergents could be explained by many critical parameters of detergents: the partition into lipid bilayer, molecular shape and flip-flop rate in the bilayer (Knol, 1999). Triton X-100 has a high degree of lipophilicity which is consistent with its rapid equilibration in lipid bilayer and high flip-flop rate between the outer and inner leaflets of membrane (le Maire et al., 1987; Kragh-Hansen et al., 1998). Based on cryo-EM observations (Knol et al., 1998; Lopez et al., 1998), it has been speculated that Triton X-100 has a molecular shape allowing lipid bilayer to exist over a broad range of detergent concentrations without disrupting liposomes (Knol et al., 1998). This stability of Triton X-100 saturated liposomes makes membrane protein incorporation efficiently and unidirectionally over a broad detergent concentration range. In contrast, detergents with the shape of inverted cones (DDM and OG, may be also DM) partition into lipid bilayer very slowly and cause the liposomes to form sheets at R_{sat} followed by long thread-like micelles at higher detergent

concentrations (Knol et al., 1998; Lambert et al., 1998). If membrane proteins only randomly incorporate into the membrane sheets that are formed relatively slowly upon removing detergents, unstable proteins might lose their activity and/or form aggregates (Groth and Walker, 1996; Knol et al., 1996).

Once the best detergent has been determined, other parameters such as the lipid-to-protein ratio (LPR), temperature, and detergent removal must be optimized. The activity of many membrane proteins depends strongly on the lipid-to-protein ratio (Richard et al., 1990; Pitard et al., 1996; le Coutre et al., 1997; Spooner et al., 2000). To study the factor of lipid-to-protein ratio, the initial concentration of protein is very important. The higher this initial concentration is, the lower is the amount of detergent brought with the protein into the equilibrated lipid-detergent mixtures (Rigaud and Levy, 2003; Poolman, 2005), assuming free detergent micelles (generally <50 kDa) are removed when concentrating via a 100 kDa-cutoff filter. Therefore, the protein volume used for reconstitution was always 10% of the total lipid-protein mixture. Proteoliposomes prepared at LPR of 20 (w/w) showed peptide transport. However, no peptide transport was observed at a LPR of 200 (data not shown). Interestingly, no significant difference in protein incorporation efficiency was observed for the above two LPRs as analyzed by freeze-fracture EM (see below). TAPL activity decreased drastically upon concentrating, suggesting TAPL aggregation may occur in the concentrating process. The detailed studies on LPR were difficult since low LPR (<20 (w/w)) needs further concentrating of proteins, resulting in complete loss of TAPL activity (data not shown).

For some relatively stable membrane proteins, the standard protocol for reconstitution is the incubation of proteins with destabilized liposomes for 30–60 min at room temperature followed by successive additions of Bio-Beads to remove detergents at room temperature and/or 4 °C (Pitard et al., 1996; Borths et al., 2005; Geertsma et al., 2008; Zehnpfennig et al., 2009). The protein incorporation is improved by mixing the liposomes and protein at 20 °C rather than 4 °C, which is probably related to increased fluidity of the lipid bilayer and/or a change in micellar size (Hjelmeland, 1980; Knol et al., 1998; Knol, 1999). Therefore, different temperatures (30, 25 or 4 °C) were tested for incubation of protein with destabilized liposomes. Working in the cold room (4 °C) all the time gives higher transport activities and an increased reproducibility (data not shown), indicating TAPL inactivation may happen at higher temperatures. On the other hand, the detergent adsorption rate by Bio-Beads doubles every 12 °C, although the total binding capacity is independent of temperature (Levy et al., 1990; Rigaud et al., 1997; Rigaud et al., 1998). However, the fast detergent removal could also be

harmful for the protein, if the detergent removal is faster than membrane insertion of the protein. Therefore, Bio-Beads were added four times with a concentration of 40 mg/ml and incubated for 1 h, overnight, 2 h and another 2 h at 4 °C for slow and complete removal of detergents as well as preventing TAPL denaturation.

Once the purified membrane protein has been mixed with detergent-destabilized liposomes, subsequent controlled, slow removal of detergent is needed for the formation of tightly sealed proteoliposomes. The detergent removal can be performed using different techniques: (i) dilution; (ii) dialysis, (iii) gel filtration, or (iv) adsorption via polystyrene beads (Rigaud *et al.* 1995, 2003). The first two methods are mostly limited to remove detergents with high CMC. The gel filtration is a rapid technique that sometimes causes incomplete and/or inhomogeneous protein incorporation as well as heterogeneous size distribution of proteoliposomes (Rigaud *et al.*, 1998; Rigaud and Levy, 2003). To remove the mild and low CMC detergents, such as DDM or Triton X-100, using polystyrene beads is a more efficient way with sufficient reproducibility. A similar observation was also made for removing Triton X-100 with dialysis, gel filtration (Sephadex G-50) and Bio-Beads in TAPL reconstitution trials. TAPL showed almost no transport after removal of detergents with dialysis and gel filtration, comparing with Bio-Beads adsorption. Moreover, proteoliposomes prepared with Bio-Beads are tightly sealed (N. Kreissig, R. Tampé, and R. Abele, unpublished data), and could be snap-frozen in liquid N₂ followed by storage at -80 °C for couples of weeks, which all facilitate the characterization of reconstituted TAPL.

Given the mammalian origin of TAPL, it was surprising that TAPL was inactive when reconstituted in lipid extracts from bovine heart, brain, or liver but showed the similar activity as in crude membranes when reconstituted in the *E. coli* lipid extracts. Although the activities of TAPL are similar in the total and polar *E. coli* lipids, I prefer the polar extract due to easier extrusion during the liposome preparation and high reproducibility. Whether the lack of transport activity in bovine lipid extracts is due to the lipid composition, impurities in the extract, or incomplete sealing of the liposomes was not further investigated. The addition of DOPC to the *E. coli* lipids substantially increased the transport activity of TAPL. Hence, phosphatidylcholine, which is the bulk phospholipid in most mammalian membranes, but absent in *E. coli* (DiRusso and Nystrom, 1998; van Meer *et al.*, 2008), seems to have a stimulating effect on TAPL activity. Furthermore, introducing negatively charged phospholipids to pure DOPC increased TAPL activity. However, this is not only due to the negative charge of the lipid head group, since phosphatidylserine and phosphatidic acid are

preferred, whereas no transport is detected with PG.

Cholesterol is only found in eukaryotes, particularly in the animal plasma membranes, lysosomes, endosomes and Golgi apparatus. The concentration of cholesterol is especially high in the animal plasma membranes (20–30%) (Voet and Voet, 2004). Cholesterol can also be included into phospholipid mixtures to provide greater stability and better impermeability of the reconstituted proteoliposomes to ions and small polar molecules (Rigaud and Levy, 2003). However, the reconstitution in lipid mixtures containing DOPC and *E. coli* lipids doped with 5–30% cholesterol or a mixture of cholesterol (10%) and sphingomyelin (20%) resembling lysosomal lipid environment did not recover TAPL activity. TAPL appeared to be aggregated but not incorporated into liposomes in the presence of cholesterol and sphingomyelin since the transporter was found at the bottom of a sucrose gradient (10–45% sucrose) after centrifugation (data not shown).

To confirm TAPL incorporation into liposomes, freeze-fracture EM was performed. The size of proteoliposomes was heterogenous and smaller (mean diameter of 100 nm) than expected. No difference in protein incorporation was observed when using different LPRs (200 or 20, w/w). In general, only low incorporation was detected with a lot of empty liposomes. One explanation for this data could be the low incorporation efficiency of TAPL into liposomes, which is independent of LPR. Nevertheless, the theoretical protein molecules per liposome would be 1 or 10 (LPR of 200 or 20, w/w), assuming the molecular weight for TAPL and phospholipids of 172 kDa and 700 Da, respectively, the averaged liposome diameter of 100 nm and the lipid headgroup area of 0.7 nm^2 . Therefore, it may be difficult to detect in each liposome a TAPL molecule at the given LPR with freeze-fracture EM considering the presence of slight protein aggregation during reconstitution, protein loss in EM sample treatment, and visualization of only less than 50% of the surface of each liposome. Remarkably, in the dual-color fluorescence-burst analysis (DCFBA) (using a LPR of 40), almost each liposome was filled with fluorescent peptides in an ATP- and TAPL-dependent manner, indicating most of the liposomes contained active TAPL (data not shown). In DCFBA, the cross-correlation signal of a liposome doped with fluorescently labeled lipid analogs and a fluorescence-labeled peptide is recorded.

5.2 Oligomeric status

Using the size exclusion chromatography and blue native PAGE, TAPL purified in the presence of digitonin or DDM had the size of a dimer, which was consistent with the

homodimer formation confirmed by the pull down assay (Wolters et al., 2005), dihydrofolate reductase protein-fragment complementation assay in SKOV3 cells (Leveson-Gower et al., 2004) and cross-linking assay (Ohara et al., 2008). The dimerization region seems to be within the TMD of core-TAPL since the core-TAPL also migrates at the size corresponding to a dimer on BN-PAGE (data not shown).

Determining the oligomeric status of integral membrane proteins is notorious difficult since the amount of associated detergents and lipids are usually unknown (Slotboom et al., 2008). The mass ratios of detergent-to-protein are in the range of 1–5, depending on the volume ratio of the hydrophobic and hydrophilic domains of membrane proteins (Yernool et al., 2003; Wei et al., 2004; Bamber et al., 2006; Kunji et al., 2008; Slotboom et al., 2008). Moreover, in gel filtration, water-soluble proteins do not bind to detergents (Wittig and Schägger, 2008) and the elution volumes are not affected by detergents (Kunji et al., 2008). Therefore, gel filtration using soluble protein standards is a low-resolution method for determining the molecular weight of membrane proteins like TAPL, unless bound detergents are investigated carefully by observing the hydrodynamic radii in detergent series (Bamber et al., 2006). In gel filtration, the digitonin-purified TAPL had a single monodisperse species with a hydrodynamic radius corresponding to a soluble protein of 200 kDa. The result shows only a 20% deviation from the theoretical molecular weight (172 kDa) of TAPL dimer without any information of bound detergents and lipids. The DDM-purified TAPL was not as pure as digitonin-purified protein and showed a broad peak roughly corresponding to the same hydrodynamic radius as digitonin-purified TAPL. Digitonin and DDM were reported to account for 80% and 70% of mass of the yeast mitochondrial ADP/ATP exchanger, respectively (Bamber et al., 2006). Therefore, it seems that 20% weight contribution of the bound detergents to detergent-TAPL complex was underestimated. Remarkably, α -hemolysin from *Staphylococcus aureus* binds less DDM (0.3 g/g protein) (Yernool et al., 2003). Moreover, the possibility that TAPL exists as monomer in the presence of digitonin and DDM can be ruled out by the pull down assay of different tagged TAPL (Figure 4-3). Thus, TAPL forms a dimer in the presence of digitonin and DDM.

Determination of the molecular mass and oligomeric status by blue native PAGE also have more than 10% error due to various amount of lipids and/or Coomassie blue dyes bound to membrane proteins, although most of the bound detergents are replaced by Coomassie blue during electrophoresis (von Jagow et al., 1977; Schägger et al., 1990; Heuberger et al., 2002; Wittig and Schägger, 2008). For example, the respiratory chain complex III (~500 kDa) still

binds 80–100 lipid molecules (56–70 kDa) after isolated chromatographically (Schägger et al., 1990), and various amounts of dyes bind to the respiratory chain complexes (0.4, 0.35, 0.5 and 0.59 g/g for complex I, III, IV and V, respectively) after BN-PAGE (Wittig and Schägger, 2008). Moreover, some membrane transporters were reported to bind even higher amount of Coomassie dyes (0.8 g/g) (Heuberger et al., 2002). Therefore, it is not surprising that the determined apparent molecular weight (200 kDa) of TAPL dimer has 20% deviation from the theoretical value. In some of the BN-PAGE trials, TAPL solubilized by digitonin did not only form dimers but also higher oligomers. However, the formation of higher oligomers could be an artifact caused by protein overexpression, solubilization conditions or different properties among distinct batches of detergents. Interestingly, the Strep-tagged TAPL solubilized with digitonin often shows the presence of different oligomers with dimers as the dominant population, which is really puzzling to explain. The BN-PAGE of solubilized endogenous TAPL from mammalian cells might help to address the oligomeric status of this ABC transporter under physiological conditions. Nevertheless, BN-PAGE for endogenous TAPL needs to be optimized in terms of solubilization and detection.

5.3 Substrate specificity

Based on the data presented herein together with our earlier study (Wolters et al., 2005), the substrate specificity of TAPL has been deciphered. TAPL recognizes peptides via the N- and C-terminal residues and also the free N- and C-termini. The sequence in between can be highly variable in length and composition, allowing the translocation of a broad spectrum of peptides by one transporter (Figure 5-1). Clearly, the C-terminal position has the strongest effect on peptide selectivity, since modification at this position has the strongest impact on transport activity. Moreover, the variability at this position is also higher than at the N-terminal position. Positions 2 and 3 of the peptide seem to have minor effects on peptide selectivity. Those positions had no influence in the D-amino acid scan, whereas fluorescein or aspartate at these positions only marginally disfavored peptide transport. Since fluorescein as well as the side chain of Asp are negatively charged at physiological pH, electrostatic repulsion can cause decreased transport rates. Further electrostatic interactions appear to be responsible for the preferred transport of positively charged peptides. Two scenarios can be considered: (i) the environment of the peptide-binding pocket or the translocation pathway is negatively charged and therefore favors positively charged peptides, or (ii) the negatively charged membrane increases the local concentration of positively charged peptides in the vicinity of the

transporter, which partially explains the dependence of peptide transport on the concentration of phosphatidylserine in the proteoliposomes.

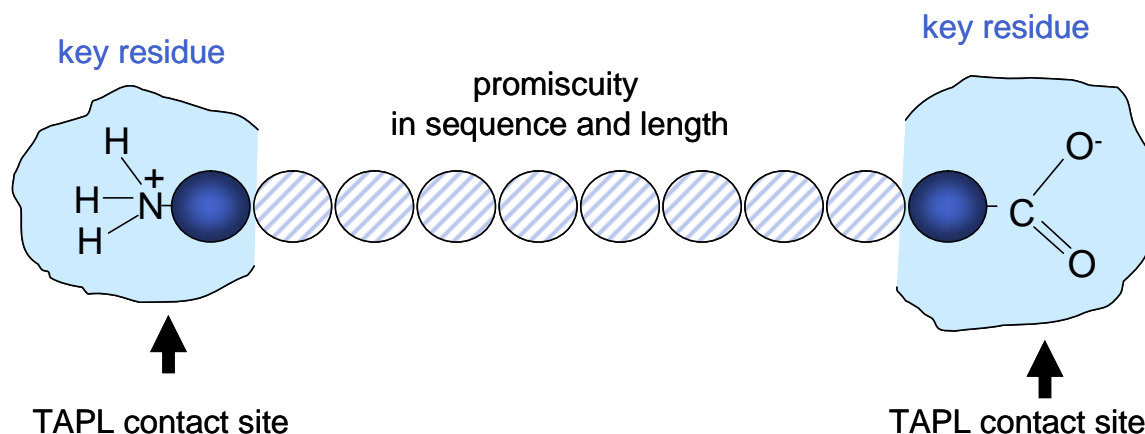


Figure 5-1. Peptide recognition by TAPL. The key residues contacting TAPL are depicted in *blue circles*, and the uncritical ones which are promiscuous in sequence and length are shown in *line-filled circles*.

Besides this global effect, there are also minor differences between the single positions. TAPL shows some preference for peptides with an Asp at position 4. Moreover, a peptide with a negatively charged fluorescein at position 4 is favored in transport. Therefore, it is feasible that the negative charge at this position is counterbalanced by positive charged residues in the peptide-binding pocket. Derived from the fluorescein scan, the second last position in the peptide seems to have a high degree of freedom. It could be conceivable that the side chain at this position does not stay in contact with TAPL but points into the liquid-filled environment. The selectivity of TAPL and the related heterodimeric antigenic peptide transporter TAP, which share 40% sequence identity (Zhang et al., 2000), show a strong overlap. Not only free N- and C-termini but also the key positions and selectivity principles are almost identical. Moreover, the C-terminal residue shows the highest impact on peptide selectivity (Heemels et al., 1993; Momburg et al., 1994; Uebel et al., 1995; van Endert et al., 1995; Gromme et al., 1997; Uebel et al., 1997). However, there are distinct differences. Positions 2 and 3 of the peptide are also critical for recognition by TAP (Hinshelwood et al., 1995; van Endert et al., 1995; Uebel et al., 1997), whereas these residues have only a minor impact on TAPL selectivity. The importance of positions 2 and 3 for selectivity of TAP is slightly dependent on the method used for analysis. By peptide binding and competition assays, positions 2 and 3 show the same impact on TAP binding as position 1 (van Endert et al., 1995; Uebel et al., 1997). However, by transport assays in semipermeabilized cells, which rely on trapping peptides in the endoplasmic reticulum by glycosylation, minor effects of positions 2 and 3 for

peptide selectivity were detected (Neefjes et al., 1995).

TAPL transports peptides with a broad length specificity ranging from 6- to at least 59-mer but low affinity (Wolters et al., 2005). In contrast, TAP translocates peptides between 8 and 16 amino acids in length with high affinity, whereas 6-mer peptides are no substrate (Neefjes et al., 1993; Androlewicz and Cresswell, 1994; van Endert et al., 1994). If the peptide selectivity of TAPL results from the binding step, as shown for TAP (Androlewicz and Cresswell, 1994; Neumann and Tamp e, 1999; Gorbulev et al., 2001), the differences must reside in the binding pocket. Based on peptide photocross-linking studies and truncation studies, the peptide-binding region of TAP1 and TAP2 is localized at the cytosolic loop between transmembrane helix 4 and 5 of the core complex (peptide-binding region 1 (PBR1)) and a stretch of 15 residues C-terminal of the last transmembrane helix connecting the TMD with the NBD (PBR2) (Nijenhuis and Hammerling, 1996; Ritz et al., 2001). The substrate-binding pocket in the TAP complex seems to be formed between TAP1 and TAP2 subunits, since peptides neither bind to nor are transported by single subunits (Meyer et al., 1994; van Endert et al., 1994), although homodimers can be formed (Antoniou et al., 2002; Oancea et al., 2009). Moreover, the asymmetry of the binding pocket restricts the orientation of the peptide, since TAP2 alleles in rats determine the selectivity for the C-terminal residue (Heemels et al., 1993; Powis et al., 1996; Wang et al., 1996). In contrast, TAPL forms a homodimeric complex, which has no sequence-based asymmetry (Leveson-Gower et al., 2004; Wolters et al., 2005). Interestingly, the putative PBR1 of TAPL shows a much higher sequence identity to TAP1 than TAP2, whereas PBR2 is more homologous to TAP2 than TAP1. Based on the fluorescence cross-correlation spectroscopy experiments with TAP (M. Herget, R. Tamp e, and R. Abele, unpublished data) and on the sequence comparison of both peptide transporters, I assume that TAP contains one peptide-binding site formed mainly by PBR1 of TAP1 and PBR2 of TAP2, whereas the two corresponding regions (PBR2 in TAP1 and PBR1 in TAP2) are inactive as regards binding. On the other hand, TAPL can bind one peptide simultaneously to each subunit, since two active peptide-binding pockets are present. The different modes of peptide binding could also explain the broader length specificity of TAPL in comparison with TAP.

5.4 ATP hydrolysis

To study the transport mechanism of TAPL, ATP hydrolysis was measured in the detergent solubilized and reconstituted states. Reconstituted TAPL showed 6-fold higher ATPase activity than the digitonin solubilized form, suggesting lipids are important for keeping the function of

this ABC transporter. Similar observations were also made for other ABC transporters. For example, the ATP hydrolysis of ABCB1 (P-gp) and ABCC3 (MRP3) drastically increases (2–5 fold, depending on lipid compositions) in the presence of lipids (Lerner-Marmarosh et al., 1999; Chloupkova et al., 2007). Lipid compositions might affect the function of TAPL by changing the conformation or inhibiting the structural flexibility with curvature stress and/or lateral pressure as proposed for other membrane proteins (Gruner, 1985; Cantor, 1997; Lundbaek et al., 1997; Bezrukov, 2000; Curnow et al., 2004).

Peptide transport and ATP hydrolysis seem to be uncoupled for TAPL since no peptide stimulation was detected. In contrast, TAP shows peptide stimulated ATP hydrolysis which is 2.8-fold over basal ATPase activity. The ATPase activity shows hyperbolic dependency on peptide concentration (with V_{\max} of $\sim 2 \mu\text{mol min}^{-1} \text{mg}^{-1}$). In addition, the Michaelis-Menten constant for ATP hydrolysis ($K_{M(\text{pep})}$) directly correlates with the affinity constant (K_D) for the peptide, indicating a strict correlation between peptide binding and stimulated ATP hydrolysis (Gorbulev et al., 2001). The maximal transport rate (V_{\max}) of TAPL was roughly calculated to be $\sim 0.3 \text{ nmol min}^{-1} \text{mg}^{-1}$ (~ 0.05 peptide/min), which was in the same range of P-gp ($\sim 110 \text{ pmol min}^{-1} \text{mg}^{-1}$) and MRP1 (ABCC1, $\sim 125 \text{ pmol min}^{-1} \text{mg}^{-1}$), but one order of magnitude lower than MRP3 ($\sim 4.7 \text{ nmol min}^{-1} \text{mg}^{-1}$) (Dong et al., 1996; Mao et al., 2000; Zehnpfennig et al., 2009). Comparing with the transport activity, the basal ATPase activity for either purified ($\sim 45 \text{ nmol min}^{-1} \text{mg}^{-1}$; 7.8 ATPs/min) or reconstituted TAPL ($\sim 270 \text{ nmol min}^{-1} \text{mg}^{-1}$; 46 ATPs/min) was much higher. One explanation for the uncoupled ATP hydrolysis could be that a lot of purified and reconstituted TAPL was not active in transport but can still hydrolyze ATP. Nevertheless, the transport activity of TAPL could also be underestimated due to unknown amount of incorrectly inserted protein after purification and reconstitution. Notably, the uncoupled ATPase activity was also reported for other ABC transporters like P-gp, BtuCD and Pdr5 (Al-Shawi et al., 2003; Borths et al., 2005; Ernst et al., 2008). Moreover, completely coupled ATP hydrolysis and substrate transport (assuming 2 ATPs are hydrolyzed per substrate) was only observed for the OpuA system (Patzlaff et al., 2003; Poolman, 2005). More generally, the ATPase and transport rates differ by 1–3 orders of magnitude (Davidson and Nikaido, 1990; Chen et al., 2001; Patzlaff et al., 2003; Borths et al., 2005).

On the other hand, the uncoupled ATPase activity was believed to be evolutionarily conserved since a constant turnover of ATP induced conformational changes that always keep the cytosolic substrate binding sites accessible (Al-Shawi et al., 2003; Ernst et al., 2008). Instead of wasting energy, the basal ATPase activity was believed to keep the transporter in the

transport-competent state for rapid detoxification from the cells (Ernst et al., 2008). This seems to be true for TAPL, since this transporter might serve as a vacuum cleaner to remove a large variety of cytosolic peptides constantly and efficiently.

5.5 TAPL cys-less and single cysteine mutants

For studying the structure, dynamics and transport mechanism of TAPL, a TAPL cys-less mutant was generated. TAPL cys-less had 3-fold increased peptide transport activity over TAPL wt but consistent peptide transport kinetic constants for peptide and ATP. The functional cys-less mutant is a basis for introducing single cysteines into strategic positions and an optimal negative control for site-specific labeling reaction. Based on primary structural alignment with Sav1866, TAPL single cysteine mutants were introduced into putative rigid helical regions of TAPL cys-less. All single cysteine mutants were expressed by the baculovirus expression system and characterized for peptide transport activity. The mutants in the highly variable TMD showed similar activity as TAPL wt, however, the mutant L701C in the NBD had impaired peptide transport. The latter is close to the conserved H-loop motif and might interfere with ATP hydrolysis. Those functional single cysteine mutants are good starting points for cysteine-specific labeling. The distance changes between two labels will provide much information about the molecular dynamics during transport cycle. Besides pulsed EPR measurements, chemical cross-linking and FRET can also be used to study TAPL structural dynamics.

The strategy of site-directed labeling on single cysteines has been successfully applied to study transport mechanism of several ABC transporters in detergent micelles and liposomes (Borbat et al., 2007; Grote et al., 2008; Goetz et al., 2009; Grote et al., 2009). For example, the conformational changes during transport cycle of the Gram-negative bacteria lipid A exporter MsbA were investigated by pulsed dipolar EPR and fluorescence homotransfer (Borbat et al., 2007). The distance distributions between single cysteines labeled with spin- or fluorescent-probes revealed large-scale movements of MsbA homodimer upon ATP hydrolysis.

5.6 Haf-4 and Haf-9

Due to the high sequence identity with the peptide transporter TAPL, the intestinal half size transporters from *C. elegans*, Haf-4 and Haf-9 were first analyzed for their peptide transport activity. Haf-4, Haf-9 and both proteins co-expressed showed significant ATP-dependent peptide transport when expressed in *Sf9* insect cells. Nevertheless, the transport activities are

quite low comparing to TAPL for a 9-mer peptide. The explanation for the low activity could be the different substrate specificity as TAPL, missing of important cofactors for their function or distinct temperature requirements. The transport activities of Haf-4 and Haf-9 showed the similar temperature dependence as TAPL. The physiological temperature of *C. elegans* (25 °C) is not optimal for transport. Similar as TAPL, both transporters do not seem to localize in the ER since almost no glycosylated peptide was detected in the transport assay, which fits well with their lysosomal localization in *C. elegans* (Kawai et al., 2009). The slight transport observed in the glycosylation assay could come from transporters which still reside in the ER. The peptide transport activity of Haf-4 may contribute to the formation of the large intestinal granules, as indicated by data from an inactive Walker A mutant (K539M). This mutant is supposed to be ATP hydrolysis deficient and cannot rescue the phenotype in *haf-4* deletion mutant (*gk240*). Moreover, TAPL could rescue Haf-4 function in *gk240* (Bauer, 2006). Whether this is true for Haf-9 or not, needs to be clarified too.

Also similar to their human ortholog TAPL, Haf-4 and Haf-9 appear to form homodimers as indicated by the peptide transport activities. However, they also interact heterologously. The situation is similar to the two subunits of the TAP transporter, an active heterodimeric complex formed by TAP1 and TAP2 (Powis et al., 1991; Spies and DeMars, 1991), whereas there are also reports about TAP1 and TAP2 forming homodimers (Antoniou et al., 2002; Oancea et al., 2009). Nevertheless, TAP1 or TAP2 alone is not active in peptide binding and transport (Meyer et al., 1994). Remarkably, co-expressed Haf-4 and Haf-9 seem only form heteromers. The heteromers have significantly decreased peptide transport. Therefore, the questions about whether both Haf-4 and Haf-9 colocalize in the same granule, and if yes, what is the function of the heteromers need to be answered by further experiments. It is likely that heterologous interaction is a negative regulation mechanism for Haf-4 and Haf-9 function.

Haf-4 and Haf-9 from *C. elegans* were reported to be expressed in intestinal granules from larval to adult stage, and required for the formation of enlarged non-acidic granules. In addition to granule defects, other phenotypes such as reduced brood size, slow growth and prolonged fecundation cycles were also observed in *haf-4* and *haf-9* deletion animals. These phenotypes are all attributable to intestinal granule defects since nutrients are not expected to be supplied adequately. Therefore, Haf-4 and Haf-9-positive granules were speculated to be involved in the storage and transport of nutrients including peptides. Haf-4 and Haf-9 may be required for the normal growth and spermatogenesis at the larval stage; in adult stage, their expressions may lead to the proper oogenesis (Kawai et al., 2009). More interestingly, Haf-4

was shown as a functional ortholog of TAPL which restores the granule phenotype in *haf-4* deletion animal (*gk240*) and increases the life span of the animal under starving conditions (Bauer, 2006). Together with the ATP-dependent peptide transport activity of Haf-4 and Haf-9 characterized in current project, I speculate that both half transporters are involved in autophagy which is strongly induced by starvation (Finn and Dice, 2005). Notably, this physiological function of TAPL orthologs may reflect the ancestral role of TAPL.

6 Abbreviations

ABC	ATP-binding cassette
ADP	Adenosine-5'-diphosphate
AEBSF	4-(2-aminoethyl)-benzotriazolium hexafluorophosphate
AMP	Adenosine-5'-monophosphate
AMPPNP	5'-Adenylyl- β , γ -imidodiphosphate
ANS	8-Anilinonaphthalene-1-sulfonic acid
APS	Ammonium persulfate solution
ATP	Adenosine-5'-triphosphate
ATP γ S	Adenosine-5'-(γ -thio) triphosphate
BSA	Bovine serum albumine
CFTR	Cystic fibrosis transmembrane conductance regulator
CHAPS	3-[(3-cholamidopropyl)dimethylammonio]-1-propanesulfonate
CHO-K1	Chinese hamster ovary cells
ConA	Concanavalin A
CPM	Counts per minute
CTP	Cytidine-5'-triphosphate
DCFBA	Dual-color-fluorescence-burst analysis
DDM	<i>n</i> -Dodecyl- β -D-maltoside
DM	<i>n</i> -Decyl- β -D-maltoside
DMF	Dimethylformamide
DMSO	Dimethyl sulfoxide
dNTP	Deoxyribonucleotides
DOPC	1,2-dioleoyl- <i>sn</i> -glycero-3-phosphocholine
DOPE	1,2-dioleoyl- <i>sn</i> -glycero-3-phosphoethanolamine
DOPS	1,2-dioleoyl- <i>sn</i> -glycero-3-phospho-L-serine
DOPA	1,2-dioleoyl- <i>sn</i> -glycero-3-phosphate
DTT	1,4-Dithiothreitol
ECL	Enhanced chemiluminescence
EDTA	Ethylenediaminetetraacetic acid
EEA1	Early endosomal antigen 1
eGFP	Enhanced green fluorescent protein

Egg PG	Egg L- α -phosphatidylglycerol
EGTA	Ethyleneglycoltetraacetic acid
ER	Endoplasmic reticulum
EPR	Electron paramagnetic resonance
Fos-14	Foscholine-14
FRET	Fluorescence energy transfer
GFP	Green fluorescent protein
GTP	Guanosine-5'-triphosphate
HEK-293	Human embryonic kidney 293 cells
HEPES	<i>N</i> -2-Hydroxyethylpiperazine- <i>N'</i> -2-ethanesulfonic acid
5-IAF	5-Iodoacetamidofluorescein
ICLs	Intracellular loops
IMAC	Immobilized metal affinity chromatography
IPTG	Isopropyl- β -D-thiogalactopyranoside
LAMP	Lysosome-associated membrane protein
LAMP-2A	Lysosome-associated membrane protein 2A
LMP-1	LAMP homologue in <i>C. elegans</i>
LPR	Lipid-to-protein ratio
MALDI-TOF	Matrix-assisted laser desorption/ionisation-time of flight
MHC	Major histocompatibility complex
MOI	Multiplicity of infection
MOPS	3-(<i>N</i> -Morpholino)propanesulfonic acid
NAD	Nicotinamide adenine dinucleotide
NBD	Nucleotide-binding domain
NHS	<i>N</i> -hydroxyl succinimide
Ni-NTA	Nickel-nitrilotriacetic acid
OG	<i>n</i> -Octyl- β -D-glucopyranoside
PA	Phosphatidic acid
PBR	Peptide-binding region
PDB	Protein data bank
PG	Phosphatidylglycerol
P-gp	P-glycoprotein
PBS	Phosphate-buffered saline

PEI	Polyethylene imine
<i>Pfu</i>	<i>Pyrococcus furiosus</i>
PI-mix	Protease inhibitor mix
PVDF	Polyvinylidene difluoride
R9LQK	RRYQKSTEL (peptide)
SEC	Size exclusion chromatography
SBR	Signal-to-background ratio
SDS	Sodium dodecyl sulfate
<i>Sf</i>	<i>Spodoptera frugiperda</i>
TAE	Tris-acetate-EDTA
TAP	Transporter associated with antigen processing
TAPL	TAP-like
TAPL C-less	TAP-like cysteine less
TAPL wt	TAP-like wild-type
TBS	Tris-buffered saline
TEMED	<i>N,N,N',N'</i> -Tetramethylethylene diamine
TFA	Trifluoroacetic acid
TMD	Transmembrane domain
TRICINE	<i>N</i> -(Tri(hydroxymethyl)methyl) glycine
TRIS	Tris(hydroxymethyl)aminomethane
UTP	Uridine-5'-triphosphate
Zn-IDA	Zinc-iminodiacetic acid

7 References

- Abele, R. and Tampé, R. (2004) The ABCs of immunology: structure and function of TAP, the transporter associated with antigen processing. *Physiology (Bethesda)*, **19**, 216-224.
- Al-Shawi, M.K., Polar, M.K., Omote, H. and Figler, R.A. (2003) Transition state analysis of the coupling of drug transport to ATP hydrolysis by P-glycoprotein. *J Biol Chem*, **278**, 52629-52640.
- Al-Shawi, M.K. and Senior, A.E. (1993) Characterization of the adenosine triphosphatase activity of Chinese hamster P-glycoprotein. *J Biol Chem*, **268**, 4197-4206.
- Aller, S.G., Yu, J., Ward, A., Weng, Y., Chittaboina, S., Zhuo, R., Harrell, P.M., Trinh, Y.T., Zhang, Q., Urbatsch, I.L. and Chang, G. (2009) Structure of P-glycoprotein reveals a molecular basis for poly-specific drug binding. *Science*, **323**, 1718-1722.
- Ambudkar, S.V., Cardarelli, C.O., Pashinsky, I. and Stein, W.D. (1997) Relation between the turnover number for vinblastine transport and for vinblastine-stimulated ATP hydrolysis by human P-glycoprotein. *J Biol Chem*, **272**, 21160-21166.
- Ambudkar, S.V., Kim, I.W., Xia, D. and Sauna, Z.E. (2006) The A-loop, a novel conserved aromatic acid subdomain upstream of the Walker A motif in ABC transporters, is critical for ATP binding. *FEBS Lett*, **580**, 1049-1055.
- Ambudkar, S.V., Lelong, I.H., Zhang, J., Cardarelli, C.O., Gottesman, M.M. and Pastan, I. (1992) Partial purification and reconstitution of the human multidrug-resistance pump: characterization of the drug-stimulatable ATP hydrolysis. *Proc Natl Acad Sci U S A*, **89**, 8472-8476.
- Androlewicz, M.J. and Cresswell, P. (1994) Human transporters associated with antigen processing possess a promiscuous peptide-binding site. *Immunity*, **1**, 7-14.
- Antoniou, A.N., Ford, S., Pilley, E.S., Blake, N. and Powis, S.J. (2002) Interactions formed by individually expressed TAP1 and TAP2 polypeptide subunits. *Immunology*, **106**, 182-189.
- Bachmann, M.F., Oxenius, A., Pircher, H., Hengartner, H., Ashton-Richardt, P.A., Tonegawa, S. and Zinkernagel, R.M. (1995) TAP1-independent loading of class I molecules by exogenous viral proteins. *Eur J Immunol*, **25**, 1739-1743.
- Bamber, L., Harding, M., Butler, P.J. and Kunji, E.R. (2006) Yeast mitochondrial ADP/ATP carriers are monomeric in detergents. *Proc Natl Acad Sci U S A*, **103**, 16224-16229.

- Bauer, B. (2006) Charakterisierung der physiologischen Funktion des Transportproteins ABCB9 mit Hilfe von *Caenorhabditis elegans* Deletionsmutanten. *Institute of Biochemistry*. Geothe University Frankfurt, Frankfurt am Main, Vol. Diploma.
- Baykov, A.A., Evtushenko, O.A. and Avaeva, S.M. (1988) A malachite green procedure for orthophosphate determination and its use in alkaline phosphatase-based enzyme immunoassay. *Anal Biochem*, **171**, 266-270.
- Beitz, E. (2000) T(E)Xtopo: shaded membrane protein topology plots in LAT(E)X2epsilon. *Bioinformatics*, **16**, 1050-1051.
- Bezrukov, S.M. (2000) Functional consequences of lipid packing stress *Current Opinion in Colloids and Interface Science*, **5**, 237-243.
- Biemans-Oldehinkel, E., Doeven, M.K. and Poolman, B. (2006) ABC transporter architecture and regulatory roles of accessory domains. *FEBS Lett*, **580**, 1023-1035.
- Borbat, P.P., Surendhran, K., Bortolus, M., Zou, P., Freed, J.H. and McHaourab, H.S. (2007) Conformational motion of the ABC transporter MsbA induced by ATP hydrolysis. *PLoS Biol*, **5**, e271.
- Borst, P. and Elferink, R.O. (2002) Mammalian ABC transporters in health and disease. *Annu Rev Biochem*, **71**, 537-592.
- Borths, E.L., Poolman, B., Hvorup, R.N., Locher, K.P. and Rees, D.C. (2005) In vitro functional characterization of BtuCD-F, the Escherichia coli ABC transporters for vitamin B12 uptake. *Biochemistry*, **44**, 16301-16309.
- Boulter, J.M., Taylor, A.M. and Watts, A. (1996) Asymmetric and functional reconstitution of band 3 into pre-formed phosphatidylcholine vesicles. *Biochim Biophys Acta*, **1280**, 265-271.
- Cantor, R.S. (1997) The lateral pressure profile in membranes: a physical mechanism of general anesthesia. *Biochemistry*, **36**, 2339-2344.
- Chen, J., Lu, G., Lin, J., Davidson, A.L. and Quioco, F.A. (2003a) A tweezers-like motion of the ATP-binding cassette dimer in an ABC transport cycle. *Mol. Cell*, **12**, 651-661.
- Chen, J., Sharma, S., Quioco, F.A. and Davidson, A.L. (2001) Trapping the transition state of an ATP-binding cassette transporter: evidence for a concerted mechanism of maltose transport. *Proc. Natl Acad. Sci. USA*, **98**, 1525-1530.
- Chen, J.H., Chang, X.B., Aleksandrov, A.A. and Riordan, J.R. (2002) CFTR is a monomer: biochemical and functional evidence. *J Membr Biol*, **188**, 55-71.

- Chen, M., Abele, R. and Tampé, R. (2003b) Peptides induce ATP hydrolysis at both subunits of the transporter associated with antigen processing. *J Biol Chem*, **278**, 29686-29692.
- Chicz, R.M., Urban, R.G., Gorga, J.C., Vignali, D.A., Lane, W.S. and Strominger, J.L. (1993) Specificity and promiscuity among naturally processed peptides bound to HLA-DR alleles. *J Exp Med*, **178**, 27-47.
- Chloupkova, M., Pickert, A., Lee, J.Y., Souza, S., Trinh, Y.T., Connelly, S.M., Dumont, M.E., Dean, M. and Urbatsch, I.L. (2007) Expression of 25 human ABC transporters in the yeast *Pichia pastoris* and characterization of the purified ABCC3 ATPase activity. *Biochemistry*, **46**, 7992-8003.
- Cresswell, P., Ackerman, A.L., Giodini, A., Peaper, D.R. and Wearsch, P.A. (2005) Mechanisms of MHC class I-restricted antigen processing and cross-presentation. *Immunol Rev*, **207**, 145-157.
- Curnow, P., Lorch, M., Charalambous, K. and Booth, P.J. (2004) The reconstitution and activity of the small multidrug transporter EmrE is modulated by non-bilayer lipid composition. *J Mol Biol*, **343**, 213-222.
- Dani, A., Chaudhry, A., Mukherjee, P., Rajagopal, D., Bhatia, S., George, A., Bal, V., Rath, S. and Mayor, S. (2004) The pathway for MHCII-mediated presentation of endogenous proteins involves peptide transport to the endo-lysosomal compartment. *J Cell Sci*, **117**, 4219-4230.
- Davidson, A.L. and Chen, J. (2004) ATP-binding cassette transporters in bacteria. *Annu Rev Biochem*, **73**, 241-268.
- Davidson, A.L., Dassa, E., Orelle, C. and Chen, J. (2008) Structure, function, and evolution of bacterial ATP-binding cassette systems. *Microbiol Mol Biol Rev*, **72**, 317-364, table of contents.
- Davidson, A.L. and Nikaido, H. (1990) Overproduction, solubilization, and reconstitution of the maltose transport system from *Escherichia coli*. *J. Biol. Chem.*, **265**, 4254-4260.
- Dawson, R.J.P., Hollenstein, K. and Locher, K.P. (2007) Uptake or extrusion: crystal structures of full ABC transporters suggest a common mechanism. *Mol. Microbiol.*, **65**, 250-257.
- Dawson, R.J.P. and Locher, K.P. (2006) Structure of a bacterial multidrug ABC transporter. *Nature*, **443**, 180-185.
- Dawson, R.J.P. and Locher, K.P. (2007) Structure of the multidrug ABC transporter Sav1866 from *Staphylococcus aureus* in complex with AMP-PNP. *FEBS Lett.*, **581**, 935-938.

- De Vendittis, E., Palumbo, G., Parlato, G. and Bocchini, V. (1981) A fluorimetric method for the estimation of the critical micelle concentration of surfactants. *Anal Biochem*, **115**, 278-286.
- Dean, M. and Annilo, T. (2005) Evolution of the ATP-binding cassette (ABC) transporter superfamily in vertebrates. *Annu Rev Genomics Hum Genet*, **6**, 123-142.
- Dean, M., Rzhetsky, A. and Allikmets, R. (2001) The human ATP-binding cassette (ABC) transporter superfamily. *Genome Res.*, **11**, 1156-1166.
- Demirel, O., Waibler, Z., Kalinke, U., Grunebach, F., Appel, S., Brossart, P., Hasilik, A., Tampé, R. and Abele, R. (2007) Identification of a lysosomal peptide transport system induced during dendritic cell development. *J Biol Chem*, **282**, 37836-37843.
- DiRusso, C.C. and Nystrom, T. (1998) The fats of Escherichia coli during infancy and old age: regulation by global regulators, alarmones and lipid intermediates. *Mol Microbiol*, **27**, 1-8.
- Dong, M., Penin, F. and Baggetto, L.G. (1996) Efficient purification and reconstitution of P-glycoprotein for functional and structural studies. *J Biol Chem*, **271**, 28875-28883.
- Ernst, R., Kueppers, P., Klein, C.M., Schwarzmuller, T., Kuchler, K. and Schmitt, L. (2008) A mutation of the H-loop selectively affects rhodamine transport by the yeast multidrug ABC transporter Pdr5. *Proc Natl Acad Sci U S A*, **105**, 5069-5074.
- Eskandari, S., Wright, E.M., Kreman, M., Starace, D.M. and Zampighi, G.A. (1998) Structural analysis of cloned plasma membrane proteins by freeze-fracture electron microscopy. *Proc Natl Acad Sci U S A*, **95**, 11235-11240.
- Eytan, G.D., Regev, R. and Assaraf, Y.G. (1996) Functional reconstitution of P-glycoprotein reveals an apparent near stoichiometric drug transport to ATP hydrolysis. *J Biol Chem*, **271**, 3172-3178.
- Fersht, A.R. (1997) Nucleation mechanisms in protein folding. *Curr Opin Struct Biol*, **7**, 3-9.
- Finn, P.F. and Dice, J.F. (2005) Ketone bodies stimulate chaperone-mediated autophagy. *J Biol Chem*, **280**, 25864-25870.
- Gaillard, I., Slotboom, D.J., Knol, J., Lolkema, J.S. and Konings, W.N. (1996) Purification and reconstitution of the glutamate carrier GltT of the thermophilic bacterium *Bacillus stearothermophilus*. *Biochemistry*, **35**, 6150-6156.
- Geertsma, E.R., Nik Mahmood, N.A., Schuurman-Wolters, G.K. and Poolman, B. (2008) Membrane reconstitution of ABC transporters and assays of translocator function. *Nat Protoc*, **3**, 256-266.

- Geourjon, C., Orelle, C., Steinfels, E., Blanchet, C., Deleage, G., Di Pietro, A. and Jault, J.M. (2001) A common mechanism for ATP hydrolysis in ABC transporter and helicase superfamilies. *Trends Biochem Sci*, **26**, 539-544.
- Gerber, S., Comellas-Bigler, M., Goetz, B.A. and Locher, K.P. (2008) Structural basis of trans-inhibition in a molybdate/tungstate ABC transporter. *Science*, **321**, 246-250.
- Goetz, B.A., Perozo, E. and Locher, K.P. (2009) Distinct gate conformations of the ABC transporter BtuCD revealed by electron spin resonance spectroscopy and chemical cross-linking. *FEBS Lett.*, **583**, 266-270.
- Gorbulev, S., Abele, R. and Tampé, R. (2001) Allosteric crosstalk between peptide-binding, transport, and ATP hydrolysis of the ABC transporter TAP. *Proc Natl Acad Sci U S A*, **98**, 3732-3737.
- Gottesman, M.M., Fojo, T. and Bates, S.E. (2002) Multidrug resistance in cancer: role of ATP-dependent transporters. *Nat Rev Cancer*, **2**, 48-58.
- Gromme, M., van der Valk, R., Sliedregt, K., Vernie, L., Liskamp, R., Hammerling, G., Koopmann, J.O., Momburg, F. and Neefjes, J. (1997) The rational design of TAP inhibitors using peptide substrate modifications and peptidomimetics. *Eur J Immunol*, **27**, 898-904.
- Grote, M., Bordignon, E., Polyhach, Y., Jeschke, G., Steinhoff, H.J. and Schneider, E. (2008) A comparative electron paramagnetic resonance study of the nucleotide-binding domains' catalytic cycle in the assembled maltose ATP-binding cassette importer. *Biophys J*, **95**, 2924-2938.
- Grote, M., Polyhach, Y., Jeschke, G., Steinhoff, H.J., Schneider, E. and Bordignon, E. (2009) Transmembrane signaling in the maltose ABC transporter MALFGK2-E: The periplasmic MALF-P2 loop communicates substrate availability to the ATP-bound malk dimer. *J Biol Chem*.
- Groth, G. and Walker, J.E. (1996) ATP synthase from bovine heart mitochondria: reconstitution into unilamellar phospholipid vesicles of the pure enzyme in a functional state. *Biochem J*, **318 (Pt 1)**, 351-357.
- Gruner, S.M. (1985) Intrinsic curvature hypothesis for biomembrane lipid composition: a role for nonbilayer lipids. *Proc Natl Acad Sci U S A*, **82**, 3665-3669.
- Haggie, P.M. and Verkman, A.S. (2008) Monomeric CFTR in plasma membranes in live cells revealed by single molecule fluorescence imaging. *J Biol Chem*, **283**, 23510-23513.

- Heemels, M.T., Schumacher, T.N., Wonigeit, K. and Ploegh, H.L. (1993) Peptide translocation by variants of the transporter associated with antigen processing. *Science*, **262**, 2059-2063.
- Herget, M., Oancea, G., Schrod, S., Karas, M., Tampé, R. and Abele, R. (2007) Mechanism of Substrate Sensing and Signal Transmission within an ABC Transporter: USE OF A TROJAN HORSE STRATEGY. *J. Biol. Chem.*, **282**, 3871-3880.
- Heuberger, E.H., Veenhoff, L.M., Durkens, R.H., Friesen, R.H. and Poolman, B. (2002) Oligomeric state of membrane transport proteins analyzed with blue native electrophoresis and analytical ultracentrifugation. *J Mol Biol*, **317**, 591-600.
- Higgins, C.F. (1992) ABC transporters: from microorganisms to man. *Annu Rev Cell Biol*, **8**, 67-113.
- Hinshelwood, S., Lovering, R.C., Genevier, H.C., Levinsky, R.J. and Kinnon, C. (1995) The protein defective in X-linked agammaglobulinemia, Bruton's tyrosine kinase, shows increased autophosphorylation activity in vitro when isolated from cells in which the B cell receptor has been cross-linked. *Eur J Immunol*, **25**, 1113-1116.
- Hjelmeland, L.M. (1980) A nondenaturing zwitterionic detergent for membrane biochemistry: design and synthesis. *Proc Natl Acad Sci U S A*, **77**, 6368-6370.
- Holland, I.B. and Blight, M.A. (1999) ABC-ATPases, adaptable energy generators fuelling transmembrane movement of a variety of molecules in organisms from bacteria to humans. *J Mol Biol*, **293**, 381-399.
- Hollenstein, K., Dawson, R.J.P. and Locher, K.P. (2007a) Structure and mechanism of ABC transporter proteins. *Curr. Opin. Struct. Biol.*, **17**, 412-418.
- Hollenstein, K., Frei, D.C. and Locher, K.P. (2007b) Structure of an ABC transporter in complex with its binding protein. *Nature*, **446**, 213-216.
- Horn, C., Bremer, E. and Schmitt, L. (2003) Nucleotide dependent monomer/dimer equilibrium of OpuAA, the nucleotide-binding protein of the osmotically regulated ABC transporter OpuA from *Bacillus subtilis*. *J Mol Biol*, **334**, 403-419.
- Hung, L.W., Wang, I.X., Nikaido, K., Liu, P.Q., Ames, G.F. and Kim, S.H. (1998) Crystal structure of the ATP-binding subunit of an ABC transporter. *Nature*, **396**, 703-707.
- Hunte, C., von Jagow, G. and Schägger, H. (2002) *Membrane Protein Purification and Crystallization: A Practical Guide* Academic Press.
- Hunter, W.M. and Greenwood, F.C. (1962) Preparation of iodine-131 labelled human growth hormone of high specific activity. *Nature*, **194**, 495-496.

- Hvorup, R.N. (2007) Asymmetry in the structure of the ABC transporter binding protein complex BtuCD-BtuF. *Science*, **317**, 1387-1390.
- Janas, E., Hofacker, M., Chen, M., Gompf, S., van der Does, C. and Tampe, R. (2003a) The ATP hydrolysis cycle of the nucleotide-binding domain of the mitochondrial ATP-binding cassette transporter Mdl1p. *J Biol Chem*, **278**, 26862-26869.
- Janas, E., Hofacker, M., Chen, M., Gompf, S., van der Does, C. and Tampé, R. (2003b) The ATP hydrolysis cycle of the nucleotide-binding domain of the mitochondrial ATP-binding cassette transporter Mdl1p. *J Biol Chem*, **278**, 26862-26869.
- Jardetsky, O. (1966) Simple allosteric model for membrane pumps. *Nature*, **211**, 969-970.
- Jones, P.M. and George, A.M. (2002) Mechanism of ABC transporters: a molecular dynamics simulation of a well characterized nucleotide-binding subunit. *Proc. Natl Acad. Sci. USA*, **99**, 12639-12644.
- Jones, P.M. and George, A.M. (2004) The ABC transporter structure and mechanism: perspectives on recent research. *Cell Mol Life Sci*, **61**, 682-699.
- Kadaba, N.S., Kaiser, J.T., Johnson, E., Lee, A. and Rees, D.C. (2008) The high-affinity E. coli methionine ABC transporter: structure and allosteric regulation. *Science*, **321**, 250-253.
- Kamakura, A., Fujimoto, Y., Motohashi, Y., Ohashi, K., Ohashi-Kobayashi, A. and Maeda, M. (2008) Functional dissection of transmembrane domains of human TAP-like (ABCB9). *Biochem Biophys Res Commun*, **377**, 847-851.
- Kawai, H., Tanji, T., Shiraishi, H., Yamada, M., Iijima, R., Inoue, T., Kezuka, Y., Ohashi, K., Yoshida, Y., Tohyama, K., Gengyo-Ando, K., Mitani, S., Arai, H., Ohashi-Kobayashi, A. and Maeda, M. (2009) Normal Formation of a Subset of Intestinal Granules in *Caenorhabditis elegans* Requires ABC Transporters HAF-4 and HAF-9, Which Are Highly Homologous to Human Lysosomal Peptide Transporter TAPL (TAP-like). *Mol Biol Cell*.
- Knol, J. (1999) Membrane Reconstitution and Functional Analysis of a Sugar Transport Protein. *Biochemistry Department*. University of Groningen, Groningen, Vol. Ph.D.
- Knol, J., Sjollem, K. and Poolman, B. (1998) Detergent-mediated reconstitution of membrane proteins. *Biochemistry*, **37**, 16410-16415.
- Knol, J., Veenhoff, L., Liang, W.J., Henderson, P.J., Leblanc, G. and Poolman, B. (1996) Unidirectional reconstitution into detergent-destabilized liposomes of the purified lactose transport system of *Streptococcus thermophilus*. *J Biol Chem*, **271**, 15358-15366.

- Kobayashi, A., Hori, S., Suita, N. and Maeda, M. (2003) Gene organization of human transporter associated with antigen processing-like (TAPL, ABCB9): analysis of alternative splicing variants and promoter activity. *Biochem Biophys Res Commun*, **309**, 815-822.
- Kobayashi, A., Kasano, M., Maeda, T., Hori, S., Motojima, K., Suzuki, M., Fujiwara, T., Takahashi, E., Yabe, T., Tanaka, K., Kasahara, M., Yamaguchi, Y. and Maeda, M. (2000) A half-type ABC transporter TAPL is highly conserved between rodent and man, and the human gene is not responsive to interferon-gamma in contrast to TAP1 and TAP2. *J Biochem*, **128**, 711-718.
- Koch, J., Guntrum, R., Heintke, S., Kyritsis, C. and Tampé, R. (2004) Functional dissection of the transmembrane domains of the transporter associated with antigen processing (TAP). *J Biol Chem*, **279**, 10142-10147.
- Koopmann, J.-O., Albring, J., Hueter, E., Bulbuc, N., Spee, P., Neefjes, J., Haemmerling, G.J. and Momburg, F. (2000) Export of Antigenic Peptides from the Endoplasmic Reticulum Intersects with Retrograde Protein Translocation through the Sec61p Channel. *Immunity*, **13**, 117-127.
- Koopmann, J.O., Post, M., Neefjes, J.J., Hammerling, G.J. and Momburg, F. (1996) Translocation of long peptides by transporters associated with antigen processing (TAP). *Eur J Immunol*, **26**, 1720-1728.
- Kragh-Hansen, U., le Maire, M. and Moller, J.V. (1998) The mechanism of detergent solubilization of liposomes and protein-containing membranes. *Biophys J*, **75**, 2932-2946.
- Kunji, E.R., Harding, M., Butler, P.J. and Akamine, P. (2008) Determination of the molecular mass and dimensions of membrane proteins by size exclusion chromatography. *Methods*, **46**, 62-72.
- Lambert, O., Levy, D., Ranck, J.L., Leblanc, G. and Rigaud, J.L. (1998) A new "gel-like" phase in dodecyl maltoside-lipid mixtures: implications in solubilization and reconstitution studies. *Biophys J*, **74**, 918-930.
- Landmesser, H., Stein, A., Bluschke, B., Brinkmann, M., Hunke, S. and Schneider, E. (2002) Large-scale purification, dissociation and functional reassembly of the maltose ATP-binding cassette transporter (MalFGK(2)) of *Salmonella typhimurium*. *Biochim Biophys Acta*, **1565**, 64-72.

- Lankat-Buttgereit, B. and Tampé, R. (2002) The transporter associated with antigen processing: function and implications in human diseases. *Physiol Rev*, **82**, 187-204.
- le Coutre, J., Narasimhan, L.R., Patel, C.K. and Kaback, H.R. (1997) The lipid bilayer determines helical tilt angle and function in lactose permease of Escherichia coli. *Proc Natl Acad Sci U S A*, **94**, 10167-10171.
- le Maire, M., Moller, J.V. and Champeil, P. (1987) Binding of a nonionic detergent to membranes: flip-flop rate and location on the bilayer. *Biochemistry*, **26**, 4803-4810.
- Lerner-Marmarosh, N., Gimi, K., Urbatsch, I.L., Gros, P. and Senior, A.E. (1999) Large scale purification of detergent-soluble P-glycoprotein from Pichia pastoris cells and characterization of nucleotide binding properties of wild-type, Walker A, and Walker B mutant proteins. *J Biol Chem*, **274**, 34711-34718.
- Leveson-Gower, D.B., Michnick, S.W. and Ling, V. (2004) Detection of TAP family dimerizations by an in vivo assay in mammalian cells. *Biochemistry*, **43**, 14257-14264.
- Levy, D., Bluzat, A., Seigneuret, M. and Rigaud, J.L. (1990) A systematic study of liposome and proteoliposome reconstitution involving Bio-Bead-mediated Triton X-100 removal. *Biochim Biophys Acta*, **1025**, 179-190.
- Li, C., Ramjeesingh, M., Wang, W., Garami, E., Hewryk, M., Lee, D., Rommens, J.M., Galley, K. and Bear, C.E. (1996) ATPase activity of the cystic fibrosis transmembrane conductance regulator. *J Biol Chem*, **271**, 28463-28468.
- Li, C., Roy, K., Dandridge, K. and Naren, A.P. (2004) Molecular assembly of cystic fibrosis transmembrane conductance regulator in plasma membrane. *J Biol Chem*, **279**, 24673-24684.
- Lich, J.D., Elliott, J.F. and Blum, J.S. (2000) Cytoplasmic processing is a prerequisite for presentation of an endogenous antigen by major histocompatibility complex class II proteins. *J Exp Med*, **191**, 1513-1524.
- Lizee, G., Basha, G., Tiong, J., Julien, J.P., Tian, M., Biron, K.E. and Jefferies, W.A. (2003) Control of dendritic cell cross-presentation by the major histocompatibility complex class I cytoplasmic domain. *Nat Immunol*, **4**, 1065-1073.
- Locher, K.P. (2009) Review. Structure and mechanism of ATP-binding cassette transporters. *Philos Trans R Soc Lond B Biol Sci*, **364**, 239-245.
- Locher, K.P., Lee, A.T. and Rees, D.C. (2002) The E. coli BtuCD structure: a framework for ABC transporter architecture and mechanism. *Science*, **296**, 1091-1098.

- Loo, T.W., Bartlett, M.C. and Clarke, D.M. (2002) The "LSGGQ" motif in each nucleotide-binding domain of human P-glycoprotein is adjacent to the opposing walker A sequence. *J Biol Chem*, **277**, 41303-41306.
- Lopez, O., de la Maza, A., Coderch, L., Lopez-Iglesias, C., Wehrli, E. and Parra, J.L. (1998) Direct formation of mixed micelles in the solubilization of phospholipid liposomes by Triton X-100. *FEBS Lett*, **426**, 314-318.
- Lundbaek, J.A., Maer, A.M. and Andersen, O.S. (1997) Lipid bilayer electrostatic energy, curvature stress, and assembly of gramicidin channels. *Biochemistry*, **36**, 5695-5701.
- Malnati, M.S., Marti, M., LaVaute, T., Jaraquemada, D., Biddison, W., DeMars, R. and Long, E.O. (1992) Processing pathways for presentation of cytosolic antigen to MHC class II-restricted T cells. *Nature*, **357**, 702-704.
- Mao, Q., Deeley, R.G. and Cole, S.P. (2000) Functional reconstitution of substrate transport by purified multidrug resistance protein MRP1 (ABCC1) in phospholipid vesicles. *J Biol Chem*, **275**, 34166-34172.
- Marshall, J., Fang, S., Ostedgaard, L.S., O'Riordan, C.R., Ferrara, D., Amara, J.F., Hoppe, H.t., Scheule, R.K., Welsh, M.J., Smith, A.E. and et al. (1994) Stoichiometry of recombinant cystic fibrosis transmembrane conductance regulator in epithelial cells and its functional reconstitution into cells in vitro. *J Biol Chem*, **269**, 2987-2995.
- Matsuo, M., Kioka, N., Amachi, T. and Ueda, K. (1999) ATP binding properties of the nucleotide-binding folds of SUR1. *J Biol Chem*, **274**, 37479-37482.
- McDevitt, C.A., Collins, R.F., Conway, M., Modok, S., Storm, J., Kerr, I.D., Ford, R.C. and Callaghan, R. (2006) Purification and 3D structural analysis of oligomeric human multidrug transporter ABCG2. *Structure*, **14**, 1623-1632.
- Metzger, J.W., Kempter, C., Wiesmuller, K.H. and Jung, G. (1994) Electrospray mass spectrometry and tandem mass spectrometry of synthetic multicomponent peptide mixtures: determination of composition and purity. *Anal Biochem*, **219**, 261-277.
- Meyer, T.H., van Endert, P.M., Uebel, S., Ehring, B. and Tampé, R. (1994) Functional expression and purification of the ABC transporter complex associated with antigen processing (TAP) in insect cells. *FEBS Lett*, **351**, 443-447.
- Momburg, F., Roelse, J., Howard, J.C., Butcher, G.W., Hammerling, G.J. and Neefjes, J.J. (1994) Selectivity of MHC-encoded peptide transporters from human, mouse and rat. *Nature*, **367**, 648-651.

- Moody, J.E., Millen, L., Binns, D., Hunt, J.F. and Thomas, P.J. (2002a) Cooperative, ATP-dependent association of the nucleotide binding cassettes during the catalytic cycle of ATP-binding cassette transporters. *J. Biol. Chem.*, **277**, 21111-21114.
- Moody, J.E., Millen, L., Binns, D., Hunt, J.F. and Thomas, P.J. (2002b) Cooperative, ATP-dependent association of the nucleotide binding cassettes during the catalytic cycle of ATP-binding cassette transporters. *J Biol Chem*, **277**, 21111-21114.
- Mourez, M., Hofnung, N. and Dassa, E. (1997) Subunit interactions in ABC transporters: a conserved sequence in hydrophobic membrane proteins of periplasmic permeases defines an important site of interaction with the ATPase subunits. *EMBO J.*, **16**, 3066-3077.
- Muller, K.M., Ebensperger, C. and Tampé, R. (1994) Nucleotide binding to the hydrophilic C-terminal domain of the transporter associated with antigen processing (TAP). *J Biol Chem*, **269**, 14032-14037.
- Mutch, D.M., Anderle, P., Fiaux, M., Mansourian, R., Vidal, K., Wahli, W., Williamson, G. and Roberts, M.A. (2004) Regional variations in ABC transporter expression along the mouse intestinal tract. *Physiol Genomics*, **17**, 11-20.
- Neefjes, J., Gottfried, E., Roelse, J., Gromme, M., Obst, R., Hammerling, G.J. and Momburg, F. (1995) Analysis of the fine specificity of rat, mouse and human TAP peptide transporters. *Eur J Immunol*, **25**, 1133-1136.
- Neefjes, J.J., Momburg, F. and Hammerling, G.J. (1993) Selective and ATP-dependent translocation of peptides by the MHC-encoded transporter. *Science*, **261**, 769-771.
- Neumann, L. and Tampé, R. (1999) Kinetic analysis of peptide binding to the TAP transport complex: evidence for structural rearrangements induced by substrate binding. *J Mol Biol*, **294**, 1203-1213.
- Nijenhuis, M. and Hammerling, G.J. (1996) Multiple regions of the transporter associated with antigen processing (TAP) contribute to its peptide binding site. *J Immunol*, **157**, 5467-5477.
- Norbury, C.C., Princiotta, M.F., Bacik, I., Brutkiewicz, R.R., Wood, P., Elliott, T., Bennink, J.R. and Yewdell, J.W. (2001) Multiple antigen-specific processing pathways for activating naive CD8+ T cells in vivo. *J Immunol*, **166**, 4355-4362.
- Oancea, G., O'Mara, M.L., Bennett, W.F., Tieleman, D.P., Abele, R. and Tampé, R. (2009) Structural arrangement of the transmission interface in the antigen ABC transport complex TAP. *Proc Natl Acad Sci U S A*, **106**, 5551-5556.

- Ohara, T., Ohashi-Kobayashi, A. and Maeda, M. (2008) Biochemical characterization of transporter associated with antigen processing (TAP)-like (ABCB9) expressed in insect cells. *Biol Pharm Bull*, **31**, 1-5.
- Oldham, M.L., Khare, D., Quioco, F.A., Davidson, A.L. and Chen, J. (2007) Crystal structure of a catalytic intermediate of the maltose transporter. *Nature*, **450**, 515-522.
- Oram, J.F. and Vaughan, A.M. (2000) ABCA1-mediated transport of cellular cholesterol and phospholipids to HDL apolipoproteins. *Curr Opin Lipidol*, **11**, 253-260.
- Paternostre, M.T., Roux, M. and Rigaud, J.L. (1988) Mechanisms of membrane protein insertion into liposomes during reconstitution procedures involving the use of detergents. 1. Solubilization of large unilamellar liposomes (prepared by reverse-phase evaporation) by triton X-100, octyl glucoside, and sodium cholate. *Biochemistry*, **27**, 2668-2677.
- Patzlaff, J.S., van der Heide, T. and Poolman, B. (2003) The ATP/substrate stoichiometry of the ATP-binding cassette (ABC) transporter OpuA. *J Biol Chem*, **278**, 29546-29551.
- Penforinis, A., Yan, G., Shi, L. and Faustman, D.L. (2003) Polymorphisms of human TAP2 detected by denaturing gradient gel electrophoresis. *Hum Immunol*, **64**, 156-167.
- Pinkett, H.W., Lee, A.T., Lum, P., Locher, K.P. and Rees, D.C. (2007) An inward-facing conformation of a putative metal-chelate type ABC transporter. *Science*, **315**, 373-377.
- Pitard, B., Richard, P., Dunach, M., Girault, G. and Rigaud, J.L. (1996) ATP synthesis by the F₀F₁ ATP synthase from thermophilic *Bacillus PS3* reconstituted into liposomes with bacteriorhodopsin. 1. Factors defining the optimal reconstitution of ATP synthases with bacteriorhodopsin. *Eur J Biochem*, **235**, 769-778.
- Poolman, B. (2005) Functional analysis of detergent solubilized and membrane-reconstituted ABC transporters. *Methods Enzymol.*, **400**, 429-459.
- Powis, S.J., Townsend, A.R., Deverson, E.V., Bastin, J., Butcher, G.W. and Howard, J.C. (1991) Restoration of antigen presentation to the mutant cell line RMA-S by an MHC-linked transporter. *Nature*, **354**, 528-531.
- Powis, S.J., Young, L.L., Joly, E., Barker, P.J., Richardson, L., Brandt, R.P., Melief, C.J., Howard, J.C. and Butcher, G.W. (1996) The rat cim effect: TAP allele-dependent changes in a class I MHC anchor motif and evidence against C-terminal trimming of peptides in the ER. *Immunity*, **4**, 159-165.
- Qu, Q., Russell, P.L. and Sharom, F.J. (2003) Stoichiometry and affinity of nucleotide binding to P-glycoprotein during the catalytic cycle. *Biochemistry*, **42**, 1170-1177.

- Ramjeesingh, M., Kidd, J.F., Huan, L.J., Wang, Y. and Bear, C.E. (2003) Dimeric cystic fibrosis transmembrane conductance regulator exists in the plasma membrane. *Biochem J*, **374**, 793-797.
- Ramjeesingh, M., Li, C., Kogan, I., Wang, Y., Huan, L.J. and Bear, C.E. (2001) A monomer is the minimum functional unit required for channel and ATPase activity of the cystic fibrosis transmembrane conductance regulator. *Biochemistry*, **40**, 10700-10706.
- Rath, A., Glibowicka, M., Nadeau, V.G., Chen, G. and Deber, C.M. (2009) Detergent binding explains anomalous SDS-PAGE migration of membrane proteins. *Proc Natl Acad Sci U S A*, **106**, 1760-1765.
- Rees, D.C., Johnson, E. and Lewinson, O. (2009) ABC transporters: the power to change. *Nat Rev Mol Cell Biol*, **10**, 218-227.
- Richard, P., Rigaud, J.L. and Graber, P. (1990) Reconstitution of CF0F1 into liposomes using a new reconstitution procedure. *Eur J Biochem*, **193**, 921-925.
- Rigaud, J.L. and Levy, D. (2003) Reconstitution of membrane proteins into liposomes. *Methods Enzymol*, **372**, 65-86.
- Rigaud, J.L., Levy, D., Mosser, G. and Lambert, O. (1998) Detergent removal by non-polar polystyrene beads. *European Biophysics Journal*, **27**, 305-319.
- Rigaud, J.L., Mosser, G., Lacapere, J.J., Olofsson, A., Levy, D. and Ranck, J.L. (1997) Bio-Beads: an efficient strategy for two-dimensional crystallization of membrane proteins. *J Struct Biol*, **118**, 226-235.
- Ritz, U., Momburg, F., Pircher, H.P., Strand, D., Huber, C. and Seliger, B. (2001) Identification of sequences in the human peptide transporter subunit TAP1 required for transporter associated with antigen processing (TAP) function. *Int Immunol*, **13**, 31-41.
- Rivnay, B. and Metzger, H. (1982) Reconstitution of the receptor for immunoglobulin E into liposomes. Conditions for incorporation of the receptor into vesicles. *J Biol Chem*, **257**, 12800-12808.
- Rudensky, A., Preston-Hurlburt, P., Hong, S.C., Barlow, A. and Janeway, C.A., Jr. (1991) Sequence analysis of peptides bound to MHC class II molecules. *Nature*, **353**, 622-627.
- Sarkadi, B., Price, E.M., Boucher, R.C., Germann, U.A. and Scarborough, G.A. (1992) Expression of the human multidrug resistance cDNA in insect cells generates a high activity drug-stimulated membrane ATPase. *J Biol Chem*, **267**, 4854-4858.

- Saurin, W., Koster, W. and Dassa, E. (1994) Bacterial binding protein-dependent permeases [mdash] characterization of distinctive signatures for functionally related integral cytoplasmic membrane proteins. *Mol. Microbiol.*, **12**, 993-1004.
- Schägger, H., Hagen, T., Roth, B., Brandt, U., Link, T.A. and von Jagow, G. (1990) Phospholipid specificity of bovine heart bc1 complex. *Eur J Biochem*, **190**, 123-130.
- Schmitt, L. and Tampé, R. (2002) Structure and mechanism of ABC transporters. *Curr Opin Struct Biol*, **12**, 754-760.
- Seddon, A.M., Curnow, P. and Booth, P.J. (2004) Membrane proteins, lipids and detergents: not just a soap opera. *Biochim Biophys Acta*, **1666**, 105-117.
- Seeger, M.A. and van Veen, H.W. (2009) Molecular basis of multidrug transport by ABC transporters. *Biochim Biophys Acta*, **1794**, 725-737.
- Serohijos, A.W., Hegedus, T., Aleksandrov, A.A., He, L., Cui, L., Dokholyan, N.V. and Riordan, J.R. (2008) Phenylalanine-508 mediates a cytoplasmic-membrane domain contact in the CFTR 3D structure crucial to assembly and channel function. *Proc Natl Acad Sci U S A*, **105**, 3256-3261.
- Shen, L. and Rock, K.L. (2006) Priming of T cells by exogenous antigen cross-presented on MHC class I molecules. *Curr Opin Immunol*, **18**, 85-91.
- Sheppard, D.N. and Welsh, M.J. (1999) Structure and function of the CFTR chloride channel. *Physiol Rev*, **79**, S23-45.
- Sheps, J.A., Ralph, S., Zhao, Z., Baillie, D.L. and Ling, V. (2004) The ABC transporter gene family of *Caenorhabditis elegans* has implications for the evolutionary dynamics of multidrug resistance in eukaryotes. *Genome Biol*, **5**, R15.
- Slotboom, D.J., Duurkens, R.H., Olieman, K. and Erkens, G.B. (2008) Static light scattering to characterize membrane proteins in detergent solution. *Methods*, **46**, 73-82.
- Smith, P.C., Karpowich, N., Millen, L., Moody, J.E., Rosen, J., Thomas, P.J. and Hunt, J.F. (2002) ATP binding to the motor domain from an ABC transporter drives formation of a nucleotide sandwich dimer. *Mol Cell*, **10**, 139-149.
- Spies, T. and DeMars, R. (1991) Restored expression of major histocompatibility class I molecules by gene transfer of a putative peptide transporter. *Nature*, **351**, 323-324.
- Spooner, P.J., Friesen, R.H., Knol, J., Poolman, B. and Watts, A. (2000) Rotational mobility and orientational stability of a transport protein in lipid membranes. *Biophys J*, **79**, 756-766.

- Stenham, D.R., Campbell, J.D., Sansom, M.S., Higgins, C.F., Kerr, I.D. and Linton, K.J. (2003) An atomic detail model for the human ATP binding cassette transporter P-glycoprotein derived from disulfide cross-linking and homology modeling. *Faseb J*, **17**, 2287-2289.
- Stevanovic, S. and Jung, G. (1993) Multiple sequence analysis: pool sequencing of synthetic and natural peptide libraries. *Anal Biochem*, **212**, 212-220.
- Uebel, S., Kraas, W., Kienle, S., Wiesmuller, K.H., Jung, G. and Tampé, R. (1997) Recognition principle of the TAP transporter disclosed by combinatorial peptide libraries. *Proc Natl Acad Sci U S A*, **94**, 8976-8981.
- Uebel, S., Meyer, T.H., Kraas, W., Kienle, S., Jung, G., Wiesmuller, K.-H. and Tamp, R. (1995) Requirements for Peptide Binding to the Human Transporter Associated with Antigen Processing Revealed by Peptide Scans and Complex Peptide Libraries. *J. Biol. Chem.*, **270**, 18512-18516.
- Uinuk-ool, T.S., Mayer, W.E., Sato, A., Takezaki, N., Benyon, L., Cooper, M.D. and Klein, J. (2003) Identification and characterization of a TAP-family gene in the lamprey. *Immunogenetics*, **55**, 38-48.
- van der Does, C. and Tampé, R. (2004) How do ABC transporters drive transport? *Biol Chem*, **385**, 927-933.
- van Endert, P.M., Riganelli, D., Greco, G., Fleischhauer, K., Sidney, J., Sette, A. and Bach, J.F. (1995) The peptide-binding motif for the human transporter associated with antigen processing. *J. Exp. Med.*, **182**, 1883-1895.
- van Endert, P.M., Tampé, R., Meyer, T.H., Tisch, R., Bach, J.F. and McDevitt, H.O. (1994) A sequential model for peptide binding and transport by the transporters associated with antigen processing. *Immunity*, **1**, 491-500.
- van Meer, G., Voelker, D.R. and Feigenson, G.W. (2008) Membrane lipids: where they are and how they behave. *Nat Rev Mol Cell Biol*, **9**, 112-124.
- Verdon, G., Albers, S.V., Dijkstra, B.W., Driessen, A.J. and Thunnissen, A.M. (2003) Crystal structures of the ATPase subunit of the glucose ABC transporter from *Sulfolobus solfataricus*: nucleotide-free and nucleotide-bound conformations. *J Mol Biol*, **330**, 343-358.
- Voet, D. and Voet, J.G. (2004) *Biochemistry*. Wiley.
- von Jagow, G., Schägger, H., Riccio, P., Klingenberg, M. and Kolb, H.J. (1977) b.c1 complex from beef heart: hydrodynamic properties of the complex prepared by a refined hydroxyapatite chromatography in triton X-100. *Biochim Biophys Acta*, **462**, 549-558.

- Wang, P., Gyllner, G. and Kvist, S. (1996) Selection and binding of peptides to human transporters associated with antigen processing and rat cim-a and -b. *J Immunol*, **157**, 213-220.
- Ward, A., Reyes, C.L., Yu, J., Roth, C.B. and Chang, G. (2007) Flexibility in the ABC transporter MsbA: alternating access with a twist. *Proc. Natl Acad. Sci. USA*, **104**, 19005-19010.
- Wei, Y., Li, H. and Fu, D. (2004) Oligomeric state of the Escherichia coli metal transporter YiiP. *J Biol Chem*, **279**, 39251-39259.
- Wiechelman, K.J., Braun, R.D. and Fitzpatrick, J.D. (1988) Investigation of the bicinchoninic acid protein assay: identification of the groups responsible for color formation. *Anal Biochem*, **175**, 231-237.
- Wiesmuller, K.-H., Feiertag, S., Fleckenstein, B., Kienle, S., Stoll, D., Hermann, M. and Jung, G. (1996) *Combinatorial Peptide and Nonpeptide Libraries: A Handbook for the Search of Lead Structures* (Jung, G., ed). Verlag Chemie, Weinheim, Germany.
- Wittig, I., Braun, H.P. and Schägger, H. (2006) Blue native PAGE. *Nat Protoc*, **1**, 418-428.
- Wittig, I. and Schägger, H. (2008) Features and applications of blue-native and clear-native electrophoresis. *Proteomics*, **8**, 3974-3990.
- Wolters, J.C., Abele, R. and Tampé, R. (2005) Selective and ATP-dependent translocation of peptides by the homodimeric ATP binding cassette transporter TAP-like (ABCB9). *J Biol Chem*, **280**, 23631-23636.
- Xu, J., Peng, H., Chen, Q., Liu, Y., Dong, Z. and Zhang, J.T. (2007) Oligomerization domain of the multidrug resistance-associated transporter ABCG2 and its dominant inhibitory activity. *Cancer Res*, **67**, 4373-4381.
- Yamaguchi, Y., Iseoka, H., Kobayashi, A. and Maeda, M. (2004) The carboxyl terminal sequence of rat transporter associated with antigen processing (TAP)-like (ABCB9) is heterogeneous due to splicing of its mRNA. *Biol Pharm Bull*, **27**, 100-104.
- Yamaguchi, Y., Kasano, M., Terada, T., Sato, R. and Maeda, M. (1999) An ABC transporter homologous to TAP proteins. *FEBS Lett*, **457**, 231-236.
- Yernool, D., Boudker, O., Folta-Stogniew, E. and Gouaux, E. (2003) Trimeric subunit stoichiometry of the glutamate transporters from *Bacillus caldoteanax* and *Bacillus stearothermophilus*. *Biochemistry*, **42**, 12981-12988.
- Yuan, Y.R., Blecker, S., Martsinkevich, O., Millen, L., Thomas, P.J. and Hunt, J.F. (2001) The crystal structure of the MJ0796 ATP-binding cassette. Implications for the structural

- consequences of ATP hydrolysis in the active site of an ABC transporter. *J Biol Chem*, **276**, 32313-32321.
- Zaitseva, J. (2005) H662 is the linchpin of ATP hydrolysis in the nucleotide-binding domain of the ABC transporter HlyB. *EMBO J.*, **24**, 1901-1910.
- Zaitseva, J., Jenewein, S., Jumpertz, T., Holland, I.B. and Schmitt, L. (2005a) H662 is the linchpin of ATP hydrolysis in the nucleotide-binding domain of the ABC transporter HlyB. *Embo J*, **24**, 1901-1910.
- Zaitseva, J., Jenewein, S., Wiedenmann, A., Benabdelhak, H., Holland, I.B. and Schmitt, L. (2005b) Functional characterization and ATP-induced dimerization of the isolated ABC-domain of the haemolysin B transporter. *Biochemistry*, **44**, 9680-9690.
- Zaitseva, J., Oswald, C., Jumpertz, T., Jenewein, S., Wiedenmann, A., Holland, I.B. and Schmitt, L. (2006) A structural analysis of asymmetry required for catalytic activity of an ABC-ATPase domain dimer. *Embo J*, **25**, 3432-3443.
- Zehnpfennig, B., Urbatsch, I.L. and Galla, H.J. (2009) Functional Reconstitution of Human ABCC3 into Proteoliposomes Reveals a Transport Mechanism with Positive Cooperativity. *Biochemistry*.
- Zhang, F., Zhang, W., Liu, L., Fisher, C.L., Hui, D., Childs, S., Dorovini-Zis, K. and Ling, V. (2000) Characterization of ABCB9, an ATP binding cassette protein associated with lysosomes. *J Biol Chem*, **275**, 23287-23294.
- Zhao, Z., Sheps, J.A., Ling, V., Fang, L.L. and Baillie, D.L. (2004) Expression analysis of ABC transporters reveals differential functions of tandemly duplicated genes in *Caenorhabditis elegans*. *J Mol Biol*, **344**, 409-417.
- Zolnerciks, J.K., Wooding, C. and Linton, K.J. (2007) Evidence for a Sav1866-like architecture for the human multidrug transporter P-glycoprotein. *Faseb J*, **21**, 3937-3948.

Acknowledgments

I want to give gratefully thanks to my supervisors PD. Dr. Rupert Abele and Prof. Dr. Robert Tampé for giving me the opportunity to work in their lab. They have provided great supervisions and fruitful discussions. I am deeply impressed by their enthusiasm for scientific questions, good knowledges, active thinking and serious attitude to every single experiment. It is a great pleasure to be their student and many things I learned from them will be very helpful in the rest of my life. Special thanks go to PD. Dr. Rupert Abele for taking so much time on reviewing my thesis and going through lots of official procedures.

I have to thank my lab members: Meike Herget, Giani Oancea, Christoph Baldauf, Özlem Demirel, Nina Kreißig, Gerda Gündisch, Irina Bangert, Franz Tumulka, Rupa Ram and Maiko Iwai for the nice working atmosphere as well as numerous helps on experiments and difficulties in lifes as a foreigner. Besides, Christoph Baldauf helped me for the German summary of this thesis. Nina Kreißig, Gerda Gündisch and Franz Tumulka did the proofreadings. I should not forget my practical students Lukas Hubener, Eileen Auth and Andreas Pollner who assisted me in the project.

Additionally, Dr. David Parcej, Dr. Daphne Nikles and PD. Dr. Joachim Koch always provide warm discussions and helps about my project. I appreciate the professional technical assistants from our technicians, especially, Ms. Gudrun Illig, Mr. Eckhard Linker and Mr. Gerhard Spatz-Kümbel. Ms. Christine le Gal has been always helping me for many complicated official procedures.

Dr. Ilka Wittig and Prof. Dr. Hermann Schägger (Zentrum der Biologischen Chemie, Universität Frankfurt) generously offered me membrane protein standards for blue native PAGE. Prof. Dr. Yuji Kohara (National Institute of Genetics, Mishima/Japan) provided the cDNA clones of *haf-9*. Dr. Winfried Haase (MPI Biophysics, Frankfurt) performed freeze-fracture EM experiments for me. The project won't proceed efficiently without the helps from these people.

I thank the additional members of my IMPReS thesis committee (Prof. Dr. Werner Kühlbrandt and Prof. Dr. Clemens Glaubitz) for taking time to participate my project progress reports and giving suggestions.

Last but not least, I thank my family for their supports during my Ph.D study.

Curriculum Vitae

Personal Informations

Name Chenguang Zhao
Status Married
Date of Birth 16/04/1977
Place of Birth Huhehaote/China

Educations

2005- Ph.D Thesis (Biochemistry), Frankfurt University, Germany
2000-2003 M.A. (Microbiology), Wuhan University, China
1996-2000 B.A. (Biotechnology), Inner Mongolia University, China

Awards and Fellowships

2007 Center for Membrane Proteomics (CMP) Frankfurt Fellowship
2005-2007 International Max-Planck-Research School Fellowship

Publications

1. **Zhao C**, Haase W, Tampé R, Abele R. 2008. *Journal of Biological Chemistry* 283: 17083-91
2. **Zhao C**, Tampé R, Abele R. 2006. *Naunyn-Schmiedeberg's Archives of Pharmacology* 372: 444-50
3. Tong X, **Zhao C**, Qi Y, Sun H. 2004. *Journal of Wuhan University (Nature Science Edition)* 50: 756-60
4. **Zhao C**, Sun H, Tong X, Qi Y. 2003. *Biochemical Journal* 374: 321-7
5. Sun H, Zhao CG, Tong X, Qi YP. 2003. *Journal of Biochemistry and Molecular Biology* 36: 214-22
6. Sun H, **Zhao C**, Tong X, Qi Y. 2003. *Chinese Journal of Biochemistry and Molecular Biology* 19: 210-4
7. Sun H, **Zhao C**, Tong X, Qi Y. 2003. *Chinese Journal of Biochemistry and Molecular Biology* 19: 96-102